Republic of Iraq
Ministry of Higher Education
and Scientific Research
University of Babylon
College of Materials Engineering
Department of Ceramic Engineering and Building Materials

Preparation and Characterization of Hard and Self-cleaning Ceramic Oxides layer by Micro-arc oxidation from Different Rock Additives

A Thesis

Submitted to the Council of the College of Materials Engineering / University of Babylon in Partial Fulfillment of the Requirements for the Master degree in Materials Engineering /Ceramic

By

Rasha Nife Rashed Jassem

Supervised by

Prof.

Samir Hamid Awad (Ph.D)

2023 A.D **1445 A.H**

بسم الله الرحمن الرحيم

وَمَا لَنَآ أَلَّا نَتَوَكَّلَ عَلَى ٱللَّهِ وَقَدْ هَدَىٰنَا سُبُلَنَا ۚ وَلَنَصْبِرَنَّ عَلَىٰ
مَآ ءَاذَيْتُمُونَا ۚ وَعَلَى ٱللَّهِ فَلْيَتَوَكَّلِ ٱلْمُتَوَكِّلُونَ ﴿١٢﴾

صدق الله العلي العظيم

سورة أبراهيم آية (12)

The Certificate of Supervisors

I certify that this thesis entitled "**Preparation and characterization of hard and self-cleaning ceramic oxides layer by micro-arc oxidation from different rock additives**" was prepared by (**Rasha Nife Rashed Jassem**) under our supervision at the department of ceramic and building Materials / College of Materials Engineering / University of Babylon in partial fulfillment of the requirements for the degree of Master in ceramic.

Signature:

Name: Prof. Samir Hamid Awad, Ph.D.

(Supervisor)

Date: / / 2023

To my Family for their endless love, Support and encouragement

Rasha

2023

Acknowledgments

Power in God, help from Him, and safety with Him; all fears of the world are worth nothing when relying on Him, all thanks be for ALLAH the Lord of all creations. The blessings of the immaculate Imams Fatima Al Zahra and Imam Abbas (peace be upon them).

I extend my deepest gratitude to my supervisor, Dr. Samir Hamid Awad, for his unwavering guidance, advice, enthusiasm, and encouragement throughout this investigation .

My journey began with a dream that my father painted for me during my childhood. With the prayers and love of my mother, that dream was fulfilled .

My late brother, the martyr (Fadel), remains the silent force behind the achievement of my goals and dreams. Every word I have written is dedicated to his memory and the love he left behind.

To my brother (Amer), your unwavering encouragement and support at every step of preparing this work have been invaluable. My sisters (Entder and Rajaa), thanks for your heartfelt resonate deeply with me. I extend my profound appreciation to my sisters (Sahraa, Sanaa and Rafall) for their unwavering support during the period of preparing this work.

Rasha
2023

Table of Contents

Table of Abbreviation and Symbols

Symbol	***Meaning***
MAO	Micro arc oxidation
SAAS	Superhydrophobic Al alloy surface
CA	Contact angle
PEO	Plasma electrolytic oxidation
MAO	Micro-arc oxidation
XRD	X-ray diffraction
SEM	Scanning electron microscope
AFM	Atomic force microscope
α	Alpha
°C	Celsius
DC	Direct Current
EDS	Energy Dispersive Spectroscopy
γ	Gamma
g	gram
L	Liter
μm	Micrometer
rpm	Revolution per minute
θ	Theta(angle)
HV	Hardness Vickers
V	Volt
λ	Wave length of incident wave
nA	nano Amber
*i*corr.	Corrosion current density

List of Figures

List of Tables

Abstract

Surface engineering of 1105-GOST4784 Al alloys by deposition of hydrophobic coatings using different techniques to improve the corrosion resistance and self – cleaning properties has gained more attention in the last years. This study is an attempt in using of Iraqi ceramic rock additives in modification of the electrolytes used in micro arc oxidation MAO process for deposition of hard and superhydrophopic Al_2O_3 ceramic coatings on Al alloys for heavy load bearing tribological and self-cleaning applications. Coating aluminum components of bridges and railings with self-cleaning materials can reduce maintenance costs and enhance the longevity of these structures in outdoor environments and self-cleaning and corrosion resistance of Al alloy coatings can be applied to architectural surfaces, such as building exteriors and facades, to reduce the accumulation of dirt, pollutants, and biological growth. This not only maintains the aesthetic appeal but also minimizes maintenance requirements.

In this study, Iraqi rock additives of calcite ($CaCO_3$) were used as electrolyte basis components, bauxite in different concentrations (1, 3, 5 and 7 g/L) and thassos rocks (1, 2, 3, 5 and 7 g/L) were used as modification components. Ceramic coatings of Al_2O_3 were deposited on Al alloy by using a homemade MAO unit with an applied voltage of (320-350) V, current of (0.1-0.3) A and a temperature of (15-25°C), and at different deposition times (10-45min). The coated surfaces were post treated using fatty acids such as myristic acid and stearic acid for important the self – cleaning properties.

Various analytical techniques and tests were used to characterize and evaluate the additives and structure, phases, mechanical and physical properties of the coatings such as scanning electron microscopy (SEM),

X-ray diffraction (XRD), roughness and topographic tests by atomic force microscope (AFM), hardness, thickness and angle of contact measurements and tests. The results proved the success of using MAO process with modified electrolytes containing Iraqi natural rock additives of calcite, bauxite, thassos and post treatment by myristic and stearic acids in deposition of porous (37.97-240.3 Ra) and thickness (445.2-2329nm) Al_2O_3. Ceramic coatings with superior properties of hardness (154.7-1700.7 HV) hydrophobicity (90.004°-113.907°) and corrosion resistance (568.61-8.48nA).

The highest contact angle of 113.907° was achieved when using a combination of calcite (20g/L), thassos (3g/L) and bauxite (3g/L). This high contact angle indicates that the surfaces are highly hydrophobic, meaning they repel water effectively. The best result for the highest hardness value recorded was 1700.7 HV when using calcite (10g/L), thassos (7g/L) and bauxite (5g/L) as additives.

Chapter One

Introduction

1-1: Overview

Aluminum and its alloys have a significant place in various industries including automotive, aerospace, high-speed rail, and nuclear power, owing to their exceptional properties. Here are some of the key attributes of aluminum and its alloys that make them valuable structural materials in these sectors low density, high Strength, thermal conductivity, and electrical conductivity. There were numerous benefits to using Al and its alloys including its excellent ductility, limited density, large specific stiffness, excellent heat conductivity, characteristics not magnetic and other properties [1].

However, Aluminum disadvantages as a structural material included the soft texture, poor wear resistance, low resistance to corrosion, and poor heat resistance, all of which have serious effect on scaled-up applications [2].

The method most frequently employed to made Al alloy surfaces super hydrophobic and self-cleaning, a tried-and-true method for preventing metals and alloys from oxidizing at high temperatures was the creation of ceramic oxide coatings on metallic surfaces. There were many different methods for depositing ceramic oxide coatings including plasma spraying, chemically vaporizing (CVD), physical vapor deposition (PVD), and sol-gel procedures [3].

These techniques have a number of disadvantages including being expensive and time-consuming due to the several processes. The temperature and chemical solution concentration, as well as the fact that the majority of the chemicals used in chemical processes were extremely corrosive and easily damage the environment had an impact on the size of the micro nanostructures created by these processes [4].

Environmentally benign weak acidic and alkaline electrolytes were used in PEO, where strong electric voltages were used to produce oxide coatings. This procedure increases the thickness of oxide coatings on the substrate by tens to hundreds of microns, considerably enhancing their heat barrier, wear resistance, and corrosion resistance properties in comparison to other traditional surface treatment procedures [5].

Ceramic coatings offer a range of advantages, making them a popular choice for various applications, especially in preserving metallic components. Ceramic coatings were often cost-effective compared to some alternative surface treatments or materials, making them an attractive choice for improving the performance and durability of metallic surfaces. Which can save time and effort in surface treatment compared to more complex methods. It were known for their excellent resistance to corrosion [6].

Alumina, often known as aluminum oxide was one of the most significant ceramic materials because of its numerous desirable qualities. It was useful for many different applications since it was chemically stable, structurally durable, optically transparent, and electrically insulating. Coating alumina components of bridges and railings with self-cleaning materials can reduce maintenance costs and enhance the longevity of these structures in outdoor environments and self-cleaning and corrosion resistance of Al alloy coatings can be applied to architectural surfaces, such as building exteriors and facades, to reduce the

accumulation of dirt, pollutants, and biological growth. This not only maintains the aesthetic appeal but also minimizes maintenance requirements [7].

The deposition of hard and thick alumina coatings through various techniques including (MAO) and anodic oxidation by spark discharge, (PCO) and (PEO) has been demonstrated to be a new and effective surface treatment technology to improve the tribological characteristics of Al alloys [8].

PEO was frequently used to create an oxidized ceramic coating in situ on the surface of aluminum (Al). The targeted ceramic coating exhibits great surface hardness, remarkable adhesion strength to the substrate and noteworthy chemical stability. It also exhibits strong electrical resistivity, corrosion resistance, high hardness and anti-wear capabilities [9].

MAO is a challenging process that depends on a variety of processing factors, including the applied voltage, the electrolytes concentration, substrate material, electrical parameters, oxidation time, processing temperature, electrolyte composition and additives. For the Al alloy to have a longer wear life, a suitable coating structure can be generated if the deposit parameters and post-treatment method of coating are appropriately chosen [10].

1-2: Objectives of the current study

The surface engineering of Al alloys by means of hardness and self-cleaning aspects using MAO process and modified electrolyte with ceramic natural rock additives such as thassos, bauxite and calcite will be of great importance in surface engineering of Al alloys for self-cleaning and heavy load bearing application. Also, it can provide valuable insights into natural rock additives effectiveness and environment conservation.

Chapter Two

Theoretical Part & Literature Survey

This chapter is divided into two sections:

- The first section one presents the definition of surface engineering and aluminum. In addition, it explains micro arc oxidation (MAO) process, deposit alumina layer, process parameters, advantages and disadvantages of process. Also, self-cleaning surface, self-cleaning coatings and (calcite, bauxite and thassos) rock additives and secondary treatment were explained.
- The second section includes the related literature survey.

2-1: Surface Engineering and Modification

"Surface engineering" is the technique of using both conventional and cutting-edge surface technologies to engineer components and substances in order to create a composite material with qualities that are not possible in either the base material or the surface material. The many surface technologies are frequently unconventional and cutting-edge surface technologies to engineering parts and materials tied to improve the designs of engineering components, however, surface engineering is best when the component is produced with knowledge of the surface treatment to be used[11-12]. Surface engineering procedures are often classified into the following categories:

- Surface preparation methods, which include cleaning and ingredient preparation for surfaces.
- Treatment of surfaces to achieve desired qualities. Surface modification can be done in a variety of ways to affect aspects of the surface including charge, biocompatibility, reactivity, energy, hydrophilicity, and roughness. The coating was one of the main surface treatments that was used to enhance properties. The classification of coatings into groups according to their methods of production is shown in figure (2-1) [13].

Presently different techniques are increasingly used to fabricate the micro-nano structure of the superhydrophobic aluminum alloy surfaces (SAAS). It can be noticed that the method used in present work is belonged to conversion coating such as, plasma electrolytic oxidation (PEO), a promising new electrochemical surface treatment method can create a thick, hard, and dense ceramic-like covering [14]. Anodic oxidation by spark discharge, plasma chemical oxidation, and micro-arc oxidation are other names for this method.

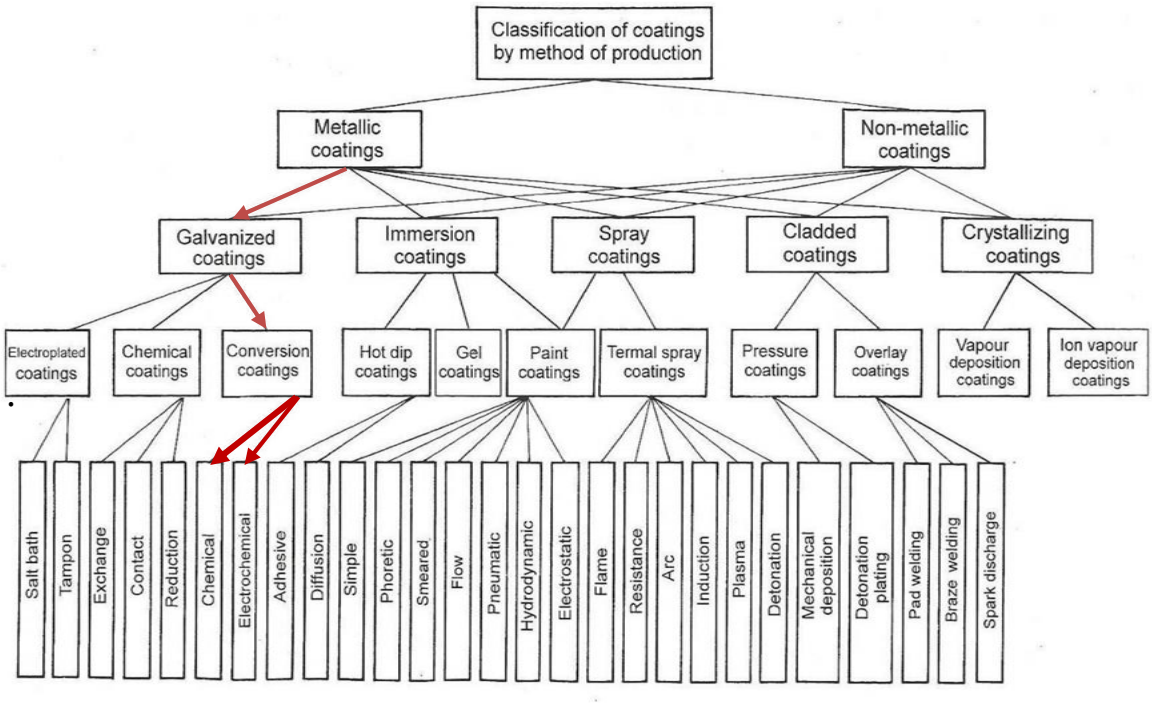

Figure (2-1): Categorization of coatings by process of production [13].

2-2: Aluminum Properties

Al (Aluminum) is one of the most versatile, economical, and attractive metallic materials for a broad range of uses from soft, highly ductile wrapping foil to the most demanding engineering applications, given to the special combinations of properties given by Al and its alloys. This use of Al alloys as structural metals is second only after steel. It is possible to design and build strong, lightweight structures that are especially useful for anything that moves including spacecraft, aircraft, and all kinds of land- and water-based vehicles. Because of their excellent properties such as low density, excellent thermal and electrical conductivity, high specific strength, and good castability [15-16].

It is of importance to creating superhydrophobic surfaces on aluminum alloys can be beneficial in inhibiting corrosion and oxidation. Superhydrophobic surfaces have the ability to repel water, preventing from coming into contact with the underlying material. This can be particularly useful in protecting aluminum alloys, as it reduces exposure to moisture and other corrosive substances. Aluminum is known for its flexibility, lightweight nature, and white-silver appearance. When exposed to oxygen, aluminum readily forms a thin oxide film on its surface, which typically impermeable and acts as a protective layer [17].

Pure aluminum naturally forms a thin barrier oxide layer of aluminum oxide on surface, which typically only a few nanometers thick. This oxide layer provides some level of protection against corrosion by stabilizing the surface and preventing further reaction with the environment. However, in harsh environments such as in the presence of aqueous salt, the corrosion resistance of aluminum can be significantly reduced, which can lead to localized damage and degradation of the metal. To enhance the corrosion resistance of Al in such environments, additional treatments can be applied [18].

The oxidation process of Al alloys is temperature-dependent, alloy-composition-dependent and sample surface condition-dependent. There is some debate in the literature on the kinetics of the process as well as the oxides formed. Aluminum and its alloys form an amorphous, shallow, thin, and resistant layer (γ- Al_2O_3) that follows parabolic kinetics during the early stages of oxidation. The first layer affects the formation of the oxide at high temperatures and this layer serves as a barrier between the metal and the atmosphere [19].

2-3: Aluminum Oxide

Aluminum oxide often known as alumina or Al_2O_3 is appealing indeed possesses several appealing properties for engineering applications that are widely employed in (microelectronics, optically, firebricks, abrasives, and catalysis) integrated circuit packaging due to thermal and chemical stability, considerable strength and qualities of thermal and electrical insulation make it a versatile material used in various fields Alumina melts at roughly 2040 °C, however defects and alloying elements generate secondary phases that can melt at much lower temperatures [20].

Alumina exists in a variety of crystalline phases or polymorphs such as (α, γ, η, δ, κ, χ, etc.) with the phase being thermodynamically stable at all high temperatures to its melting point of 2051 °C. However, alumina is a compound consisting of aluminum and oxygen atoms and has several different phases or crystal structures. The phase α- Al_2O_3 is the only thermodynamically stable phase of alumina at standard conditions. This means that all of these transformations occur at high temperatures. Across all phases of alumina, it has the highest concentration, elastic modulus, hardness, and band gap. Because of these qualities, it is the ideal material for many industrial applications, including chemical and wear protection. It takes a while for a stable modification to emerge as the crystal lattice becomes more organized. The morphology of the resulting α-Al_2O_3 particles depends on the type of metastable polymorph [21-22].

2-3-1: Aluminum Oxide Structure

There are numerous polymorphs of solid aluminum oxide (alumina), the most stable of which being α-Al_2O_3 (corundum) as shown figure (2-2). The octahedral interstices of corundum are symmetrically occupied by aluminum cations and the structure of corundum is composed of hexagonally close packing of oxide ions. In contrast, a portion of the aluminum ions occupies tetrahedral interstices in metastable alumina phases like γ - Al_2O_3 as shown figure (2-2) and δ - Al_2O_3. Tetrahedrally and square pyramidally (fivefold) coordinated aluminum sites can be found in ultrathin alumina films. Half of the octahedral spots contain aluminum cations, and the remaining third contain oxygen anions. Four octahedral molecules share one oxygen. The features of alumina are due to the oxygen present in octahedral locations, which allows for strong bonding [23-24].

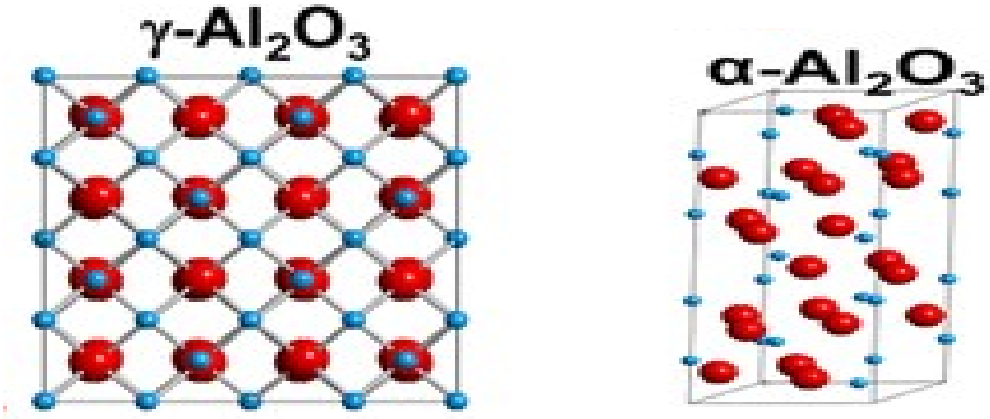

Figure (2-2): Aluminum Oxide structure for γ - Al_2O_3 and α-Al_2O_3.

2-3-2: Aluminum Oxide Applications

Alumina (*Aluminum Oxide)* is an intriguing material for versatility with several enticing features that make it suitable for various applications. Some of the applications include [25-26]:

♦ Aluminum oxide is widely used as an abrasive material due to its hardness. It is used in grinding wheels, sandpaper, polishing compounds and abrasive media for sandblasting.

♦ It has a high melting point and excellent heat resistance, making it suitable for applications in refractory materials. It is used in the production of bricks, crucibles and other high-temperature resistant products.

♦ It is a key component in the production of ceramics. It is used as a ceramic glaze, as well as in the fabrication of ceramic parts, such as cutting tools, electrical insulators and wear-resistant components.

♦ It can be used as a catalyst or catalyst support in various chemical reactions. Its high surface area and stability make it suitable for catalytic applications in petroleum refining, chemical synthesis and environmental processes.

♦ It is an excellent electrical insulator, and it is used in the production of insulating materials for electrical components and devices. It provides thermal conductivity along with electrical insulation making. It ideal for applications such as power transmission and electronic circuit boards.

- Al_2O_3 coatings are applied to various surfaces to enhance their properties. They can improve corrosion resistance, hardness, and wear resistance of materials. Aluminum oxide coatings are commonly used in the automotive, aerospace and manufacturing industries.
- It is used in dentistry for the production of dental crowns, bridges, and implants. It is also used in medical devices and implants due to its biocompatibility and resistance to bodily fluids.
- It is utilized in filtration processes due to its porous nature. It is used in the production of filter media for water treatment, air purification and industrial filtration applications.
- It is a common abrasive material used in grinding wheels and cutting tools. It provides high hardness and durability, allowing for efficient material removal in metalworking and other machining processes.

2-4: Self-cleaning Surface

Several plants leaves are completely free of dust contamination after a little rain. These leaves are referred to as "superhydrophobic" because droplets of water form spheres with very little adherence to the surface and roll off very quickly even at very slight slopes. Surface roughness on the micro and nano scales is a key property of superhydrophobic surfaces. In order to design and build superhydrophobic substrates with self-cleaning capabilities, as shown figure (2-3) lotus-like super hydrophobicity must be prepared [27-28]**.**

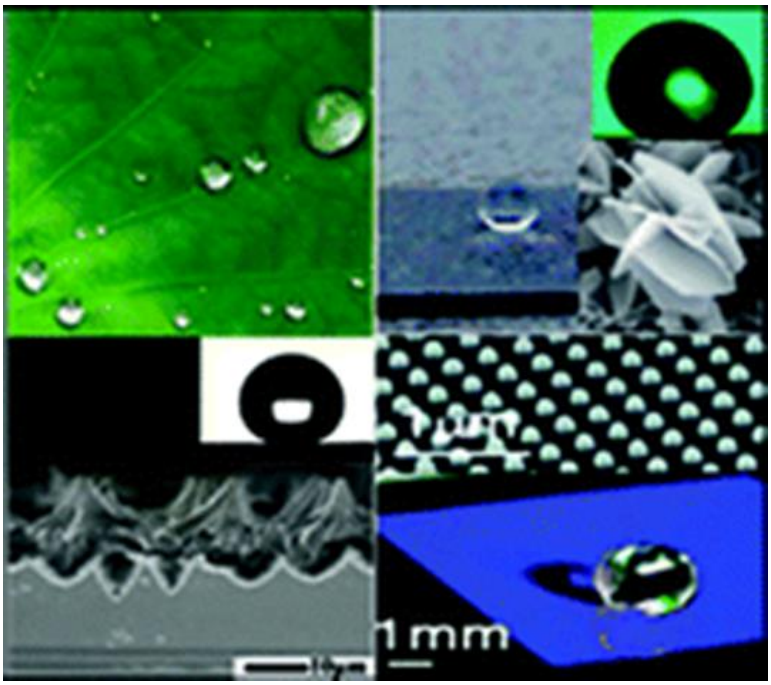

Figure (2-3): Super hydrophobic substrates with self-cleaning.

2-4-1: Self-cleaning Coatings

Self-cleaning coatings can be broadly divided into hydrophilic and hydrophobic types. Both groups clean themselves through the influence of water. A hydrophilic coating causes the water to scatter (made of fabric of water) over the substrates, removing dust or other impurities, whereas a hydrophobic method causes the water droplets to slide and roll over the surfaces, cleaning them. Yet, the hydrophilic coatings with the appropriate metal oxides have the additional ability to chemically degrade the intricate dirt deposits through a cleaning mechanism facilitated by sunshine. The surface contact angle (CA) is connected to the self-cleaning phenomena. It is the angle created between both the surface of the water droplet and the surface of the solid at the 3 phase border (solid, liquid and vapour). In general, a solid surface is said to have a hydrophilic surface if the contact

area is 90 degrees or less. Whenever the contact angle (CA) is more than 90 degrees, the surface is referred to as hydrophobic. Similarly, a surface is considered ultra (super) hydrophilic if its water contact angle is close to zero and ultra (super) hydrophobic if it has a contact angle greater than 150° . Figure (2-4) [29].

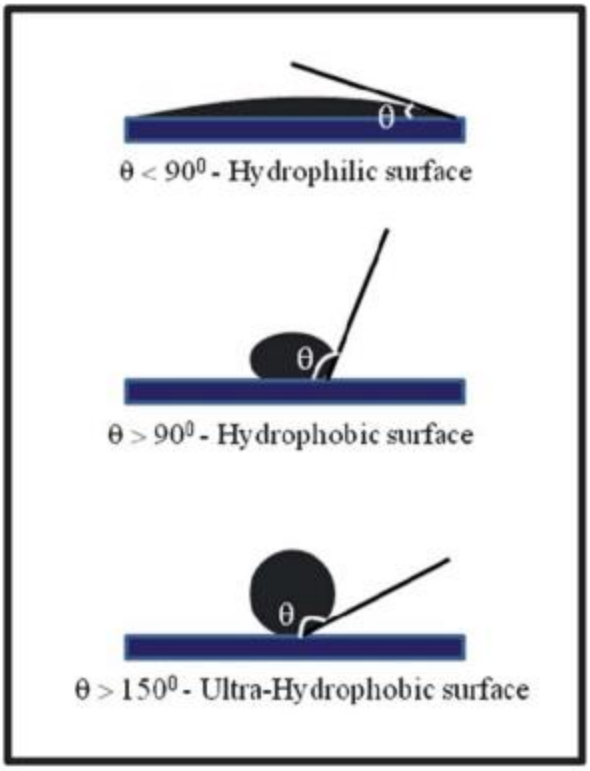

Figure (2-4): An illustration of surfaces that are hydrophilic, hydrophobic, and ultra- (super-) hydrophobic [29].

2-4-1-1:Self-cleaning through Hydrophobic Coating

Rolling water drops that hit a smooth surface collect dust from a rough, super hydrophobic surface, causing a self-cleaning phenomenon. In addition to researchers, the general public is becoming more and more interested in the self-cleaning properties of hydrophobic surfaces (Lotus Effect). The list of surfaces that can be coated with this self-cleaning hydrophobic coating is endless. Examples include the windscreens of cars, the entire body of cars, doors and windows glasses, skyscrapers, solar cell screens, textile products, sportswear, metal alloys, papers, sponges, woods, marbles and the list goes on [30].

2-5: Hydrophobic Coating Methods

Hydrophobic surfaces can currently be created using a variety of efficient methods, including as sol-gel, template, electro spinning, hydrothermal synthesis, laser fabrication, etching and electrochemical techniques. The previous research has also shown the existence of hydrophobic surfaces with micro-nano structures on metallic substrates. To change the surface topology to the necessary hierarchical micro-nano topologies for hydrophobicity, a variety of mechanical, thermal and chemical methods have been used [31].

2-5-1: Conversion Coating

A conversion coating is a chemical process used to change a metal surface from metallic to non-metallic, creating a film at the surface. Due to their importance in the metal treatment industry increased aesthetic appeal and corrosion protection. Converter coatings have been commonly used for a long time**.** Conversion coatings are created by aqueous solutions and the substrate reacting chemically or electrochemically to build an oxide layer that expands both inward and outward. The likes of conversion coatings provide a practical technique to improve the corrosion resistance of titanium, magnesium and aluminum alloys or a pre-treatment to improve the adherence of a final coating that is deposited. Conversion layers provide the option of changing the substrate surface to improve adhesion, create a clean surface or create a coating layer with active corrosion inhibitors. The electrochemical anodization process produces the most prevalent conversion layers [32].

The choice of electrolytes, including alkaline substances with phosphate, silicate and borate additions has recently received a lot of scientific attention. In addition to being cost-effective, chemical conversion coatings favored for their adhesion and quick coating development. Additionally, these can be created using basic tools and without the need of outside potential. However, the performance of the anodizing process can sometimes be less than satisfactory. Plasma electrolytic oxidation (PEO) synthesis of anti-corrosion coating on light alloys. The PEO procedure can be viewed as combining the anodizing (electrolytic oxidation) and plasma discharging procedures. Whereas the first step of the PEO method is an anodization process, the key connections of the PEO and anodizing

procedures are that both involve the oxidization of substrate using an electrolytic bath. Additionally typical is combining two or more [33-34].

2-5-1-1: Micro-Arc Oxidation

Plasma electrolytic oxidation (PEO), also known as micro-arc oxidation (MAO) is a promising method of surface treatment that could result in ceramic-like coatings increase the corrosion and wear resistance of aluminum alloys by employing environmentally safe diluted electrolytes. The MAO coating growth is a complex reaction process that is accompanied by instantaneous and localized acoustic, light and heat emission, chemical and plasma-chemical interactions, as well as a melt and quench [35].To create ceramic overcoats for aluminum components and shield them from severe oxidization on metal, micro-arc oxidizing or arc discharge oxidizing has been developed. The application of micro-arc oxidation coatings to preserve aluminum alloys is now of great interest because of its high micro-hardness, excellent electric insulation resistance and strong adherence to the substrate [36].

The PEO invention theoretically does not need the solute, instead forming an autogenous oxide layer on the surface of the Al-compound. In this manner, since neither the cathode nor the components in the electrolyte are expended the PEO innovation is a "spotless" treatment. Al composite has excellent saltwater and high temperature consumption resistance thanks to the PEO process, which effectively moulds an Al_2O_3 coating that is metallurgically adhered to the substrate and has high impedance and high soundness [37].

2-5-1-1-1: Micro-Arc Oxidation Principle

In the micro arc oxidation (MAO) process, the electrolytic cell functions as the cathode, while the metal being treated such as aluminum, magnesium, titanium or their alloys acts as the anode. The metal is immersed in an electrolyte solution and placed under an electric field environment, where it is subjected to voltages typically ranging up to 1000 volts or even higher, along with higher currents. This is illustrated in figure (2-5). A thin metal oxide insulating coating is immediately produced on the metal surface after energization. As a result, the applied voltage to the work piece gradually increases over time. As the voltage increases, some weak points in the insulating film eventually break when a specific critical value is reached. It will manifest as a micro area arc discharge phenomenon and instantly create a zone of extremely high temperature [38].

This results in the base metal and oxide melting or even vaporizing. The ceramic films layer is created by cooling the molten material after it has come into contact with the solution of electrolysis.

Since the breakdown always takes place in a relatively weak area of the aluminum oxide film, a new oxide layer is created in the area where the breakdown originally occurred. The point of breakdown then transfers to additional moderately weak regions. On the metal surface a consistent oxide deposit is continuously created [39-40].

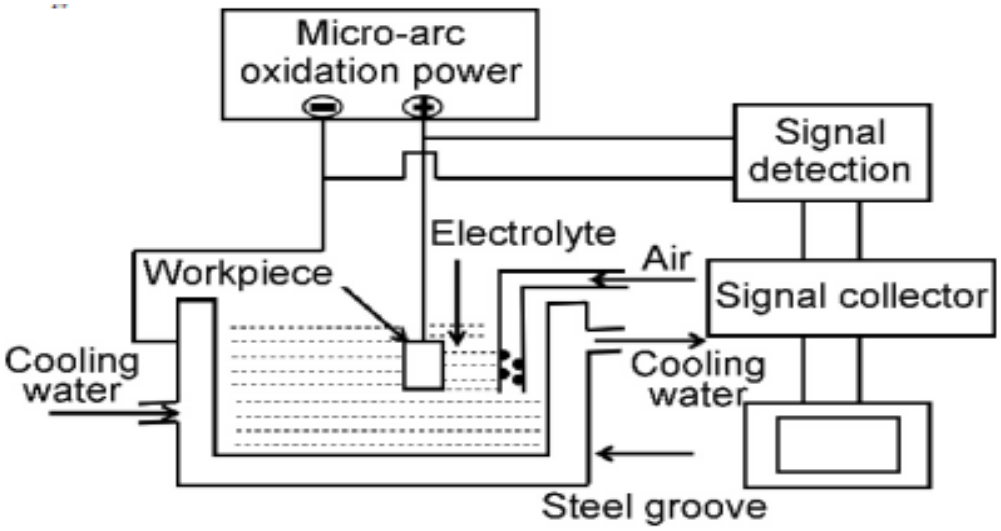

Figure (2-5): Shows a schematic diagram of the MAO technology workings [38].

2-5-1-1-2: Advantages and Disadvantages of MAO Coatings

The benefits of MAO include a coated surface with good hardness and adhesion qualities and varying porosity scales across its structure. The coating itself is where this kind of multi-structural nature originates. Surface treated with MAO at various frequencies of producing porous structures with various porosities [41]. The MAO coating also has outstanding adhesion, hardness, wear resistance, corrosion resistance, insulation, temperature resistance and impact resistance. One advantage of the MAO process can be performed at room temperature and atmospheric pressure, which makes it an environmentally friendly and cost-effective surface treatment option compared to other methods such as thermal spraying and chemical vapor deposition. It is crucial to note that the MAO coating caused less harm to the substrates fatigue performance than the hard anodic oxide coating did [42].

MAO coatings have a number of benefits, but they also have certain drawbacks. First, the generator must boost voltage to up to 1000V (almost 1 mw) using the selected parameters. Depending on the size and kind of the material, the process is hazardous because to the high energy. Furthermore, it costs more money than the anodic oxidation method. A large capacity cooler is becoming increasingly necessary to bring down the solution's temperature. Additionally, the coating is brittle and rough in the outer layers, which reduces wear resistance. MAO is drawing growing interest in the fabrication of ceramic-like coatings on aluminum, magnesium, and titanium alloys. It has great bonding strength with the substrate, high productivity, economic efficiency, environmental friendliness, high hardness and strong wear resistance [43-44].

2-5-1-1-3: Applications of MAO

There are many uses, especially in the transportation industry, including the automotive and aerospace sectors as well as the biomedical, electrical, and aerospace industries, where it is preferable to other traditional surface treatment procedures on titanium, magnesium, and aluminum alloys. These include the rotors and centered rings of turbo molecular pumps, facilities for astrobiological research during the international space stations exposures system, heat sinks, die-cast optical parts and plates for osteosynthesis, and scanned body locators and stents to address cardiac issues. Making use of MAO with varied materials. Researchers have exposure the use of MAO with different materials to enhance their properties for specific applications. In certain studies, surface structuring techniques are employed during MAO to create hydrophobic surfaces.

These surfaces repel water and can have applications in areas such as self-cleaning coatings, anti-icing surfaces, and microfluidic devices [45].

The MAO method is primarily used in several areas [46].

♦ Applications in Chemistry: It is stable to powerful acids and powerful bases at moderate temperatures. Because of this, it can be applied in the chemical and food sectors.

♦ Mechanical Applications: This MAO process creates an oxide layer with hardness. The increased value of hardness is one of the elements that raise the resistance to sliding, abrasive, and wear. More limited lubrication procedures can benefit from the friction coefficient's effectiveness.

♦ Thermal Applications: Because the oxide layer has a lower thermal inductivity than the other metal, it can be used to both distribute heat evenly and to boost thermal shock resistance.

♦ Applications for electric and electronic systems: Include using it as an insulator coating on electrical and electronic components. Additionally, it works well for cylindrical, conical or cavital interior parts that need a strong coating.

2-5-1-1-4: Parameters affecting on Micro arc Oxidation

The quality of the MAO coating is influenced by several factors, and controlling these factors is crucial for obtaining a high-quality coating. The factors that affect the properties of the MAO coating include current density, anode and cathode currents ratio, MAO processing time, temperature and composition of the electrolyte. One of the challenges in the MAO process is finding the optimal process parameters to achieve the

desired coating properties [47]. The following are some of the factors that can affect the micro arc oxidation process of aluminum alloys:

1- Current density

The current density, which is the ratio of the applied current to the surface area of the aluminum alloy, can also affect the micro arc oxidation process. A higher current density can lead to a higher discharge intensity and a thicker oxide layer [48].

2- Processing time

The processing time is another important factor that can affect the micro arc oxidation process. A longer processing time generally results in a thicker oxide layer [49].

3- Electrolyte temperature

The temperature of the electrolyte can affect the micro arc oxidation process. A higher electrolyte temperature can lead to a higher oxide layer thickness, but too high a temperature can also lead to overheating and other problems [50].

4- Applied voltage

The applied voltage is an important factor that affects the micro arc oxidation process. The voltage determines the intensity of the electrical discharge that occurs between the aluminum alloy surface and the electrolyte. A higher voltage leads to a higher discharge intensity, resulting in a thicker oxide layer [51].

5- Alloy composition

The composition of the aluminum alloy can also affect the micro arc oxidation process. Different alloy compositions can have different microstructures and chemical compositions, which can affect the formation and properties of the oxide layer [52].

6- Electrolyte composition

It is important to note that the selection of electrolyte for MAO process depends on various factors, such as the type of metal substrate, desired coating properties, and application requirements. Therefore, the electrolyte composition and concentration should be optimized to achieve the desired coating characteristics [53].

Additionally, the MAO process involves complex electrochemical reactions, and the electrolyte plays a crucial role in controlling the reactions and the resulting coating structure and properties. Therefore, understanding the effect of electrolyte on the MAO process is essential for optimizing the process and improving the coating performance. In summary, the electrolyte used in the MAO process can significantly affect the coating structure and properties. Alkaline silicates and phosphate electrolyte solutions are commonly used, with phosphate electrolytes being favored for their thicker coatings and better corrosion resistance [54-55]. In this study, alkaline silicates and phosphate electrolyte were used as a matrix for the coating solution. Overall, the use of this matrix material in self-cleaning coatings is an area of ongoing research and development, with the potential to provide a range of benefits in various applications.

2-6: Post treatments of Self-cleaning Coatings

The primary purpose of the micro-arc oxidation (MAO) process is indeed to improve the surface properties of aluminum alloys, such as hardness, wear resistance and corrosion resistance by creating a ceramic oxide layer on the surface. As MAO itself does not confer self-cleaning capabilities, additional coatings with self-cleaning functionalities would need to be applied after the MAO process to achieve the desired self-cleaning properties. This post-treatment can introduce hydrophobic or other self-cleaning characteristics to the surface, which can help repel contaminants and keep the surface clean [56]. Here are show post treatments of self-cleaning coatings by a simple and environmentally friendly method that can be applied to Al alloys after the MAO process in this study:

- Fatty acids are long-chain carboxylic acids, and some common examples include oleic acid, lauric acid, palmitic acid, myristic acid and stearic acid. These fatty acids are typically derived from the hydrolysis of natural fats and oils found in animals and plants. These fatty acids play a crucial role in the formulation of cosmetic creams, cakes, soaps, pastes, and other personal care products, contributing to their texture, stability and overall performance [57].
- Methanol (CH_3OH) is a colorless liquid with a mild alcoholic odor when pure. It is highly volatile and readily evaporates at room temperature, similar to other common alcohols, a flammable liquid. Its vapors can form flammable mixtures with air, highly miscible with water, meaning it can mix with water in all proportions. It is also miscible with many other polar and non-polar solvents, including alcohols, esters, ketones, and most organic solvents. Solubility is only slightly soluble in fats and oils.

This property is useful in certain applications where it is necessary to keep fats and oils separate from water-based solutions. These properties make methanol a versatile solvent and chemical intermediate used in various industrial processes, including as fuel, antifreeze, solvent and in the production of chemicals and materials [58].

- Chloroform is also known as trichloromethane, methane trichloride, trichloroform, methyl trichloride, and formyl trichloride. A chemical compound with the molecular formula ($CHCl_3$). It is a colorless, heavy, sweet-smelling liquid that was historically used as an anesthetic during medical procedures. However, its use as an anesthetic has largely been phased out due to safety concerns and the development of safer alternatives. Chloroforms solubility refers to its ability to dissolve in different substances, particularly in water and other solvents. It is moderately soluble in water. The solubility of chloroform in water increases with temperature. Its solubility is influenced by factors like temperature, pressure and the presence of other dissolved substances. It is more soluble in organic solvents such as ethanol, acetone, and ether. Its ability to dissolve in organic solvents is due to its non-polar nature [59].

2-7: Additives

2-7-1: Calcium Carbonate

Calcium carbonate ($CaCO_3$) is a chemical compound that can be found abundantly in various natural sources such as eggshells, gastropod shells, pearls and shellfish bones. In addition to its presence in biological materials, calcium carbonate is also found in rocks as minerals calcite or aragonite. Limestone a well-known sedimentary rock is primarily composed of calcite and is one of the most common sources of calcium carbonate in the earths crust. The formation of lime scale occurs when calcium ions from hard water combine with carbonate ions resulting in the precipitation of calcium carbonate [60].

Calcium carbonate ($CaCO_3$) is indeed an abundant inorganic biomaterial that can exist in different structures, including calcite, vaterite and aragonite. Thermodynamically, under normal conditions, calcite (β-$CaCO_3$) is the most stable form of $CaCO_3$. However, under specific synthesis temperatures, other polymorphs such as aragonite (λ-$CaCO_3$) and vaterite (μ-$CaCO_3$) can be formed [61].

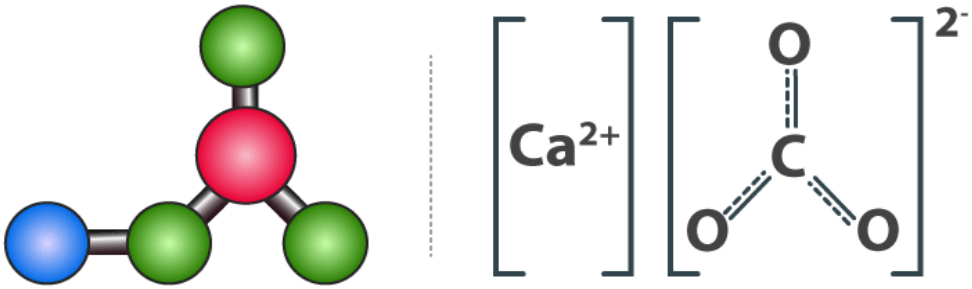

Figure (2-6): Calcium carbonate structure [61].

$CaCO_3$ Applications:

The structure and phase transformation of $CaCO_3$ are of great interest to researchers in various fields due to the diverse applications of this biomaterial [62-63]. Some common applications of $CaCO_3$ include:

- Environmental applications: $CaCO_3$ is utilized in water treatment processes, such as pH adjustment and water softening. It can also be used for the removal of heavy metals from industrial wastewater.
- Construction and building materials: $CaCO_3$ is a key component in the production of cement, concrete and lime. It provides strength and stability to these materials and is also used as a filler in paints, coatings and adhesives.
- Formation of deposits: $CaCO_3$ has been studied for its ability to form deposits on hard surfaces, such as stainless steel and silica, under different bulk solution conditions and surface properties.
- Self-cleaning coatings: Transparent self-cleaning coatings have been synthesized using organic Polydimethylsiloxane (PDMS) polymers and inorganic nano-$CaCO_3$ particles
- Scratch resistance: $CaCO_3$ has been used as a filler in rapid alkyd-based wood coatings to improve their scratch resistance
- Composite films: $CaCO_3$ has been used in polyurethane composite films to enhance their self-healing mineralization and anti-corrosive performance.

2-7-2: Bauxite

Bauxite ($Al_2H_2O_4$) is indeed a mineral composite that typically consists of several minerals, including gibbsite ($Al(OH)_3$), boehmite (γ-AlO(OH)), kaolinite ($Al_2Si_2O_{54}$), hematite (Fe_2O_3), anatase (TiO_2) and quartz (SiO_2). These minerals can vary in their relative proportions, resulting in a wide range of attributes for different bauxite deposits. In terms of aluminum class, bauxite is the primary source of aluminum ore the mineralogy of bauxite is also important as it determines the processing methods required to extract alumina from the ore [64-65].

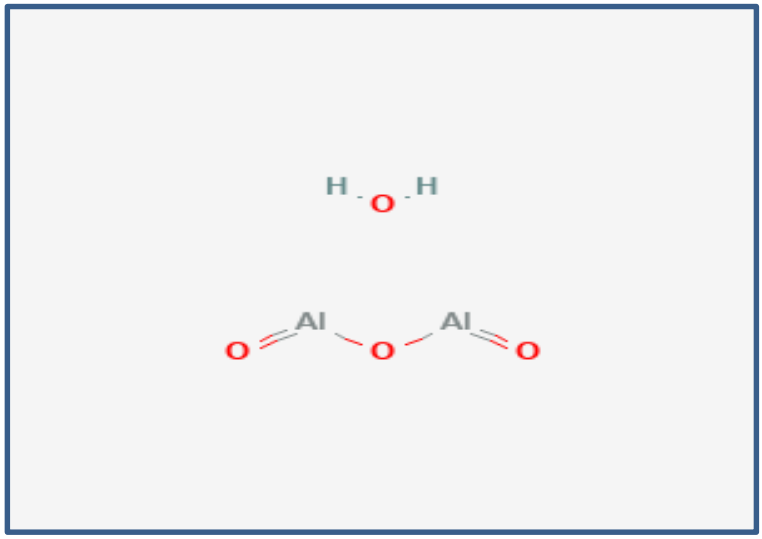

Figure (2-7): Chemical structure depiction.

Bauxite is described as a soft white to gray to reddish brown rock with a pisolitic structure. Pisolitic refers to the presence of small rounded nodules within the rock. It has an earthy luster and a relatively low specific gravity, typically ranging from 2.0 to 2.5. Bauxite is a naturally occurring heterogeneous material, meaning it is not uniform throughout.

It primarily consists of one or more aluminum hydroxide minerals, such as gibbsite, boehmite or diaspore. Along with these aluminum hydroxide minerals, bauxite contains various mixtures of silica, iron oxide, titania, alumina silicate and other impurities in minor or trace amounts. The specific composition of bauxite can vary depending on its location and geological conditions. It is found naturally in Al- Anbar and the western desert of Iraq [66].

Bauxite Applications:

Bauxite, which is an ore of aluminum, has several important applications in various industries. These are just a few examples of the applications of bauxite. Its versatility and abundance make it a valuable resource in various industries worldwide [67-69]. Here are some common applications of bauxite:

- Aluminum production: Bauxite is the primary source of aluminum metal. It is refined to extract alumina, which is then electrolytically processed to obtain pure aluminum. Aluminum is widely used in transportation (e.g., cars, airplanes), construction, packaging, electrical wiring and many other industries due to its lightweight, corrosion resistance and excellent conductivity.
- Refractory materials: Bauxite is used in the production of refractory materials, which heat-resistant substances were used to line high-temperature furnaces, kilns and reactors. The high alumina content of bauxite makes it suitable for manufacturing refractory bricks and shapes that can withstand extreme temperatures.

- Cement production: Bauxite with high alumina content can be used as a raw material in the production of cement. It acts as a fluxing agent, providing the necessary aluminum oxide and iron oxide to create the desired chemical composition during the cement manufacturing process.
- Ceramics and pottery: Bauxite is used in the production of ceramics and pottery, providing a source of alumina for the glazes and enamels used on the surfaces. It can enhance the strength, hardness and resistance to chemicals and heat in ceramic materials.
- Plasma sprayed coatings: Bauxite has been mixed with fly ash to create plasma sprayed coatings with improved adhesion strength and surface roughness.
- Composite coatings: Bauxite has been used to modify nano-TiO_2 composite coatings to enhance the self-cleaning and hardness property of brick surfaces using the spin coating technique

2-7-3: Thassos

Thassos marble is unique in that it can only be found on the small island in the Aegean Sea, adding to its rarity and value. The quality of thassos marble is remarkable. It is typically found in pure blocks that resemble clear sugar cubes, giving a pristine and elegant appearance [70].

The grains in white thassos marble are small ranging from 1 to 2 mm^2 in size and visible to the naked eye. The crystal surfaces of this marble exhibit a high level of light reflection, adding to its visual appeal. In terms of purity, thassos marble is known to have nearly 100% purity particularly in the dolomite-based variety.

This makes it one of the whitest stones discovered so far. Thassos marbles exceptional purity and lack of impurities give unique properties including special thermal characteristics compared to other types of marble [71].

Thassos marble possesses several thermo physical properties that distinguish it from other types of marble. Thassos marble has relatively low thermal conductivity which means, it is not a good conductor of heat. This property makes to useful in applications where temperature insulation or resistance is desired. Thassos marble can help maintain a stable temperature in interior spaces, making suitable for areas where heat transfer needs to be minimized. Like most natural stones thassos marble exhibits thermal expansion meaning expands when exposed to higher temperatures and contracts when cooled [72-73].

Thassos Applications:

Thassos marble finds application in various areas due to exceptional qualities and aesthetic appeal. It was important to note that the specific application of thassos marble can vary depending on factors such as the type of marble (e.g., dolomitic or calcite), finish (e.g., polished, honed, or brushed) and the desired aesthetic and functional requirements of the project [74-76]. Some common applications of thassos marble include:

- Thassos marble has found extensive application in sacred sites and historic buildings in the Middle East. The Makah Haram and Imam Ali Najaf are notable examples where thassos marble is frequently used for flooring adding to the grandeur and spiritual experience of these revered locations.

- It is often utilized as a decorative element for wall cladding in interiors. It adds a touch of sophistication and brightness to spaces, making a popular choice in hotels, restaurants and high-end residences.
- Thassos marbles durability and resistance to heat and moisture make suitable for countertops and vanity tops in kitchens and bathrooms. White color provides a clean and sleek look adding a sense of luxury to the space.
- It can be used to create visually striking staircases and steps. It is smooth surface and light-reflecting properties enhance the architectural features of the staircase making a focal point.
- Thassos marbles high quality and workability make it a favored material for sculptors and artists. It has been used historically for carving sculptures and contemporary artists continue to create stunning works of art using this marble.
- It is also employed for exterior cladding of buildings, adding a touch of elegance and sophistication to facades. It withstands weathering and maintains its appearance over time, making a durable choice for outdoor applications.
- It is a popular choice for fireplace surrounds and mantels. Its heat-resistant properties and timeless beauty create a focal point in any living space.
- It can be used for decorative elements such as columns, balustrades, moldings and ornamental details in architecture and design. It adds a touch of grandeur and refinement to spaces.

2-8: Literature Survey

According to our knowledge until this time, no work have used the rock additives in the electrolyte of MAO to improve the properties of Al alloy. Therefore, we will focuses on the latest studies that have used the micro and nano additives that used to improve different properties of aluminum alloys.

In ***(2017) Mohit Vishnoi et al,*** studied the hydrophobic coating developed and characterized for its corrosion resistance and surface properties synthesize by micro arc oxidation (MAO) on Al alloy. The MAO process involves electrochemical treatment of the aluminum alloy substrate in an aqueous electrolyte. The electrolyte has been chemically treated with myristic acid. The objective is to produce a stable film on the Al alloy substrate. The contact angle measurement for water on one of the treated surfaces is found to be approximately 129°, indicating a high level of hydrophobicity [77].

In ***(2017) Noor Fadhil et al,*** studied effects of rice husks ash addition on alumina layers deposited on 2024 aluminum alloys by micro-arc oxidation(MAO). The results proved that the formation of hard ceramic coatings were values (246.8-496.6) HV. Roughness increased with deposition time increasing (2.320-6.837), thickness of coatings variation with deposition time (25-48.8). The structure of coatings was characterized by the porosity, with increasing RHA ratio from (5 to 1S) g the structure became less porous particularly with increasing deposition time to 45min. Also, the RHA addition could improve wear resistance by means of decreasing loss weight from 0.0017 to (0.0006-0.0005)g and decreasing friction coefficient from 0.66 to (0.34-0.52) [78].

In ***(2018) Farqad Saleem et al,*** studied deposition of Aluminum Oxide on Al alloy by Micro Arc Oxidation using different additives. The results showed the possibility to deposit wear resistant γ- Al_2O_3 coatings with different modification elements (Si, W, and Ca) with thickness (38-78.1) μm, and hardness (167.7-447) HV using the Iraqi rock additives. Using of (10gm) fired porcelanite (900°C) provided the highest thickness (78.1μm at 60 min deposition time), and using this porcelanite with 6gm Na_2WO_4 showed the highest hardness (447 HV at 45 min). Also, using of rock additives with nano-TiO_2, and Na_2WO_4 could give more improvement in wear resistance of Al alloys [79].

In ***(2019) Mustafa Safa Yilmaz et al,*** studied investigation of high energy single pulse effect on micro arc oxidation (MAO) process on aluminum. Since the aim of the present study was to investigate effect of pulse durations on MAO processing, other processing parameters such as duty cycle (8%), electrolyte temperature (25±5 °C), electrolyte composition (KOH, $Na_2SiO_3.5H_2O$), process time (20 minutes), anodic pulse voltage, cathodic pulse voltage and chemical composition of substrate were all kept constant. Coating layers with thickness between 50-90 μm and surface roughness between 3.1-5.2 μm were obtained. The hardness of coating layers was between 800-2000 Vickers. Coatings consist of two sub-layers, inner dense layer and outer porous layer, which were a mixture of γ-Al_2O_3 and α- Al_2O_3 [80].

In ***(2020) Xiao-Jing Li et al,*** studied microstructure and wear resistance of micro-arc oxidation ceramic coatings prepared on $2A_{50}$ aluminum alloys. The phase structure, microstructure, micro-hardness and wear resistance were determined by XRD, SEM, HVS-1000 Vickers micro-hardness tester and tribology tester. The results show that the phase of the obtained coatings is mainly composed of γ-Al_2O_3. The coating consists of the inner

dense layer and the outer loose layer. As the cathodic voltage increases, the quantity and size of the micro-pores in the coatings first decrease and then increase. Micro-arc oxidation can greatly strengthen 2A50 aluminum alloy, the micro-hardness increases from 75 HV0.5 to 1321 HV0.5 after a micro-arc oxidation under a cathodic voltage of −100 V. The friction coefficient of the ceramic coatings are in the range of 0.35–0.55, and the coating obtained under −100 V exhibits the best wear resistance [81].

In ***(2020) Xiaojuan Dong et al,*** studied fabrication of self-cleaning superhydrophobic surfaces with improved corrosion resistance on 6061 aluminum alloys. The results show that binary rough structures and an FAS film with a low surface energy on the Al alloy surfaces confer good superhydrophobicity with a water contact angle of 167.5 ± 1.1° and a sliding angle of 2.5 ± 0.7°. Meanwhile, the potentiodynamic polarization curve shows that the corrosion potential has a positively shifted trend, and the corrosion current density decreases by three orders of magnitude compared with that of the original aluminum alloy sample. In addition, the chemical stability of the as-prepared superhydrophobic surface was evaluated by dripping test using solutions with different pH values for different immersion time [82].

In ***(2022) Qiufeng Mo et al,*** studied hydrophobic composite layers for enhancing long-term corrosion resistance of Al alloy micro-arc oxidation coating. The MPTMS/IPDI layer reduced the surface defects and surface roughness and improved the corrosion resistance of the MAO coating. After introducing SiO_2 particles and TMS into the MPTMS/IPDI layer, the surface roughness of the coating further decreased from 1.725 μm to 1.1117 μm. The contact angle of the MAO-SiO_2-TMS coating reached the superhydrophobic level (150.6°), which was higher than that of the MAO-MPTMS/IPDI (85.3°) [83].

In ***(2022) Chenxu Liu et al,*** studied tribological behavior of cathode plasma electrolytic deposited $Al_2Y_4O_9$ coating on aluminum alloy. The coating, prepared in a Y $(NO_3)_3$ aqueous solution on the surface of the Al alloy, consists of $Al_2Y_4O_9$ as the major phase component, Y_2O_3 as a minor phase component, and amorphous Al_2O_3 in the grain boundaries. As the applied voltage and deposition time increased, the crystallization of the coatings was enhanced. When deposited at 130 V for 10 min, the contact angle of the ceramic coating reached 141.0 ± 2.6°, indicating an enhanced self-cleaning effect. The ceramic coating also exhibited excellent self-lubricating and anti-wear effects. The friction coefficient of the CPED-treated sample vs. ZrO_2 ball or bearing steel ball decreased from 0.55–0.65 to 0.26–0.31 when the load was 3 N and the reciprocating velocity was 10 mm/s [84].

In ***(2023) Pengxiang Lv et al,*** studied processing and analysis of micro-arc oxidation coating on 319S aluminum alloy. The results showed that in the sodium silicate solution system, with an increase in pulse width, the thickness of the coating gradually increased and the surface hardness initially increased and then decreased. With an increase in the KOH concentration, the coating thickness increased and the roughness initially decreased and then increased. When the pulse width was 3000 ms, the negative voltage was 130 V, and the KOH concentration was 1 g/L, the coating exhibited the best density, with the highest surface hardness of 1426.8 HV and the thickest dense layer of 55 μm. The reduction in surface cracks and improvement in density indicated an enhancement in the hardness and wear resistance of the coating [85].

2-8-1: Summary of Literature Survey

Table (2-1) summary of literature survey for deposition of alumina coatings by (MAO) process on Al alloy.

Researchers	Ref	Summery
Mohit Vishnoi et al.(2017)	77	Produced ceramic coatings on Al alloys by MAO the coatings are found to offer excellent corrosion resistance combined with hydrophobic property. The coating evaluated in electrolyte having chemically treated with myristic acid.
Noor Fadhil et al.(2018)	78	Formation of ceramic oxide coatings by the micro-arc oxidation (MAO) on 2024 aluminum alloy with rice husks ash containing electrolyte solution. The XRD, EDS, SEM, micro-hardness, thickness, roughness and wear tests were used to evaluate the microstructure, morphology of deposited phases and coating properties.
Farqad Saleem et al.(2018)	79	The results showed the possibility to deposit wear resistant γ- Al_2O_3 coatings with different modification elements (Si, W, and Ca). Also, using of rock additives with nano-TiO_2, and Na_2WO_4 could give more improvement in wear resistance of

		Al alloys.
Mustafa Safa Yilmaz et al.(2019)	80	Coating layers with thickness between 50-90 μm and surface roughness between 3.1-5.2 μm were obtained. The hardness of coating layers was between 800-2000 Vickers. Coatings consist of two sub-layers, inner dense layer and outer porous layer, which were a mixture of γ-Al_2O_3 and α- Al_2O_3.
Xiao-Jing Li et al.(2020)	81	The results show that the phase of the obtained coatings is mainly composed of γ-Al_2O_3. The coating consists of the inner dense layer and the outer loose layer. As the cathodic voltage increases, the micro-hardness increases from 75 HV0.5 to 1321 HV0.5 after a micro-arc oxidation under a cathodic voltage of −100 V. The friction coefficient of the ceramic coatings are in the range of 0.35–0.55, and the coating obtained under −100 V exhibits the best wear resistance.
Xiaojuan Dong et al.(2020)	82	The results show that binary rough structures and an FAS film with a low surface energy on the Al alloy surfaces confer good superhydrophobicity with a water contact angle of 167.5 ± 1.1° and a sliding angle of 2.5 ± 0.7°. Meanwhile,

		the potentiodynamic polarization curve shows that the corrosion potential has a positively shifted trend, and the corrosion current density decreases by three orders of magnitude compared with that of the original aluminum alloy sample
Qiufeng Mo et al.(2022)	83	The surface roughness of the coating further decreased from 1.725 μm to 1.1117 μm. The contact angle of the MAO-SiO_2-TMS coating reached the superhydrophobic level (150.6°), which was higher than that of the MAO-MPTMS/IPDI (85.3°).
Chenxu Liu et al.(2022)	84	As the applied voltage and deposition time increased, the crystallization of the coatings was enhanced. When deposited at 130 V for 10 min, the contact angle of the ceramic coating reached 141.0 ± 2.6°, indicating an enhanced self-cleaning effect. The ceramic coating also exhibited excellent self-lubricating and anti-wear effects. The friction coefficient of the CPED-treated sample vs. ZrO_2 ball or bearing steel ball decreased from 0.55–0.65 to 0.26–0.31 when the load was 3 N and the reciprocating velocity was 10 mm/s.

Pengxiang Lv et al.(2023)	85	When the pulse width was 3000 ms, the negative voltage was 130 V, and the KOH concentration was 1 g/L, the coating exhibited the best density, with the highest surface hardness of 1426.8 HV and the thickest dense layer of 55 μm. The reduction in surface cracks and improvement in density indicated an enhancement in the hardness and wear resistance of the coating.

2-9: Overview of Summary Literature Survey

It seems that until the current date, there is no research available regarding the use of rocks such as bauxite, thassos and calcite additives in the electrolyte of micro arc oxidation (MAO) processes to achieve characterization of hardness and self-cleaning of alumina deposited on aluminum alloys. However, researchers in the field of aluminum alloy surface treatments have not on utilizing thassos rock additives to enhance the different properties of aluminum alloys. While don't have specific information on recent developments in using thassos rock, the research is providing a study that enhances characteristics such as hardness, wear resistance and self-cleaning properties. While there has been extensive research on MAO coatings the use of specific rock additives such as bauxite, thassos and calcite to achieve the desired hardness and self-cleaning characteristics on aluminum alloys did not appear to be explored or documented.

Chapter Three

Experimental Work

3-1: Introduction

This section concentrates on providing a thorough explanation of the material and research methods required to accomplish the objectives of the current investigation. Figures (3-1) and (3-2) depicts the experimental approach used in this work.

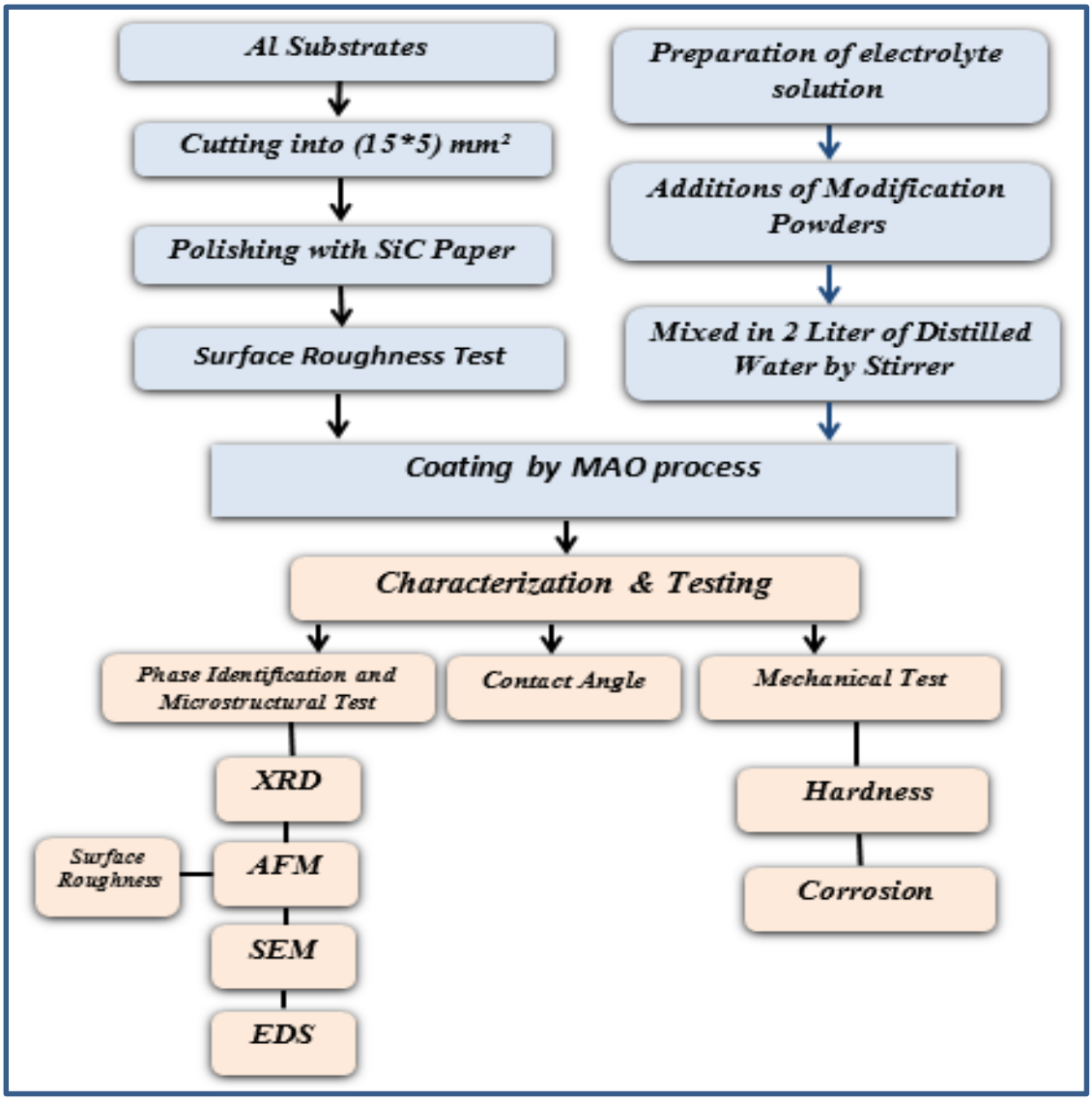

Figure (3-1): Flowchart of experimental works.

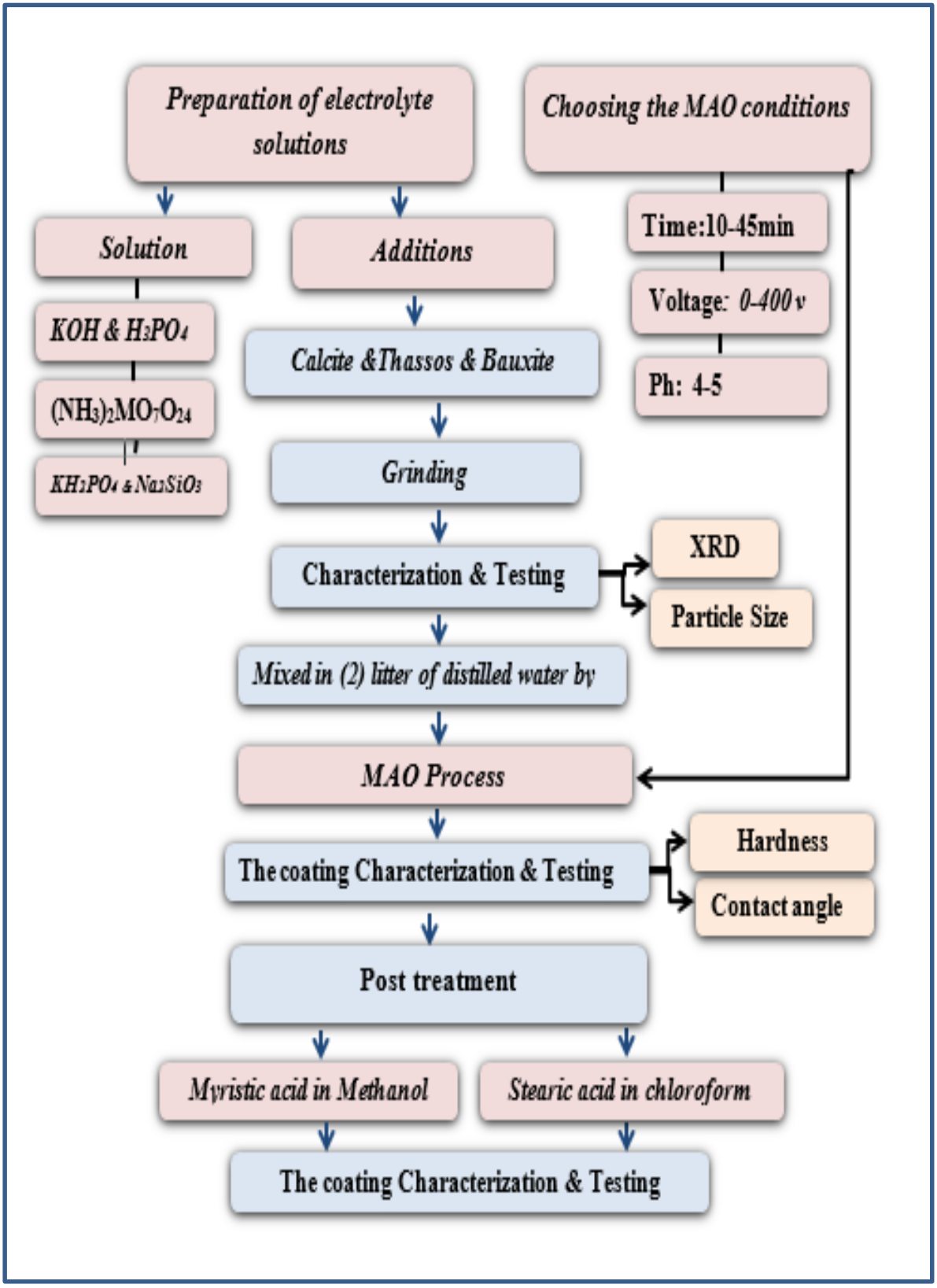

Figure (3-2): The steps involved in the MAO process.

3-2: Preparation of Powders

3-2-1: Preparation of Thassos Powder

In this work, thassos powder was prepared from rocks, according to the following steps:

- Collection appropriate amounts of thassos rocks from (Grand Mosque of Kufa).
- The rocks were washed with distilled water to remove soluble salts.
- Manually breaking up large chunks with a grinding. The powder was sorted using a sieve with a 200-mesh (75μm) pore size.
- At the laboratories of Materials Engineering College of Babylon University, the created powder was next crushed and ground into a fine powder using a planetary ball mill (High-speed tumbling ball mill SFM-1 (QM-3SP2)). Aluminum balls and bowls were included with the ball mill. Moreover, the milling took place at 350 rpm for 10 hours.
- By using of XRD, PAS and chemical composition test, powders were evaluated after milling.

3-2-1-1: Chemical Composition of Thassos

Table (3-1) shows the chemical composition of thassos. It can be observed that the greater ratios were recorded by CaO and MgO, while Fe_2O_3 and Al_2O_3 were recorded the less ratio.

Table (3-1): Chemical composition of thassos powder.

Thassos	SiO_2	Al_2O_3	Fe_2O_3	CaO	MgO	L.O.I
(Wt. %)	1.46	0.13	0.07	32.08	19.50	46.58

3-2-2: Preparation of Bauxite Powder

The process of preparing bauxite powder involved several steps:

- Iraqi bauxite rocks were obtained from Iraq Geological Survey. These rocks were manually broken down into smaller pieces using a grinding resulting in a semi-finished powder .
- The semi-finished powder obtained from kibbling was subjected to washing to remove any impurities or contaminants. After washing the powder was dried to achieve a moisture-free state .
- The dried powder was further process in the ceramic lab of the College of Material Engineering of the University of Babylon, it was ground in a ball mill for 8 hours at a rotation speed of 350 revolutions per minute (rpm). This additional grinding step aimed to achieve a finer particle size and improved homogeneity
- Following the grinding process, the powder was sieved to obtain a small granular size. Sieving helps to ensure a uniform particle size distribution .
- Powders were examined by XRD and PZA after milling.

3-2-3: Preparation of Calcite Powder

This work was done according to the following steps:

- Preparation suitable amounts of calcium carbonate rocks (99%) from lime factory (Karbala, Iraq).
- Manual kibbling using mortar to get the quasi-finished powder.
- Milling for 5 hours to get fine powder.
- After the milling, powders were tested by PZA, and XRD.

3-3: Substrates Preparation

The substrates were prepared from shaft of 1105-GOST4784 Al alloy had specific hardness values of 146.7 HV. Table (3-2) shows the chemical composition of Al substrates done at (The Central Agency for Standardization and Quality Control). The substrates were cut into dimensions of (Ø 15×5 mm^2) by machining. The surfaces of the prepared substrates were polished to achieve a smooth and uniform finish. Silicon carbide (SiC) abrasive papers with various grit sizes (280, 400, 600, 800, 1000, 1200 and 2000) were used for the polishing process, to obtain roughness Ra of about 0.282 µm.

After polishing, the substrates were degreased with acetone to remove any contaminants or residual oils from the surface. Subsequently, the substrates were cleaned with distilled water for 10 seconds to ensure a clean surface. Then they were drilled for clamping during the MAO process as indicated in figure (3-3).

Table (3-2): Chemical Composition of 1105-GOST4784 Al alloy

Element	Content (Wt. %)	Element	Content (Wt. %)
Si	0.266	Ni	0.0021
Fe	0.386	Zn	0.0423
Cu	3.530	Ti	0.0129
Mn	0.890	Pb	0.0072
Mg	0.463	V	0.0054
Cr	0.0634	Al	94.3

Figure (3-3): Substrates for MAO process.

3-4: Preparation of MAO Process

A special homemade (an indigenously designed) MAO process equipment figures (3-4) to (3-6) was used for the deposition of Al_2O_3 coatings. It has 0-500 V AC/DC power supply with maximum output current of (7) A. The Al substrate acts as (anode) in the MAO equipment and stainless steel 316L plate was used as the electrode (cathode). The anode and cathode play essential roles in the electrochemical reaction that occurs during the MAO process, leading to the formation of ceramic coatings on the Al substrate. The electrolytic solution was contained in a (2) liter container. Both electrodes were submerged vertically in the electrolyte solution. The distance between the electrodes were (3) cm, this distance is controlling the MAO process and ensuring effective current flow between the electrodes [79]. Electrolyte solution was stirred using a mechanical stirrer employed to keep the electrolyte homogeneous.

Ice containing salt was utilized in the cooling process to keep the electrolyte temperature to 5C°. It put to a large plastic container containing an electrolyte solution container. The temperature was measured using a thermometer. After the MAO treatment, the samples were rinsed in distilled water, and dried using hot air. The electrolytes were stirred using magnetic stirrer for (7) hours. Also, the pH of the electrolytes were measured by a pH meter. Before the MAO process. The electrolyte was cooled to keep constant temperature (15-30) C°.

Figure (3- 4):Components of MAO power supply ; (1) current gauge ;(2) over load; (3) voltage gauge;(4) on-off switch; (5) DC-AC current ;(6) voltage control.

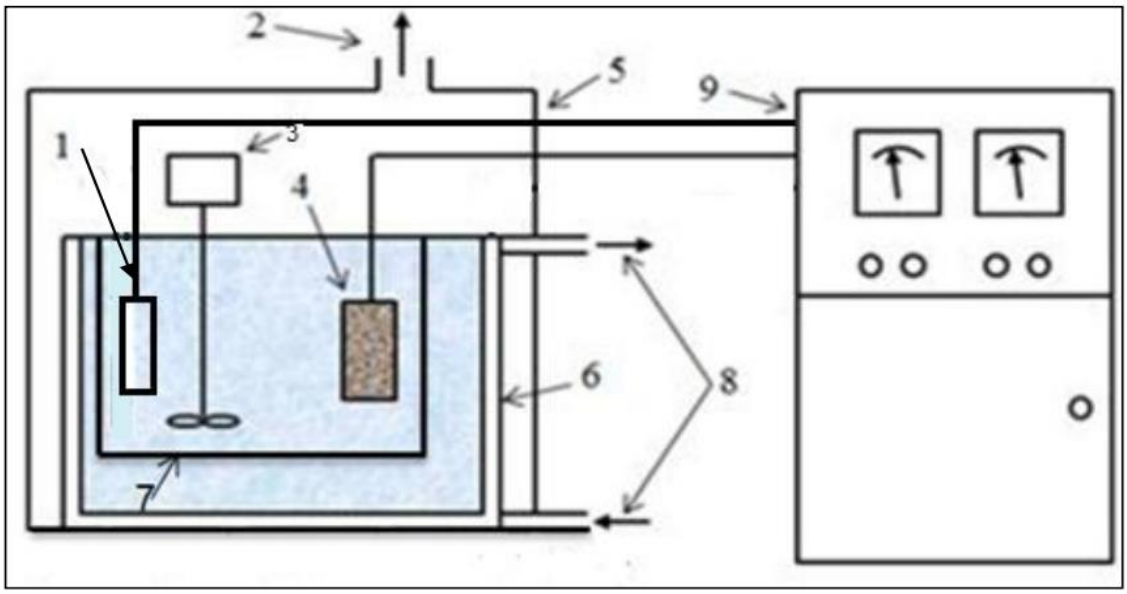

Figure (3-5): Equipment for MAO coating includes (1) a cathode, (2) a ventilation unit, (3) a stirrer, (4) an anode, and an (5) exterior plastic tank. (6) A cooling system, (7) an electrolyte container, and (8) a container for a cooling bath (9) A power source [86].

Figure (3-6): Images of the coating unit; (1) mixer, (2) coating container, (3) cooling container, (4) electrodes, (5) thermometer.

3-5: Preparation of MAO Electrolytic Solutions

3-5-1: Materials and Chemicals

Table (3-3) shows the chemicals the rock additives used in the MAO electrolytic solutions for surface modification of 1105-GOST4784 Al alloy for self-cleaning application.

Table (3-3): Components functions in MAO electrolyte.

No	Material name	Chemical formula	Source	Functions
1.	**Potassium di-hydrogen phosphate**	KH_2PO_4	India	Property modification
2.	**Phosphoric acid**	H_3PO_4	India	PH alteration
3.	**Sodium silicate**	Na_2SiO_3	India	Assistant additive
4.	**Ammonium molybdate**	$(NH_3)_2MO_7O_{24}$	India	Performance modification
5.	**Potassium hydroxide**	KOH	U.S.A	Electrolyte conductivity increasing
6.	**Calcite**	Mineral	lime factory in (Karbala, Iraq)	Hardness modification
7.	**Bauxite**	Mineral	Iraq	Hardness modification
8.	**Thassos**	Mineral	Iraq	Hardness modification
9.	**Myristic acid**	$CH_3(CH_2)_{12}COOH$	U.S.A	Contact angle modification
10.	**Stearic acid**	$C_{18}H_{36}O_2$	U.S.A	Contact angle modification
11.	**Chloroform**	$CHCL_3$	India	Contact angle modification
12.	**Methanol**	CH_3OH	India	Contact angle modification

13.	**Molybdenum disulfide**	MOS_2	India	Contact angle modification

3-5-2: Main Electrolytic Solutions and Selection

Depending on the functions mentioned, five (5) types of electrolytic solutions were choose and prepared for modification. These solutions and their selection were sequenced according to steps, shown in tables (3-4). Wherein, measurements of coatings hardness and contact angle were choose to be the main factors adopted in selection of MAO process conditions and type of electrolyte. Furthermore, for a certain electrolyte, the best ration of component addition and deposition time by means of hardness and contact angle were taken into consider selection of the subsequent electrolyte.

Table (3-4): The success main electrolytic solutions used in the MAO process.

Samples	**C**	**D1**	**MC**	**F**	**CF1**	**EF**	**(G3)1**	**G5**	**CFG 1**	**EFG**
KH2PO4	20g/L	20g/L	20g/L	20g/L	20g/L	20g/L	20g/L	20g/L	20g/L	20g/L
KOH	2g/L	2g/L	2g/L	2g/L	2g/L	2g/L	2g/L	2g/L	2g/L	2g/L
Na_2SiO3	---	10g/L	---	---	---	---	---	---	---	---
(NH3)2MO7O24	12g/L	12g/L	12g/L	12g/L	12g/L	12g/L	12g/L	12g/L	12g/L	12g/L
H3PO4	8ml	8ml	8ml	8ml	8ml	8ml	8ml	8ml	8ml	8ml
CaCO3	10g/L	15g/L	10g/L	---	20g/L	10g/L	---	---	20g/L	10g/L
Thassos	---	---	---	1-7g/L	3g/L	7g/L	---	---	3g/L	7g/L
Bauxite	---	---	---	---	---	---	3g/L	5g/L	3g/L	5g/L
MOS_2	---	---	1g/L	---	---	---	---	---	---	---
Time (min)	15	15	15	15	15	15	15	15	15	15
	45	---	45	45	---	45	---	---	---	45
PH	4-5									
Voltage	320-330									
Current	0.1-0.3									
Temp(C°)	15-20	15-20	15-20	15-20	15-20	15-20	15-20	15-20	15-20	15-20

3-6: MAO Process Coating

The steps involved in completing this process are as follows:

♦ Begin to add the chosen electrolyte solution to the glass electrolyte container shown in figure (3-6). This container holds the electrolyte solution during the MAO process.

♦ Using a cooling unit (ice that included salt) Cooling the solution to the start temperature 5˚C.

♦ The MAO unit is used to deposit the ceramic coatings on the Al substrate. This unit applies a high voltage about (320-330)V. The voltage is controlled by raising village from 0 to 320V through 10 min fixed for all samples. In this step, the DC current-Voltage values in steady state arcs during MAO process were recorded.

Figure (3-7) displays various sparks of arcs seen throughout the MAO process, figure (3-8) shows different types of coated samples using different electrolytes.

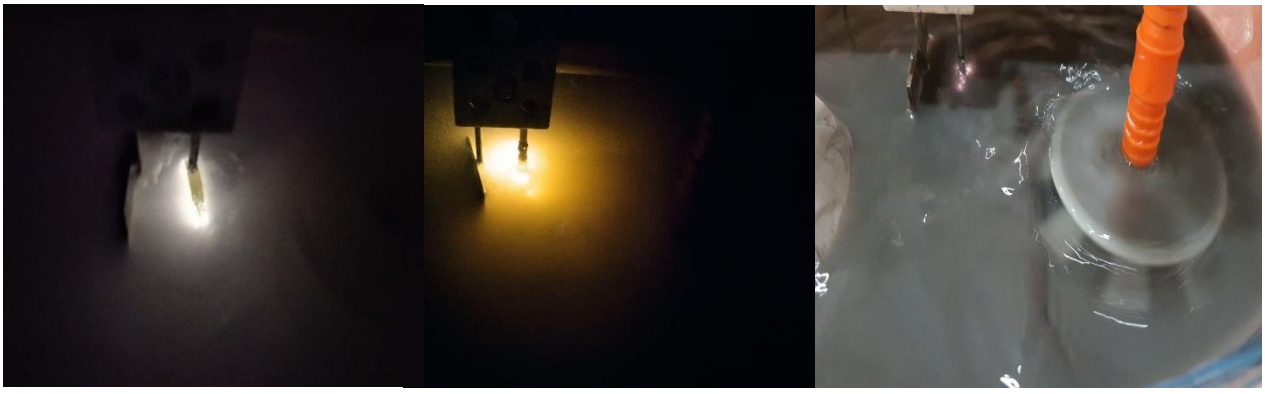

Figure (3-7): Micro sparks at different electrolytes (A, C4 and MC2).

Figure (3-8): Samples coated with (Calcite, Thassos, and Bauxite) different additions in electrolytes.

3-7: The post-treatment of MAO coatings

After ensuring the MAO-coated substrate is clean and free from contaminants

♦ Immerse the substrate for 15 min in a solution of myristic acid weighing (10g) is dissolved in 250 milliliters in methanol. Myristic acid has long hydrocarbon chains that contribute to hydrophobicity. The carboxylic acid (COOH) groups of myristic acid interact with the substrate's surface. After immersion, the substrate to dry by hot air dryer, which promotes the formation of a self-assembled monolayer (SAM) of myristic acid molecules on the surface.

- Immerse the substrate for many times in a solution of stearic acid weighing (5g), is dissolved in 100 milliliters chloroform. Allow the substrate to dry again, facilitating the formation of a SAM of stearic acid molecules on top of the existing myristic acid SAM. During immersion and drying, the fatty acid molecules undergo a self-assembly process.
- The densely packed monolayer of fatty acid molecules on the substrate creates a hydrophobic surface. Water droplets tend to bead up on this surface and roll off, carrying away dirt and contaminants. The hydrophobicity contributes to the self-cleaning effect, as water cannot easily wet the surface. By following these steps, the MAO-coated substrate is modified to become hydrophobic and self-cleaning, which is particularly advantageous in applications where maintaining clean and dry surfaces is essential. This treatment enhances the substrates performance and durability in various environments.

3-8: Instrumentation

In this section, various physical and mechanical test equipment is used to analyze and evaluate the properties of the materials or Substrate under study. Here are some common types of instrumentation that might be used in such investigations:

3-8-1: Chemical Composition Test

It are essential for determining the elemental makeup of substrate and materials. The substrate and thassos powder were determined with chemical composition tests at the Central Agency for Standardization and Quality Control, Engineering Rehabilitation and the Iraqi geological survey/central laboratories department, respectively.

3-8-2: X-Ray Diffraction (XRD)

An effective technique for identifying the structure and properties of crystalline materials. Structural characteristics of the powder (thassos, bauxite, calcite) also substrate 1105-GOST4784 Al alloy, Cukα radiation (λ = 1.5405 Å) was used at a scanning speed of about 5º/min from (10◦ to 50◦) of 2Ɵ (Bragg angle) and the power that applied is (40 kv/30 mA). And the test was performed at Babylon University / College of Material Engineering at the ceramic and building materials department. The X-ray diffract meter device (XRD 6000, Shimadzo, Japan) was used in this work. As well as, coating samples and describing their phase composition in XRD, which scanned in diffraction angle (2θ) from 10°, 20° to 90°. The test was performed at Alkhora Company in Baghdad.

3-8-3: Laser Particle Size Analysis (PSA)

(PSA) is a powerful and widely used technique for determining the size distribution of particles in a sample. In this work particle size analyzer, the Ceramic and Building Materials Department at Babylon Universitys College of Materials Engineering used type Better Size 2000 Laser. The tool provides info on particle size and distribution, and the theory it is based on is stated (Mie theory). The light travels through it with a space filter and the use of a ripping ray telescope to screen the illuminator and create a parallel, more expansive monochromic illuminator ray. The illuminator ray next irradiates the molecules in the measuring region, allowing the illuminator diffractive behavior to develop, shown in figure (3-9).

Figure (3-9): Particle size analyzer device.

3-8-4: Hardness Test

At Babylon University / College of Material Engineering at the Ceramic and building materials department, uncoated sample and coatings hardness was tested using a Laryee HVS-1000 digital Micro-hardness tester figure (3-10) with a force of 4.9N and a holding duration of 15 seconds. The average of three measurements was used to calculate the HV value.

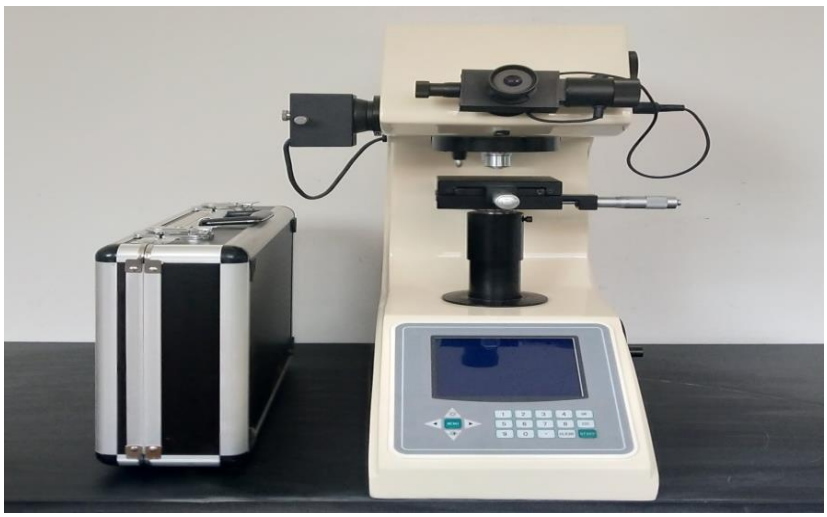

Figure (3-10): Hardness instrument

3-8-5: Contact Angle Test Instrument

The contact angle test instrument used in this study is an optical system designed to measure contact angles on surfaces. It instrument is manufactured by Holmarc Opto-Mechatronics Pvt. Ltd., in India. It equipped with an automatic unit and specialized software for contact angle measurement. This suggests that the instrument is capable of performing measurements with a high degree of precision and automation. This test was done at Babylon University's /College of Materials Engineering at Ceramic and Building Materials Department .The contact angle measurement process involved placing the surface to be tested on a base of the device. A syringe pump was used to deliver water droplets onto the surface. The instrument then recorded the angle at which the water droplet made contact with the surface. Data was displayed on a PC screen, likely through specialized software. Figure (3-11) shows a photograph for contact angle measurement and clarification image of the droplet.

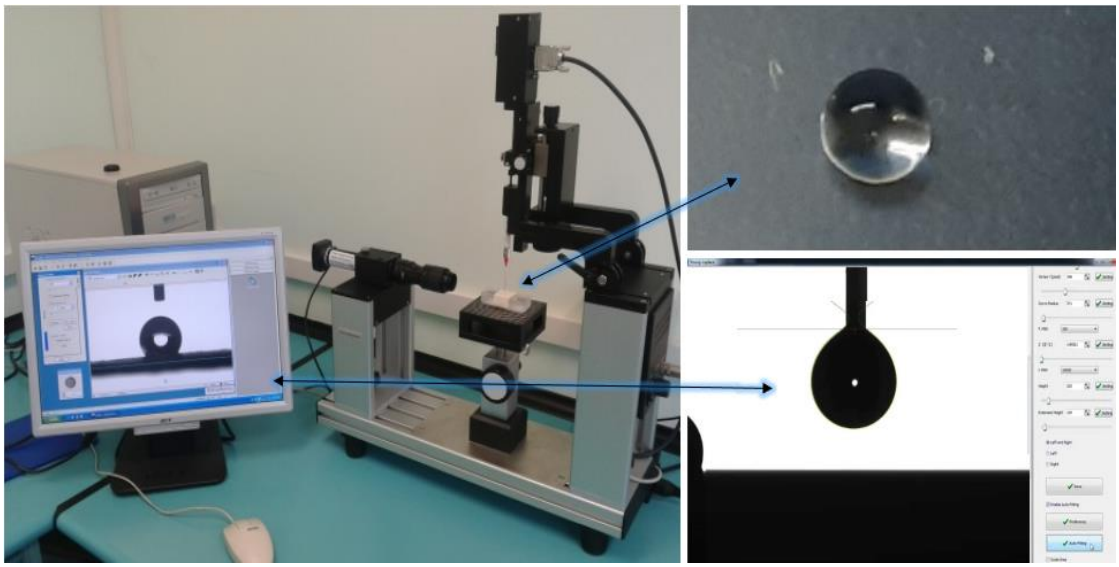

Figure (3-11): Contact angle measurement device

3-8-6: SEM Analysis

SEM was used to examine the outer morphology and structural integrity of coated samples, the experiment was carried out at Alkhora Company in Baghdad. The SEM instrument utilized is shown in figure (3-12).

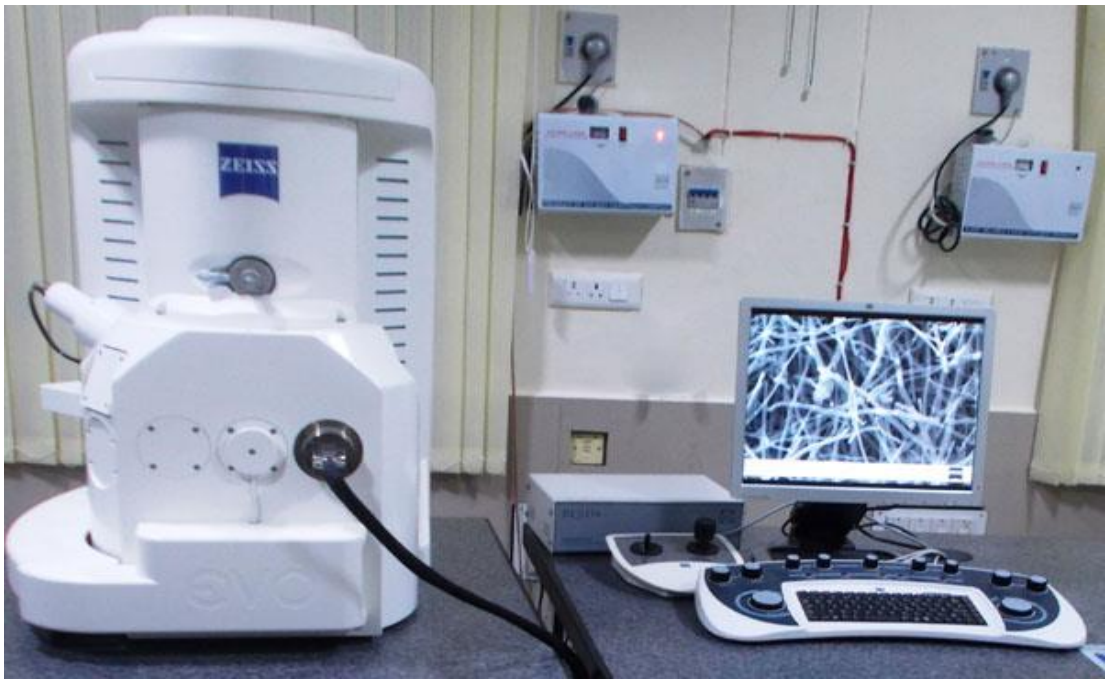

Figure (3-12): SEM microscope instrument.

3-8-7: EDS Analysis

At Alkhora Company in Baghdad, the chemical compositions of the coated sample were examined using energy dispersive spectroscopy using a Bruker Corporation X Flash 6l10-Model.

3-8-8: AFM Test

AFM has demonstrated remarkable precision just on the range of nanometer fractions to view particle size, the coatings thickness and surface roughness. The findings of tests was carried out at CAC chemistry analysis center and shown in figure (3-13).

Figure (3-13): The atomic force microscopy analyzer.

3-8-9: Corrosion Test

As an electrolyte potentiodynamic and cyclic polarization test, electrochemical tests were conducted in three electrode cells containing 3.5 g/L $NaCl_2$ solution. As indicated in figure (3.14), the counter electrode was Pt, the reference electrode was SCE, and the working electrode was a specimen. The corrosion cell consists of three electrodes:

1. The working electrode (Al alloy sample).

2. The counter electrode (platinum rod).

3. The saturated calomel electrode (SCE).

The corrosion rate (CR) was calculated by Tafel plots by using anodic and cathodic branches.

Figure (3.14): Schematic diagram of potentiodynamic polarization cell.

Chapter Four

Results & Discussions

4-1: Introduction

This chapter explains all of the characterization and experimental results, including the powder tests conducted on the materials used in MAO coating processes. The powders were analyzed for their particle size distribution, morphology and composition. The contact angle measurements revealed that the coating samples exhibited varying degrees of hydrophobicity. In addition, changes in mechanical and physical properties were observed in the coated samples. The properties investigated include (hardness, surface roughness and corrosion strength). Also, provide visual evidence of the coated surfaces through SEM and AFM images.

4-2: PSA Results

Figures (4-1), (4-2) and (4-3) show the results from the particle size analysis for (calcite, thassos and bauxite) powders used in this study. The size of calcite powder distributed over a range of (4.303µm-37.27µm) with a mean value of (21.30µm). The particle size of thassos powder distributed over a range of (0.867µm-22.96µm) with a mean value of (4.543µm). Furthermore, the particle size of bauxite powder distributed over a range of (0.264µm-19.85µm) with a mean value of (4.146µm).

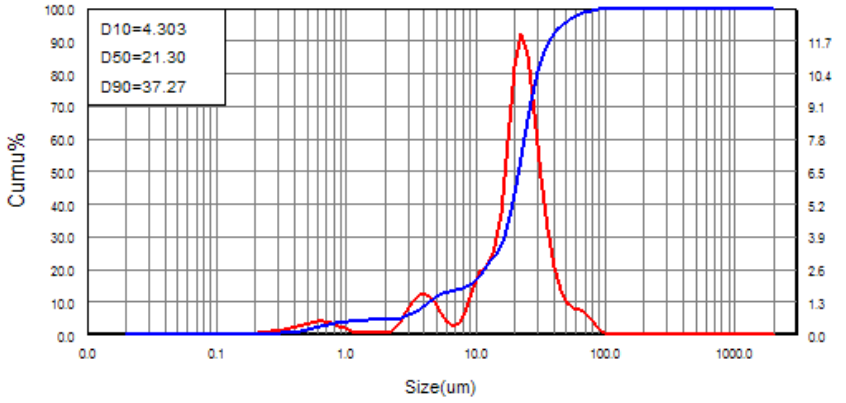

Diam um	Percent
0.200	0.01
0.500	1.41
1.000	3.95
2.000	4.42
5.000	11.74
10.000	16.53
20.000	44.12
45.000	94.24
75.000	99.17
100.000	100.00

Figure (4-1): PSA results of calcite powder.

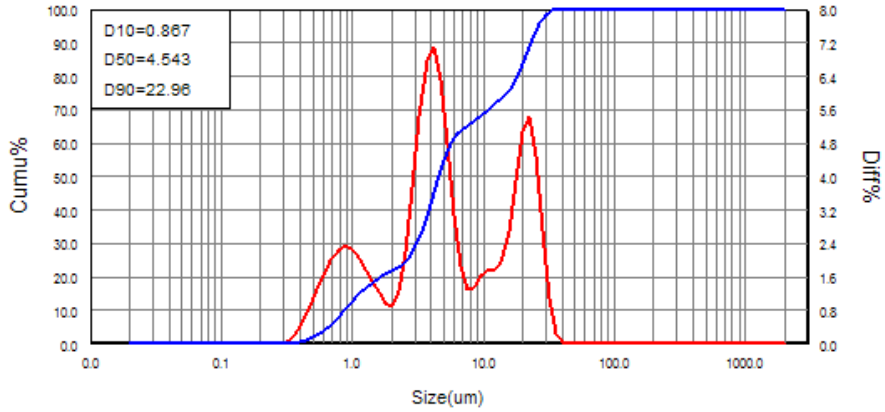

Diam um	Percent
0.100	0.00
0.200	0.00
0.500	1.71
1.000	12.72
2.000	21.54
5.000	55.03
10.000	68.54
20.000	83.85
45.000	100.00
75.000	100.00

Figure (4-2): PSA results of thassos powder.

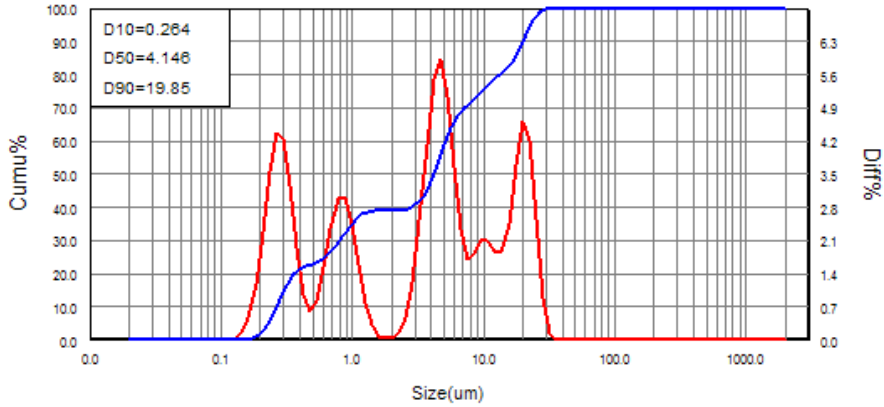

Diam um	Percent
0.100	0.00
0.200	2.22
0.500	22.93
1.000	35.22
2.000	38.99
5.000	59.04
10.000	75.19
20.000	90.27
45.000	100.00
75.000	100.00

Figure (4-3): PSA results of bauxite powder.

4-3: X-ray Diffraction Results

4-3-1: X-ray Results of powders

Figures (4-4),(4-5) and (4-6) show XRD patterns of (calcite, thassos and bauxite) powders respectively, that scanned in diffraction angle (2θ) from 10°,20° to 60°. The phases were identified by comparison with standard reference patterns from powder files (JCPDS cards). The patterns show the existence of $CaCO_3$ peaks confirmed the $CaCO_3$ existence according to the standard card number (JCPDS card No.01-072-1937). The XRD patterns of thassos powder revealed the Dolomite ($MgCO_3$), which agrees with (JCPDS card No.36-0426). The XRD patterns of bauxite powder revealed the bohemite AlO(OH) and gibbsite $Al(OH)_3$ which agrees with (JCPDS No.96-901-2275) and (JCPDS card No. 96-101-1082) respectively, this confirms the presence of bauxite, considering that these are the basic oxides that constituent the bauxite.

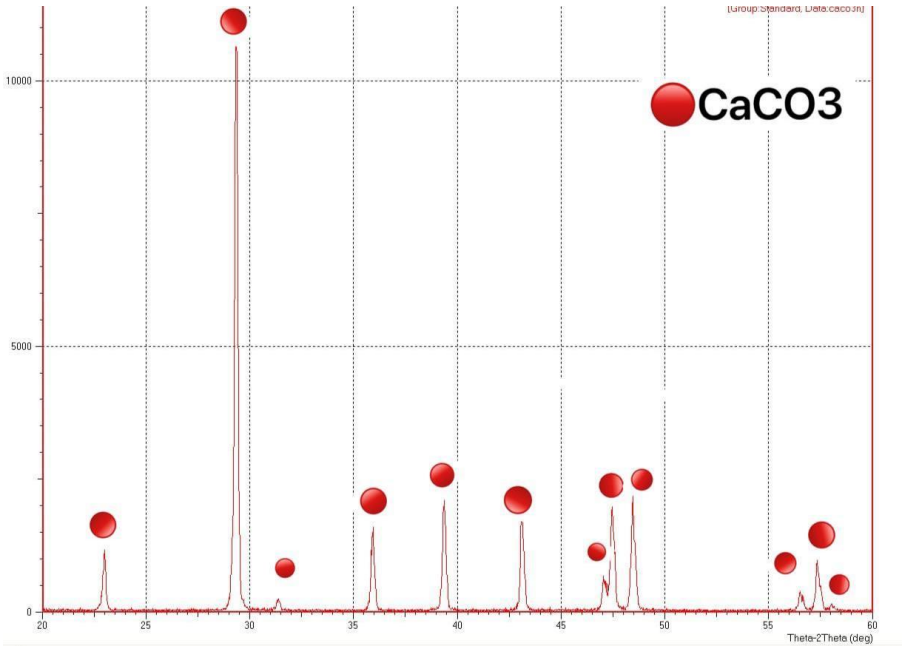

Figure (4-4): Results of XRD for calcite.

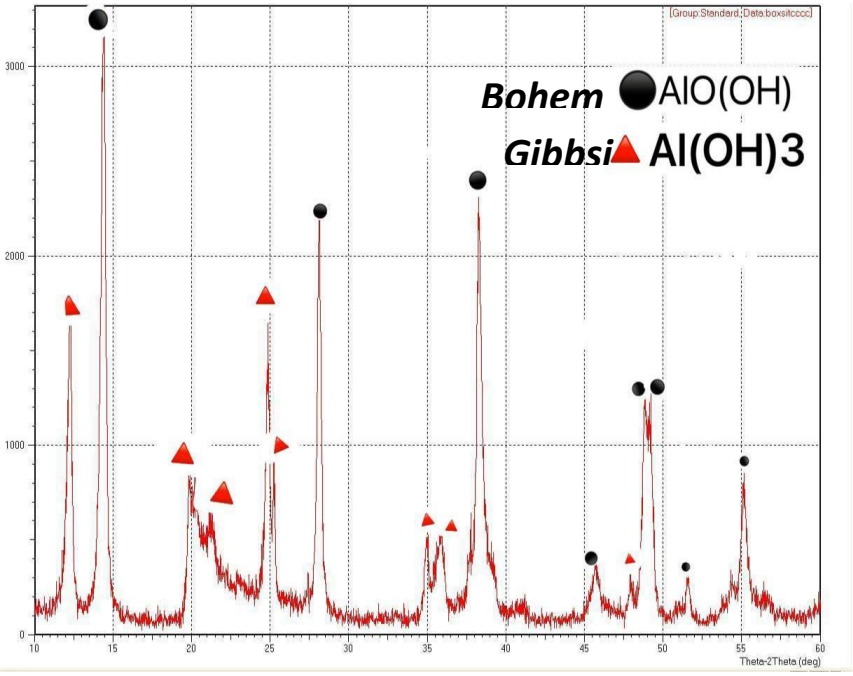

Figure (4-5): Results of XRD for bauxite.

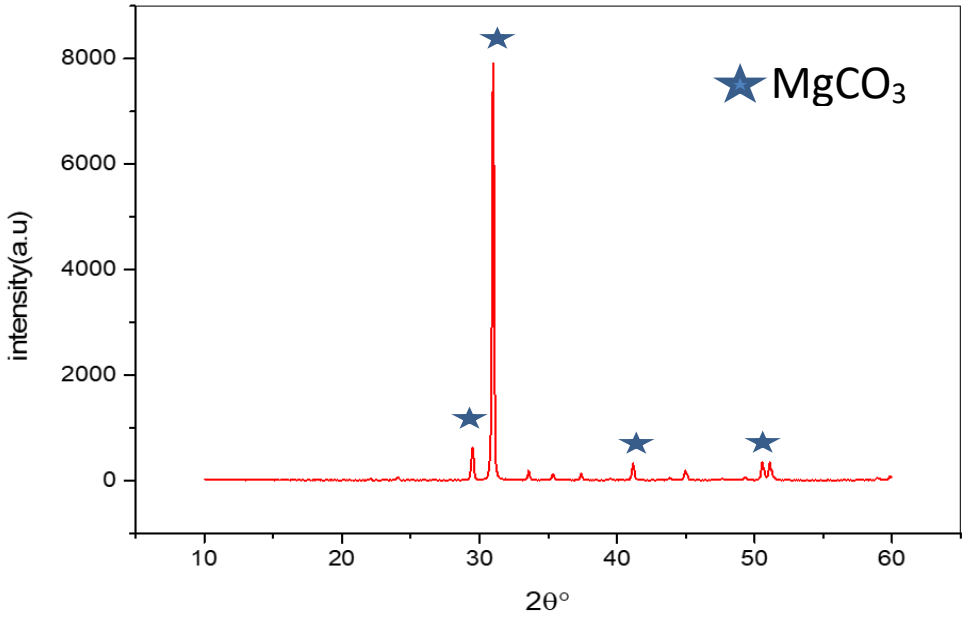

Figure (4-6): Results of XRD for thassos.

4-3-2: X-ray Results of coatings

The X-ray diffraction (XRD) results for different coatings scanned in diffraction angle (2θ) from 10° to 90° presented in figures (4-7) to (4-13) show that Al_2O_3 ceramic layers were successfully deposited onto the Al substrates. The phases were identified by comparison with standard reference patterns from files (JCPDS cards) [87-88]. Upon analyzing the XRD data, the detection of mean peaks shared across all samples can be attributed to various forms of Al and Al_2O_3 including table (4-1):

- Al peaks verified using (JCPDS card No. 00-002-1109).
- γ- Al_2O_3, confirmed with (JCPDS card No. 00-010-0425).
- Al_2O_3 (also known as Corundum), using (JCPDS card No. 01-075-0787).

The presence of γ-Al_2O_3 and α-Al_2O_3 phases in the coatings produced through the Micro-Arc Oxidation (MAO) process has a distinct impact on the hardness of the coatings. γ-Al_2O_3 is known for its relatively high surface area, which is due to its fine particle size and porous structure. It can exhibit good mechanical properties, including hardness, but it is often less hard compared to α-Al_2O_3. On the other hand, α-Al_2O_3 is typically harder and more wear-resistant than gamma alumina. It has a denser crystal structure and larger crystallite size, contributing to its higher hardness. During the MAO process, when a high-voltage electrical discharge or spark occurs between the substrate and the electrolyte solution, extremely high temperatures were generated momentarily at the spark impact point. These high temperatures can lead to the rapid dissociation and ionization of aluminum ions from the electrolyte solution [88]. As the aluminum ions were released at the point of the spark, they can react with oxygen and hydroxyl ions from the solution to form different alumina phases. High temperatures generated by the spark provide the necessary energy for the formation of various Al_2O_3 phases, which form at different temperatures due to the kinetics of phase formation varying. Moreover, the rapid cooling that follows the spark impacts the phase composition by trapping certain phases in the coating.

This cooling process can influence the final composition of the alumina phases present. The appearance of Al peaks is most likely due to two factors, the thickness of the film coated on the substrate and the penetration depth of the X-rays into the Al alloy substrate [87].

Table (4-1): Shows the XRD analysis results of samples coating.

No.	*Compound Name*	*Chemical Formula*	*Reference code*
1	Aluminum Oxide [Corundum]	α-Al_2O_3	01-075-0786 01-075-0787
2	Aluminum Oxide [gama]	γ -Al_2O_3	00-010-0425
3	Aluminum	Al	00-002-1109

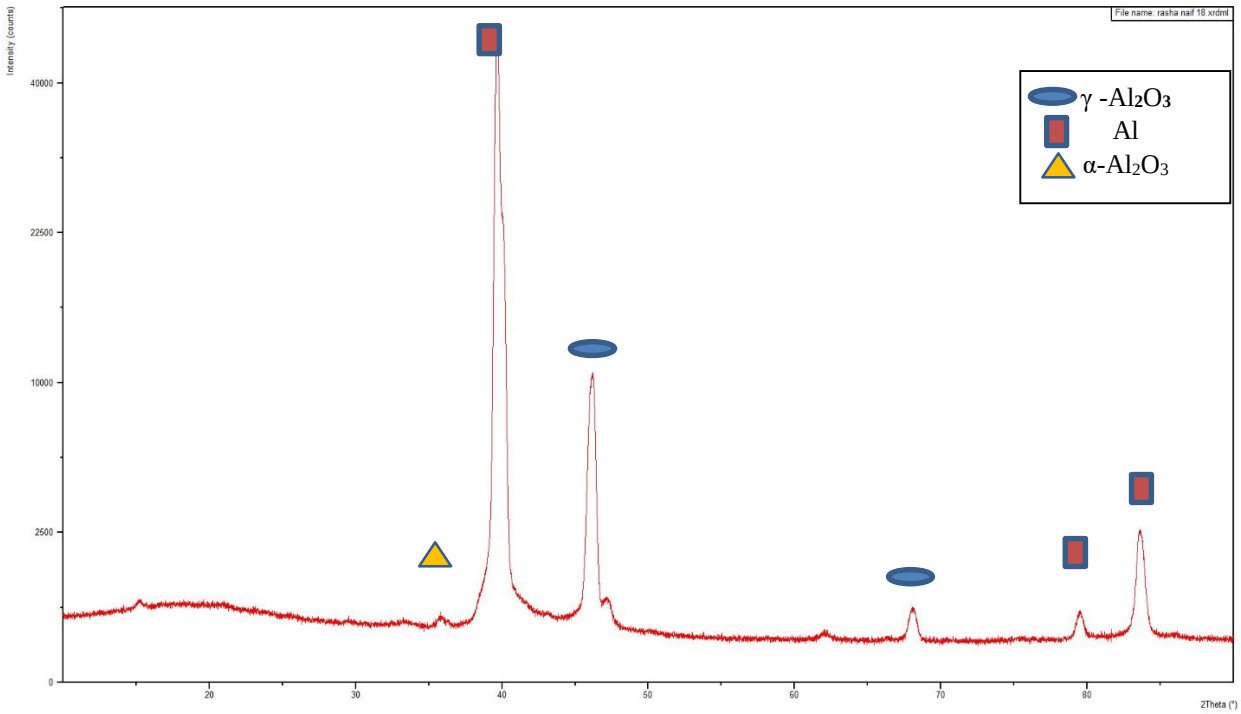

Figure (4-7): Results of XRD for sample D1 at 15 min.

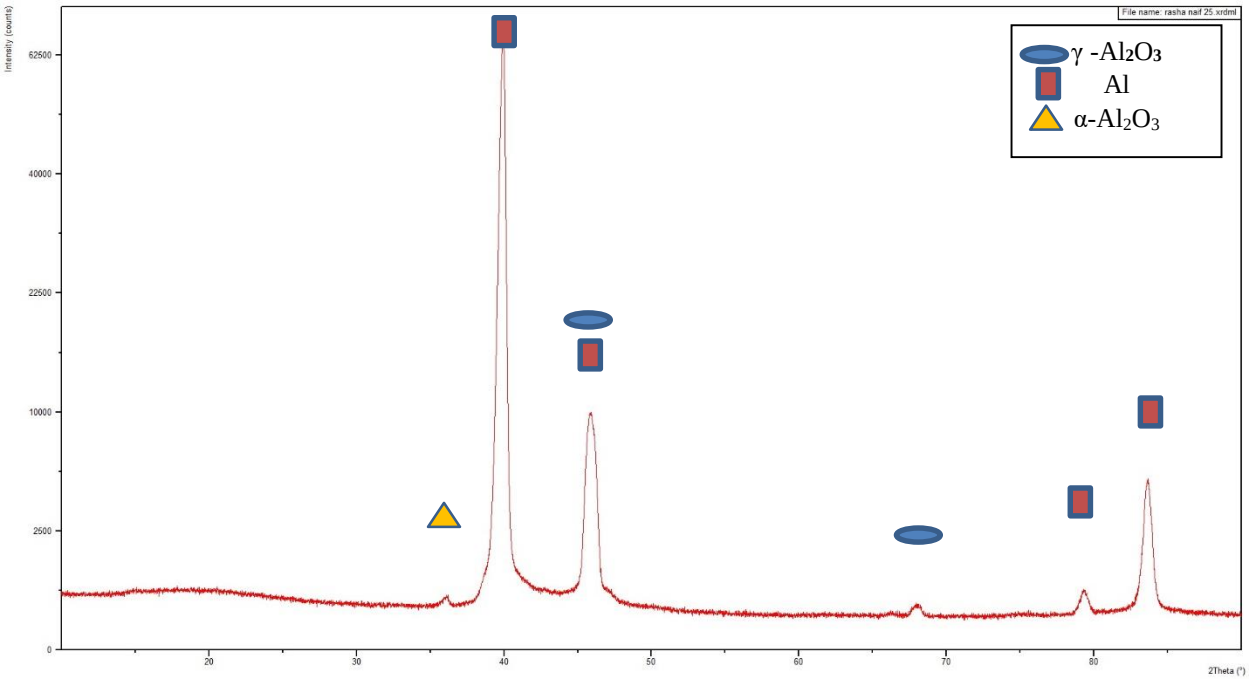

Figure (4-8): Results of XRD for sample MC2 at 45 min.

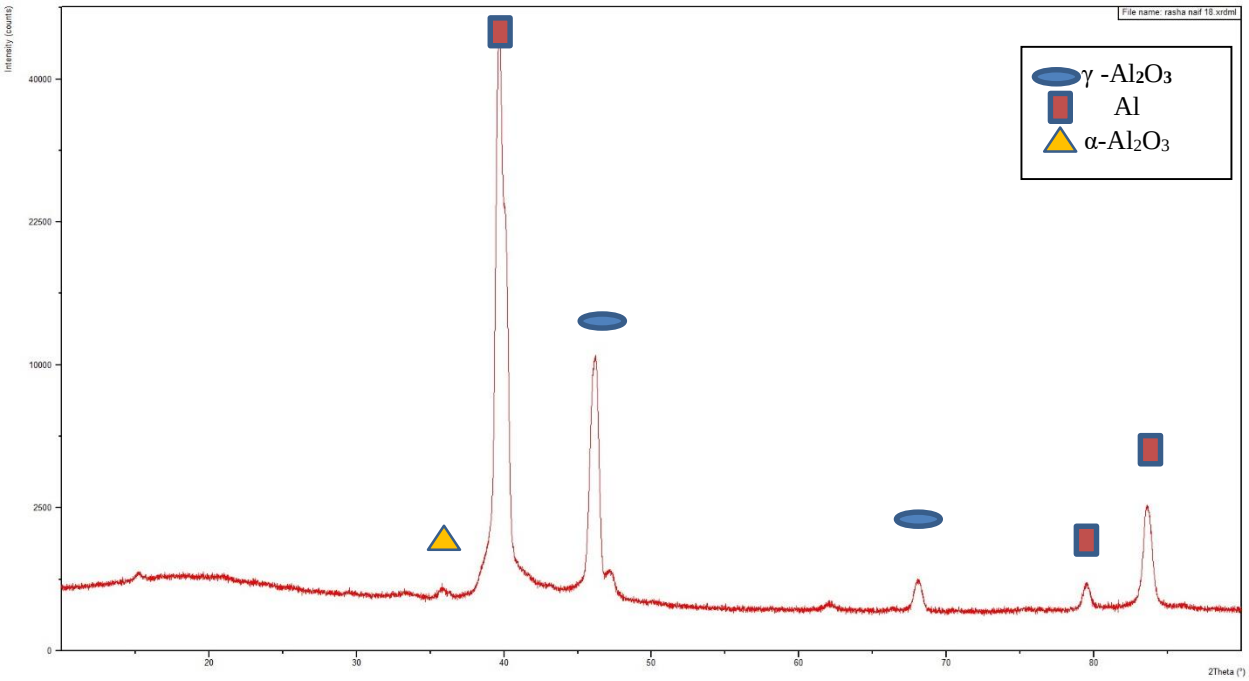

Figure (4-9): Results of XRD for F2 sample at 45min.

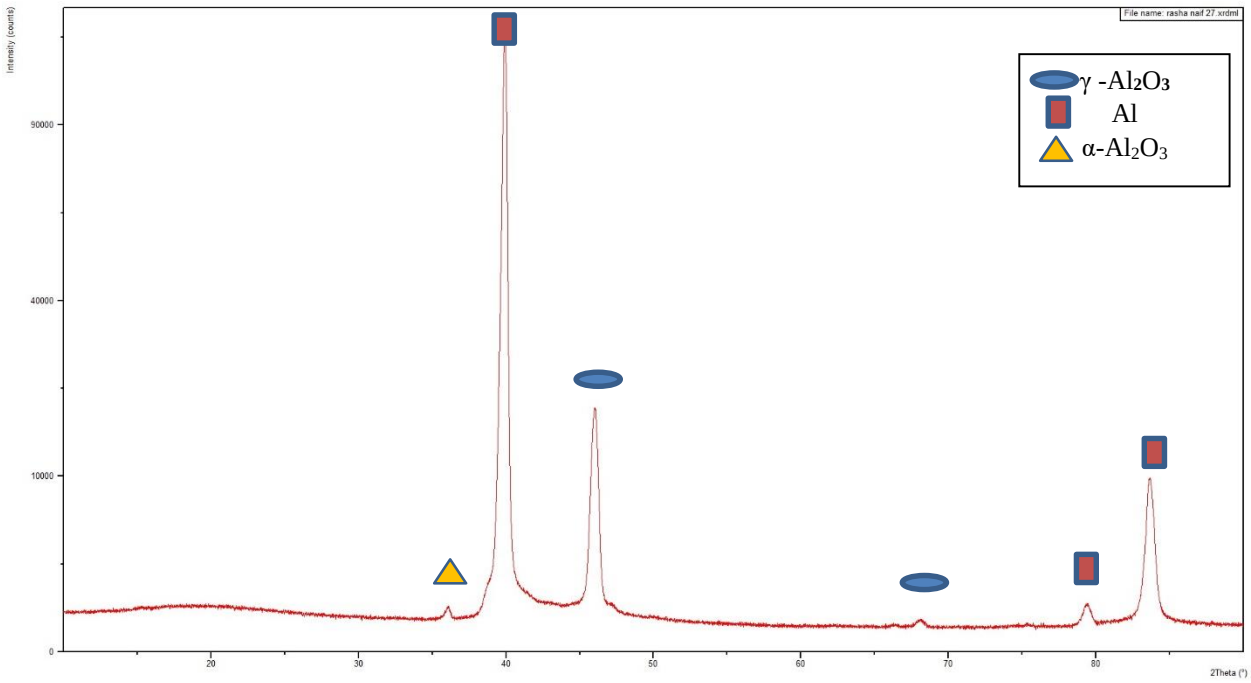

Figure (4-10): Results of XRD for CF1 sample at 15 min.

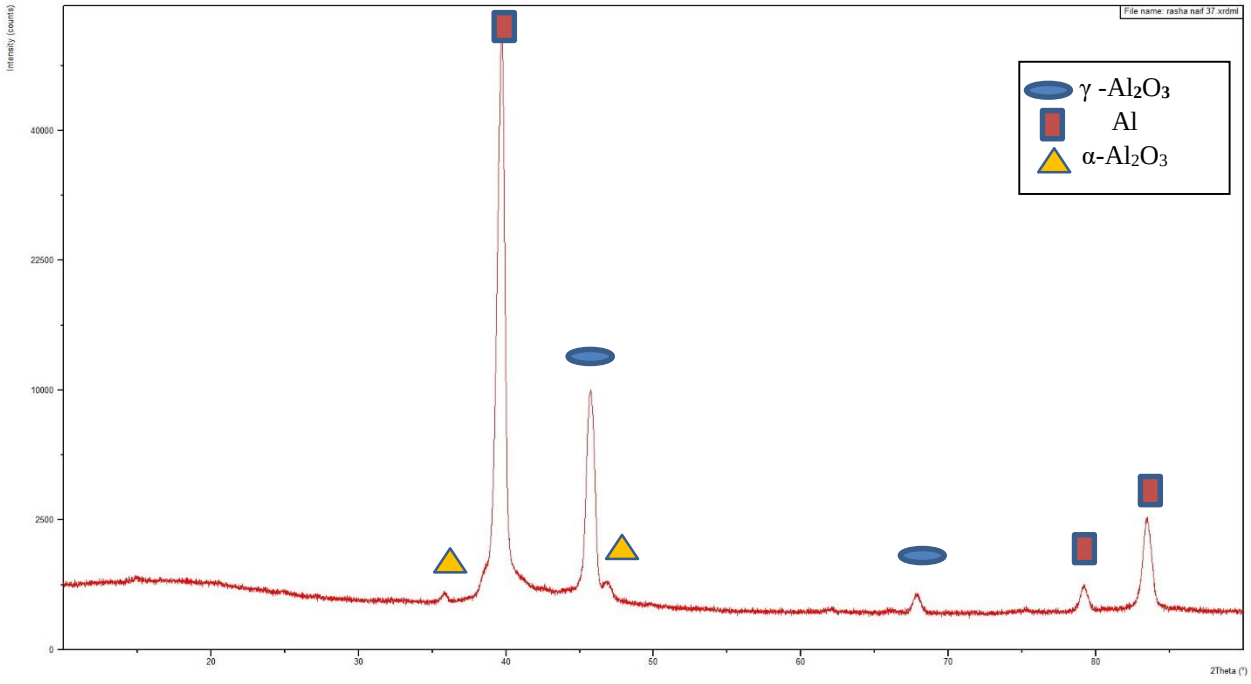

Figure (4-11): Results of XRD for G5 sample at 15 min.

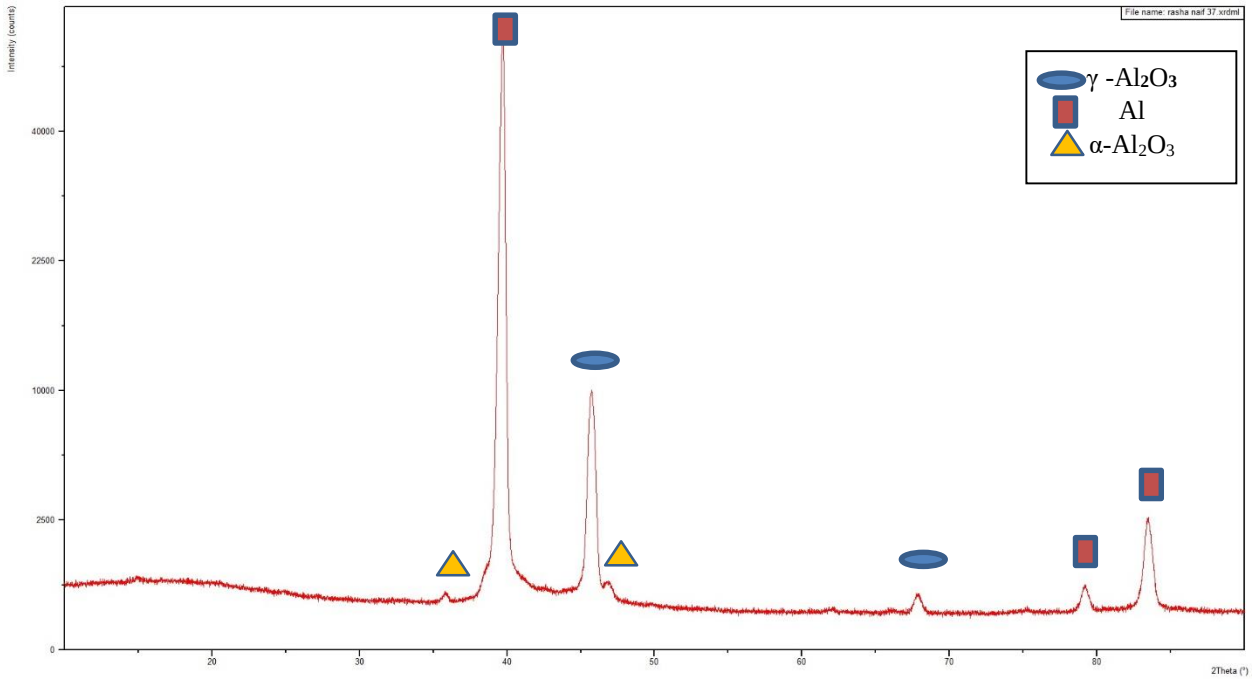

Figure (4-12): Results of XRD for CFG1 sample at 15 min.

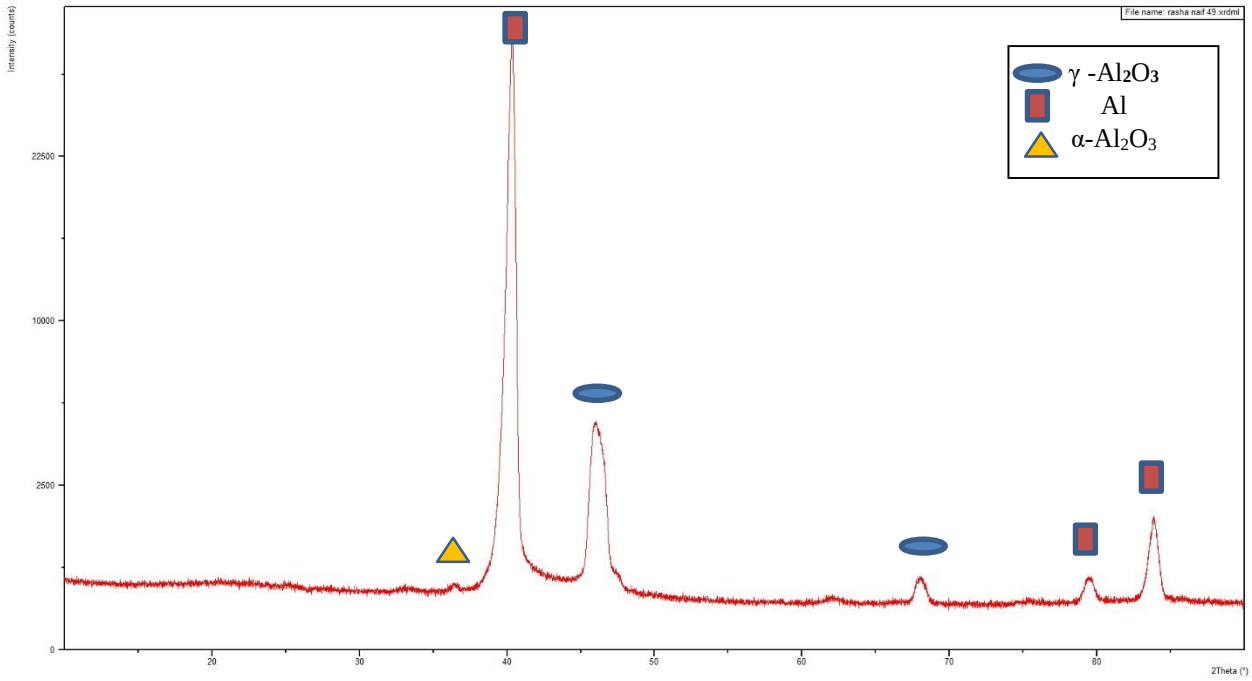

Figure (4-13): Results of XRD for EFG3 sample at 45 min.

4-4: Thickness Measurement

Results of coatings thickness are shown in figure (4-14) to (4-15). It can be observed that the coating thickness were in the range (445.2 nm -2329 nm) proving the success of the study in deposition of ceramic coatings by MAO process using natural rock additive modified electrolyte containing calcite, bauxite, and thassos additives. Generally, the higher thickness was obtained for the coatings deposited using calcite and thassos modified electrolytes (2329 nm for CF1 coating at 20 g/L calcite and 3g/L thassos) at 15 min. Where the observed increase in coating thickness implies that these additives contribute to the build-up of the coating material on the sample surfaces, MAO coating depends on several factors such as the components of the electrolyte. The electrolyte resistance and ph for different electrolytes, so the thickness of the coating depends on the material deposited and the optimal process parameters [89].

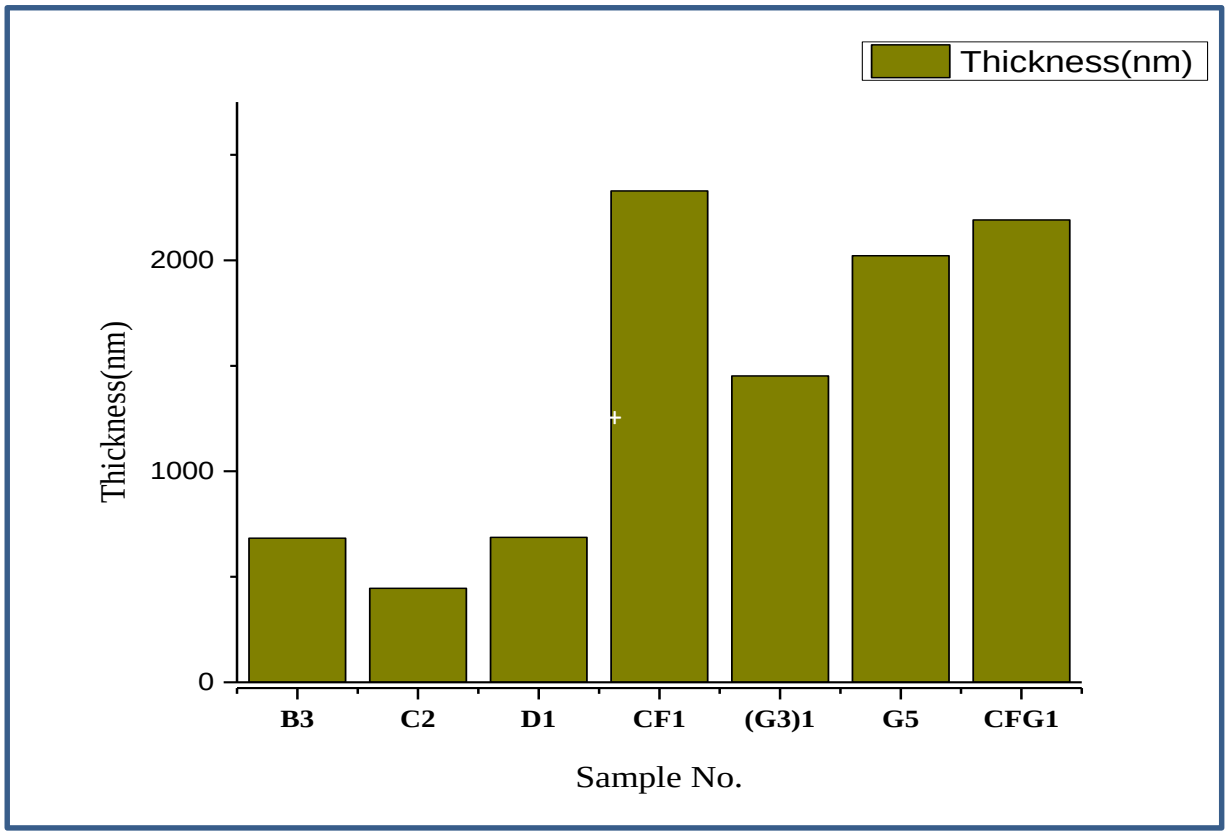

Figure (4-14): Thickness results for coatings using calcite, thassos and bauxite modified electrolyte at 15 min.

For the coatings deposited using basic electrolytes, the coating thickness was in the range (445.2 nm -687.0 nm) and the D1 coating (at 15 g/L calcite) exhibited the highest thickness for comparison with others. Also, for coatings B3 and C2 (at 3 g/L and 10 g/L calcite), the coating thickness decreased from 683.1 nm to 445.2 nm with deposition time to 15 min, and the least thickness was obtained for the coating deposited from all the coatings. Due to The thickness of the coating was influenced by the surface roughness, porosity, and corrosion resistance of the coatings [90]. Additionally, for coatings C4 (at 10 g/L calcite), it can be observed that the coating thickness increased from 445.2 nm to 520.4 nm with deposition time increasing from 15 min to 45 min. With increasing deposition, time the porosity of the coatings decreased, and the uniformity and thickness increased [91].

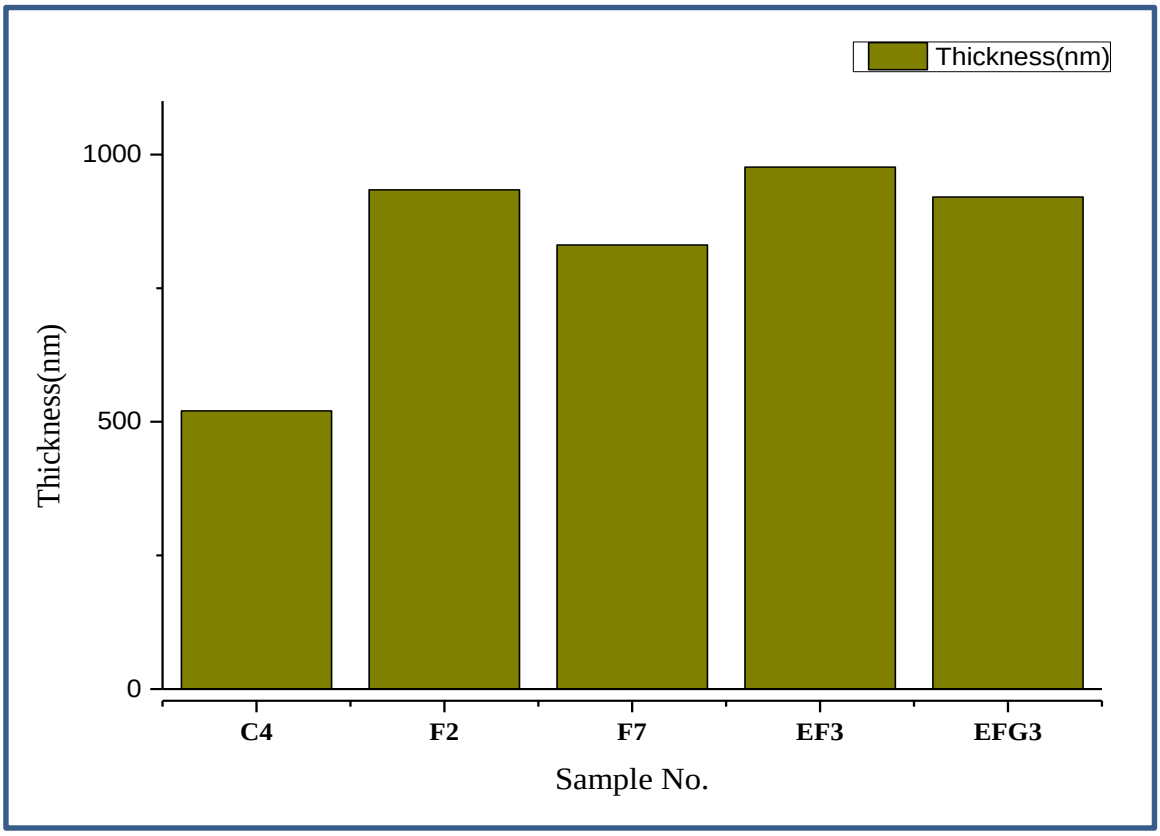

Figure (4-15): Thickness results for coatings using calcite, thassos and bauxite modified electrolyte at 45 min.

In addition, for coatings deposited using thassos modified electrolytes, the coatings thickness was in the range (830.8 nm-933.9 nm) and the F2 coating (at 2 g/L thassos) showed a high thickness with deposition time to 45 min. It might have characteristics that enhance adhesion, prevent excessive penetration of the coating solution into the substrate or promote the formation of a thicker layer on the surface. The specific interactions between thassos particles, the coating solution and the Al alloy substrate likely play a role in this process [92]. As, for coatings F7 (at 7 g/L thassos), it can be noted that the coating thickness decreased from 933.9nm to 830.8nm with deposition time to 45 min.

For the coatings deposited using calcite and thassos modified electrolytes, the coatings thickness were in the range (976.5 nm -2329 nm) and the CF1coatings (at 20g/L calcite and 3g/L thassos) showed the higher thickness among the others. Also, it is clearly that the coating thickness decreased from 2329 nm to 976.5 nm with deposition time increasing from 15 min to 45 min (EF3 coating) at 10g/L calcite and 7g/L thassos. This confirms the validity of the results in this study, where adding thassos decreased the thickness with an increase in the addition ratio and deposition time, while calcite recorded the highest thickness with a deposition time of 15 min with increased the addition of 15g/L.

for the coatings deposited using bauxite modified electrolytes, the coatings thickness were in the range (1452 nm -2022 nm) and the (G3)1 and G5 coating (at 3g/L and 5g/L bauxite) exhibited increasing thickness with deposition time to 15 min and increased addition ratio from 3g/L to 5g/L. Depending on their particle size and distribution. It can be occupy spaces in the coating and contribute to an increase in thickness [93].

Furthermore, for the coatings deposited using calcite, thassos and bauxite modified electrolytes, the coating thickness were in the range (920.5 nm -2191 nm), and the CFG1 (at 20g/L calcite, 3g/L thassos and 3g/L bauxite) coating recorded highest thickness. Due to the interaction between different additives can be complex. They affect others properties or hinder their ability to contribute to coating thickness in the desired way. Also, for coating EFG3 (at 10g/L calcite, 7g/L thassos and 5g/L bauxite) at 45 min, it is clearly that the coating thickness decreased from 2191 nm to 920.5 nm with deposition time increasing from 15 min to 45 min. However, it is also important to consider that while the combined additives might not have significantly increased coating thickness in this specific study, they could still be contributing to other beneficial properties such as hardness, corrosion resistance and contact angle.

4-5: Scanning Electron Microscope (SEM) Results

Figure from (4-16) to (4-26) shown the SEM image for surface morphology of different coatings at different magnifications. It can be observed that the coatings were characterized by pores with different sizes and uniform distribution and the particle distribution of the additives through the coating layer. Proving the success of the study in deposition of ceramic coatings by MAO process using natural rock additive modified electrolyte containing calcite, bauxite and thassos additives. Generally, the higher porosity and non-uniform distribution was obtained for the coatings deposited F2 and CF1 among the others.

In addition, the SEM for coatings shown in figures (4.16) to (4-18) proved that the coatings deposited using calcite electrolyte, it can be noted that the best surface coverage and crack coverage with the presence of calcite particles. As, for coating C4 (at 10 g/L calcite for 45 min) recorded the highest hardness among the other. It can be noticed more homogeneous surface morphology $CaCO_3$ particles that increases the density of the coating solution. In addition, the size of the pores and tunnels decreased with the addition of $CaCO_3$; this is due to the decomposition of the calcium carbonate into the pores and tunnels.

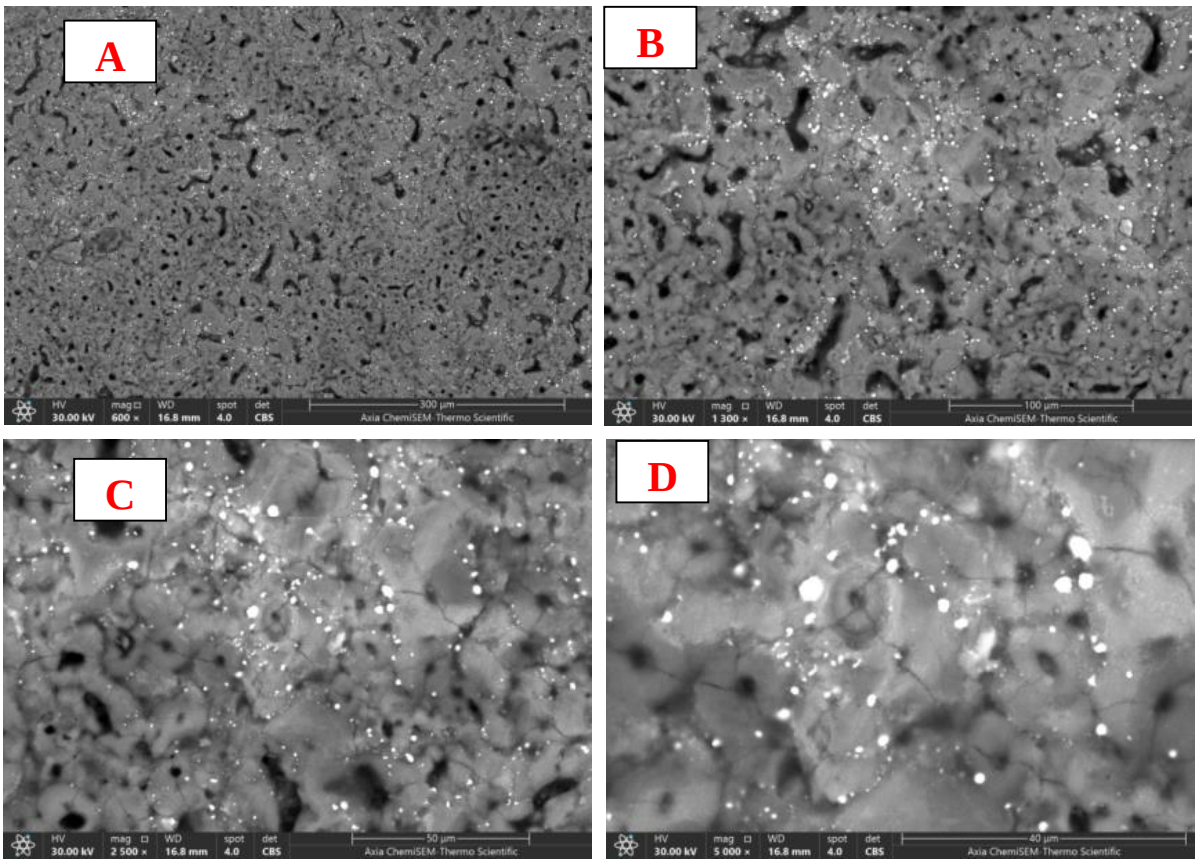

Figure (4-16): SEM results for coatings deposited using basic electrolyte (C4 coating) at 45 min.

As for the figure (4-17) to D1 coating. It can be observed that the coating gives a typical crater-like porous structure and it can be noticed that non-uniform pores distribution with the presence of micro cracks because of rapid solidification of particles on the substrate. As well as post-treatment, that was carried out after the coating process on the surface of the samples.

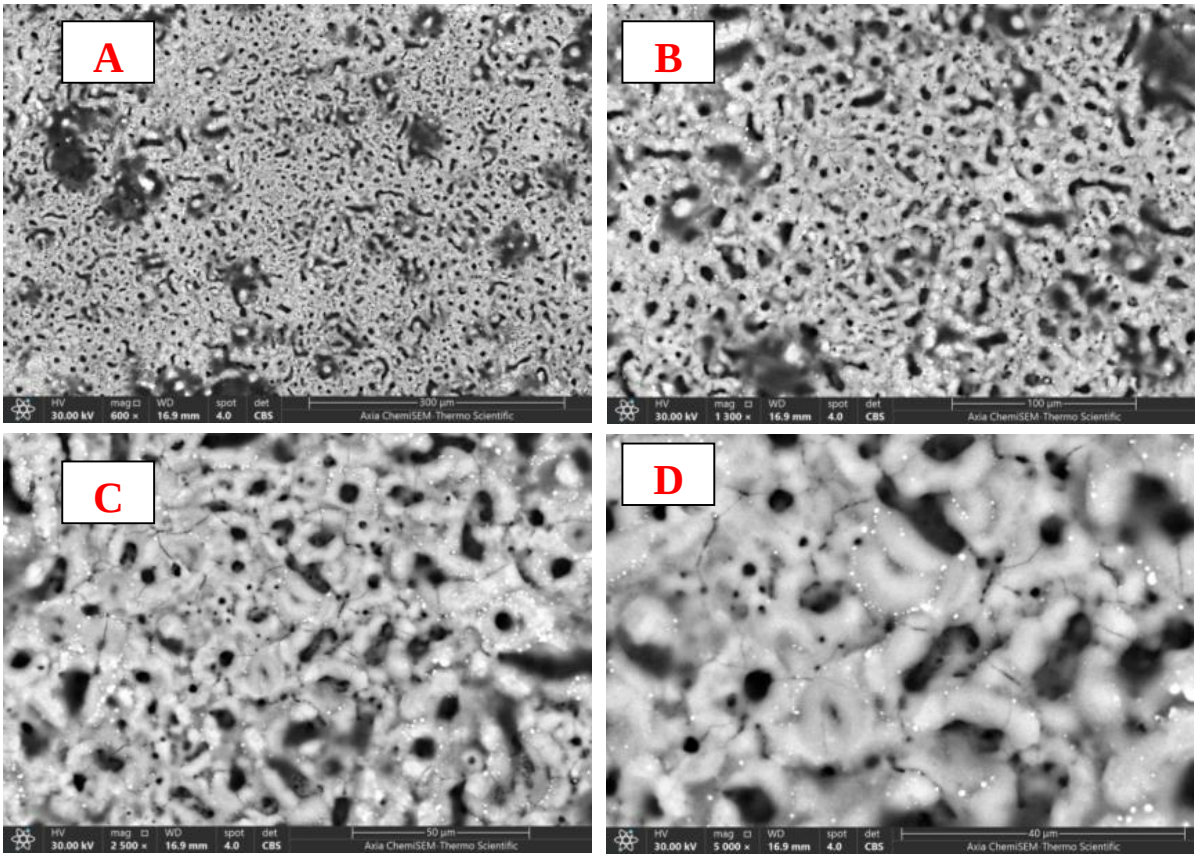

Figure (4-17): SEM results for SEM results for coatings deposited using *basic electrolyte* (D1 *coating) at 15 min*.

As well as in figure (4-18) for coating MC2 (at 10g/L calcite and 1g/L MOS_2) at 45 min, it can be exhibited micro pores, due to poor dispersion of MOS_2 within the $CaCO_3$ matrix can lead to localized regions with varying compositions. These variations can result in the formation of pores as the material is processed. It could record the highest hardness among coatings. Anyhow, it would be expected, the hardness difference can be also strongly attributed to the non-uniform distribution of pores and the deposited phase of γ-alumina.

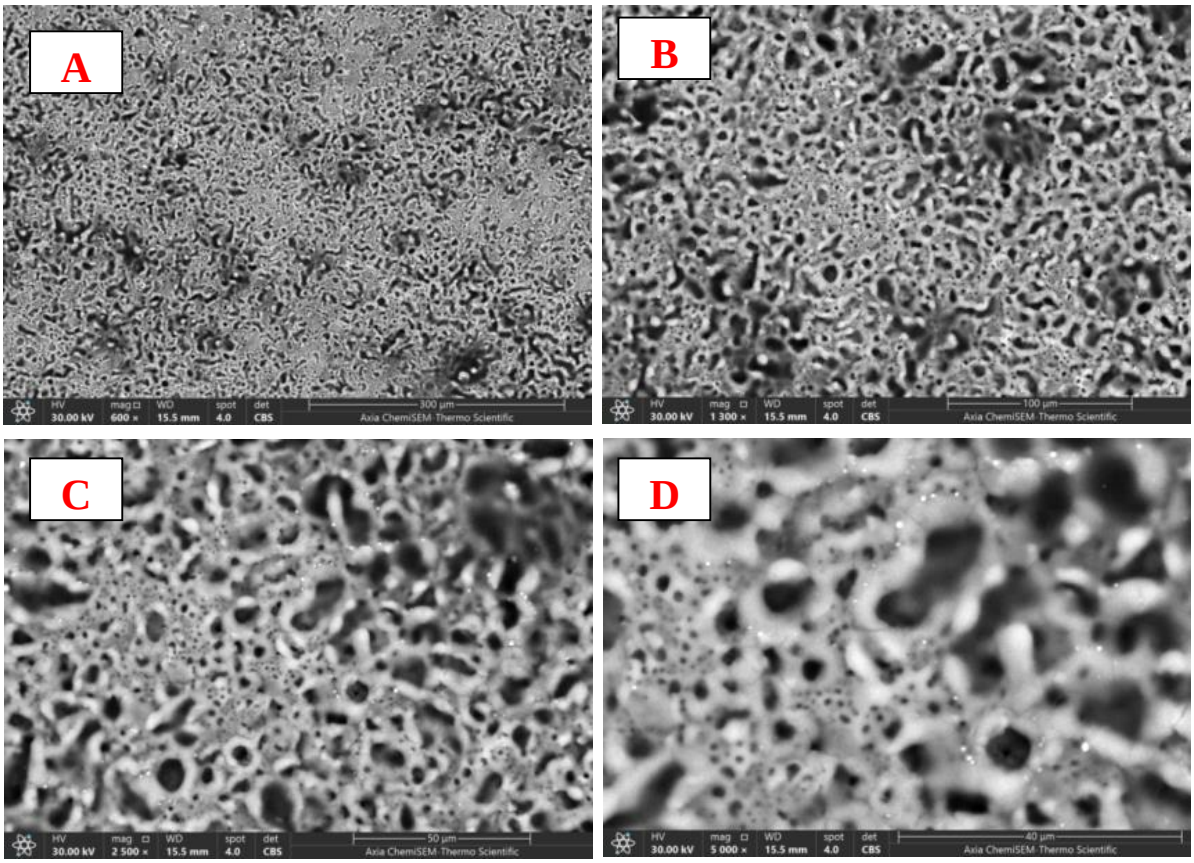

Figure (4-18): SEM results for coatings deposited using *basic electrolyte* (MC2 *coating) at 45 min*.

Where, figures (4-19) to (4-20) show the SEM images of the coatings deposited using thassos modified electrolyte, in figure (4-19) shown for coating F2 (at 2g/L thassos), it can be observed that the porosity increases with the addition but the shape of pores became less uniform and dense. as well as in figure (4-20) for coating F7 (at 7g/L thassos), we observed that the porosity decreased, due to incorporation of thassos components into the micro-pores, which leads to reduce the amount of pores in the structure. Such incorporation benefits can be that clearly sensed in hardness improvement, pores distribution and contact angle.

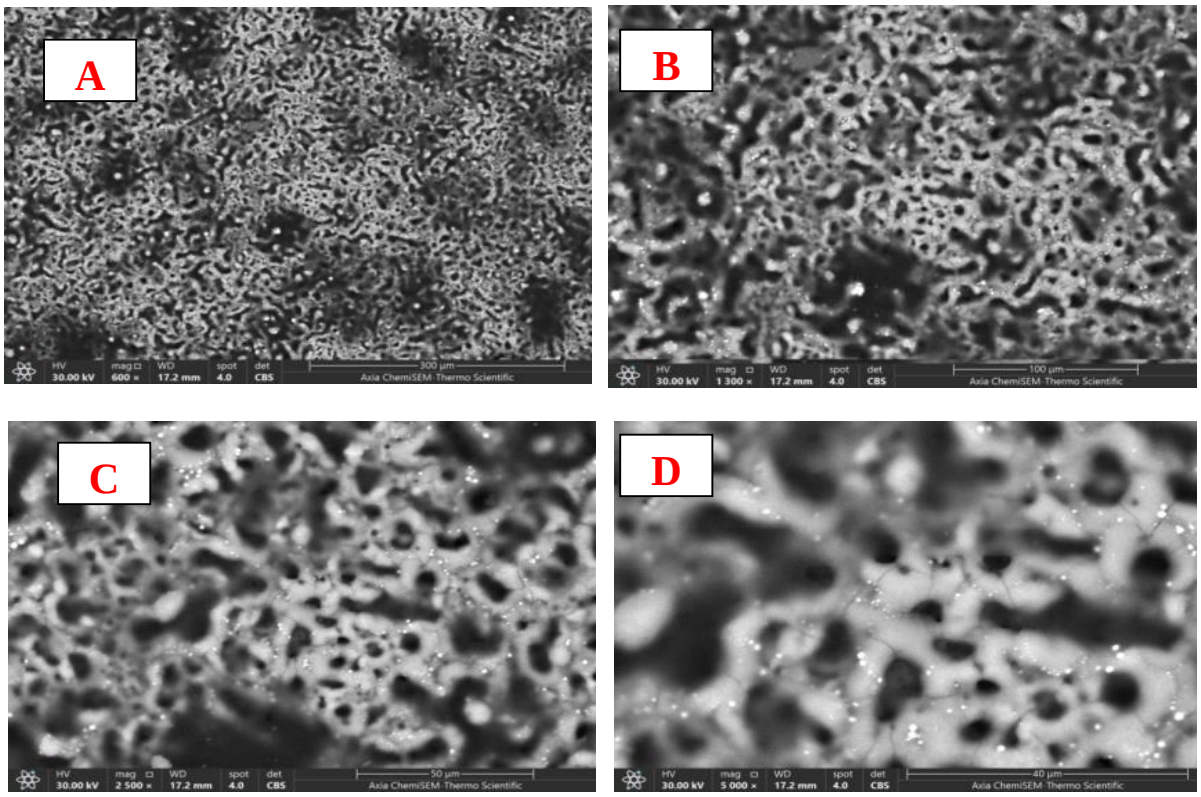

Figure (4-19): SEM results for coatings deposited using thassos modified electrolyte (F2 coating) at 45 min.

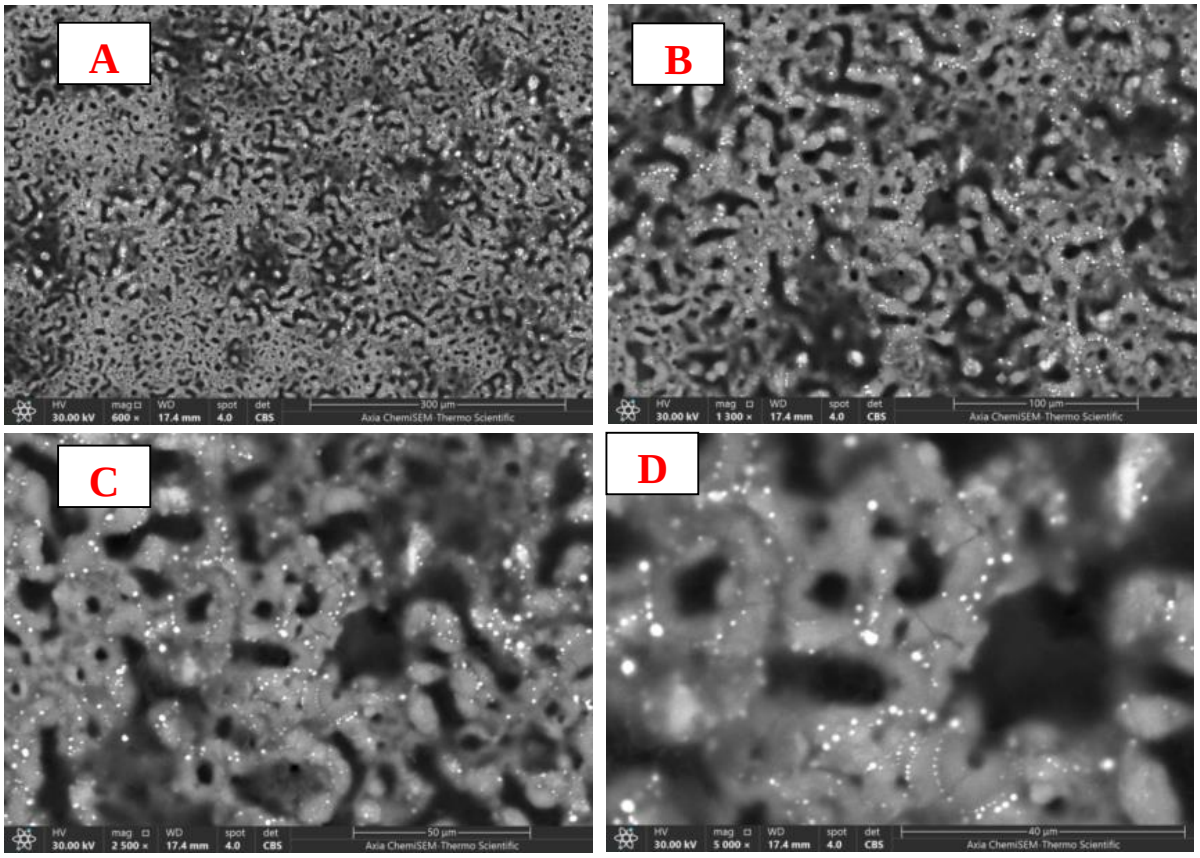

Figure (4-20): SEM results for coatings deposited using *thassos modified electrolyte* (F7 *coating) at 45 min*.

Figures (4-21) to (4-22) the SEM image of coating deposited using calcite and thassos modified electrolytes, for the coating, CF1 (at 20g/L calcite and 3g/L thassos) at 15 min, showed the higher coating thickness among others. Also, the coating porosity is highest compared to the coating EF3 (at 10g/L calcite and 7g/L thassos) with deposition time to 45 min, due to the incorporation of $CaCO_3$ and thassos can be filled or partially fill any existing pores within the coating. This can lead to non-uniform pore distribution or even a reduction in the overall number and size of pores.

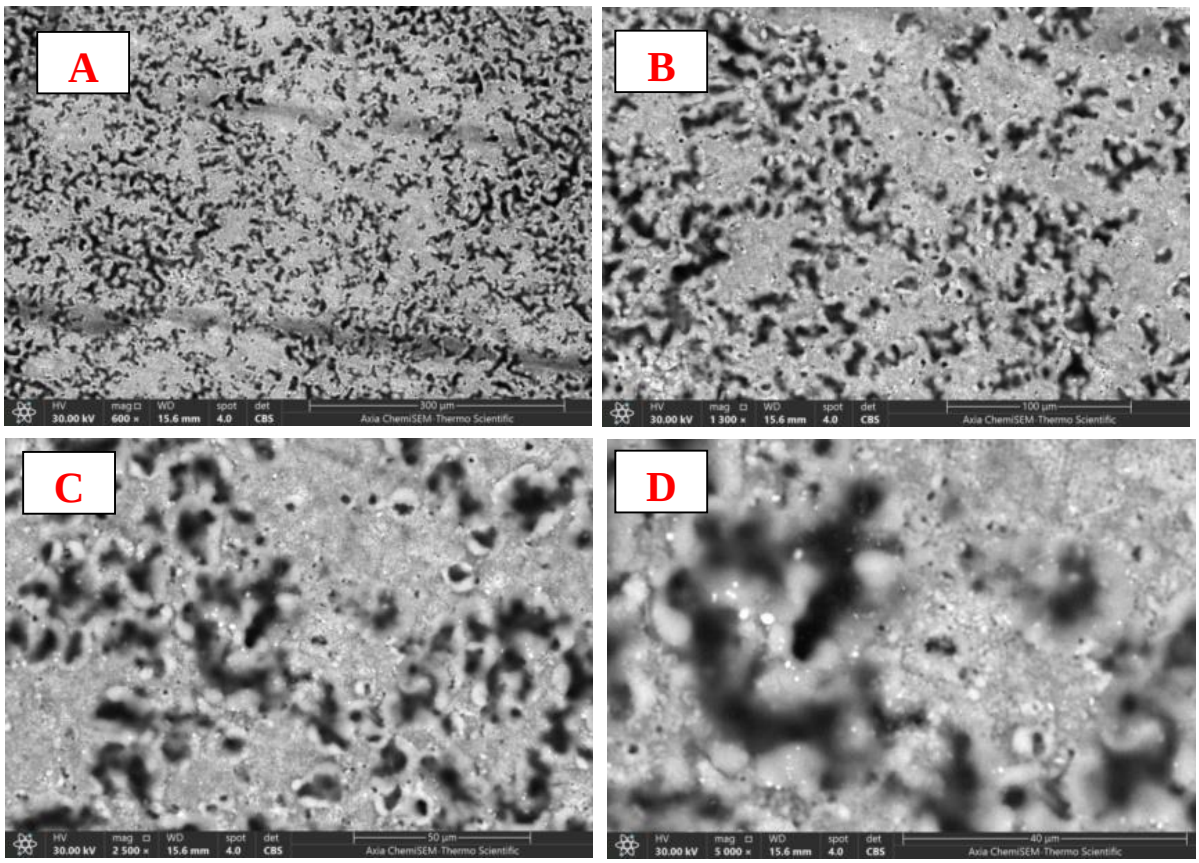

Figure (4-21): SEM results for coatings deposited using calcite and thassos modified electrolyte (CF1 coating) at 15 min.

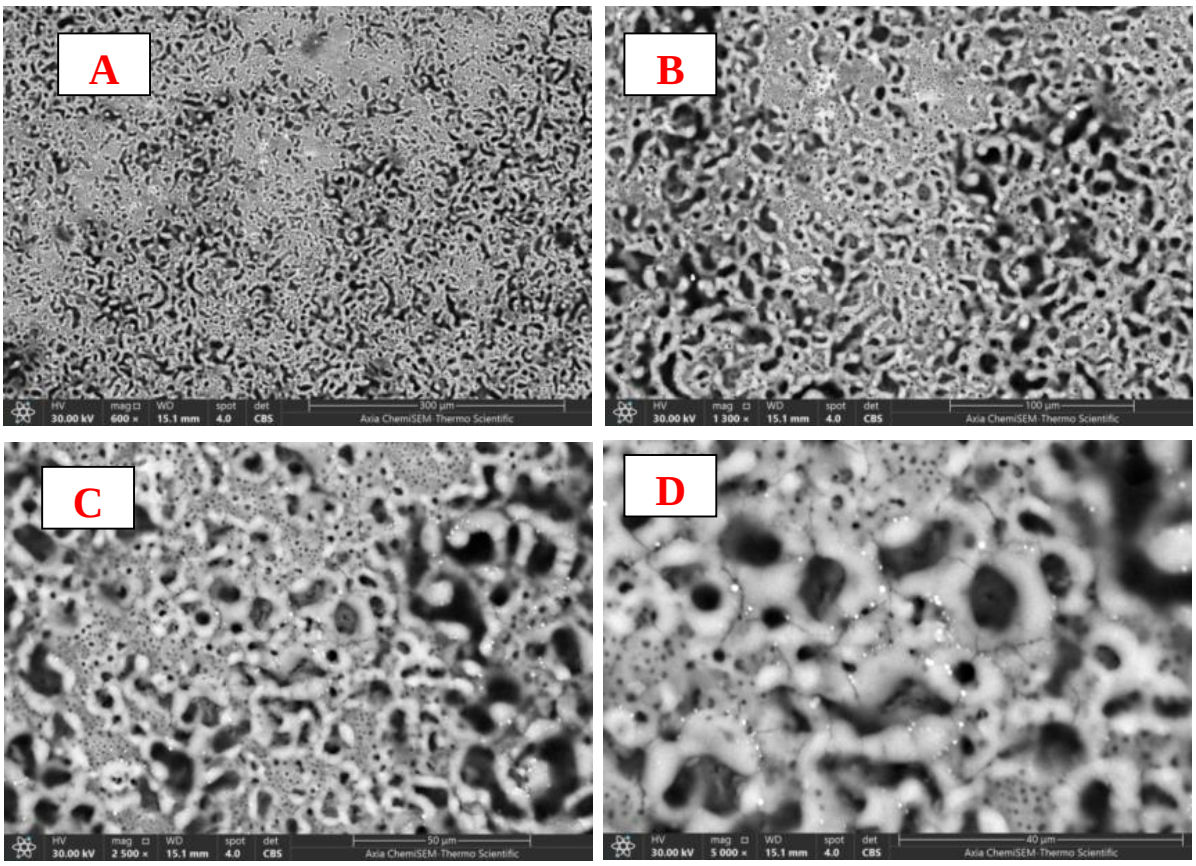

Figure (4-22): SEM results for coatings deposited using calcite and thassos modified electrolyte (EF3 coating) at 45 min.

Figures (4-23) to (4-24) for SEM image of coating deposited using bauxite modified electrolytes, it can be noticed that the coatings (G3)1 and G5 (at 3g/L and 5g/L bauxite) at 15 min, large micro particles of bauxite dispersed throughout the matrix of the coating. This suggests that the bauxite particles could not been finely dispersed or have not fully integrated into the coating material. Instead, they appear to be relatively large and distinct within the coating.

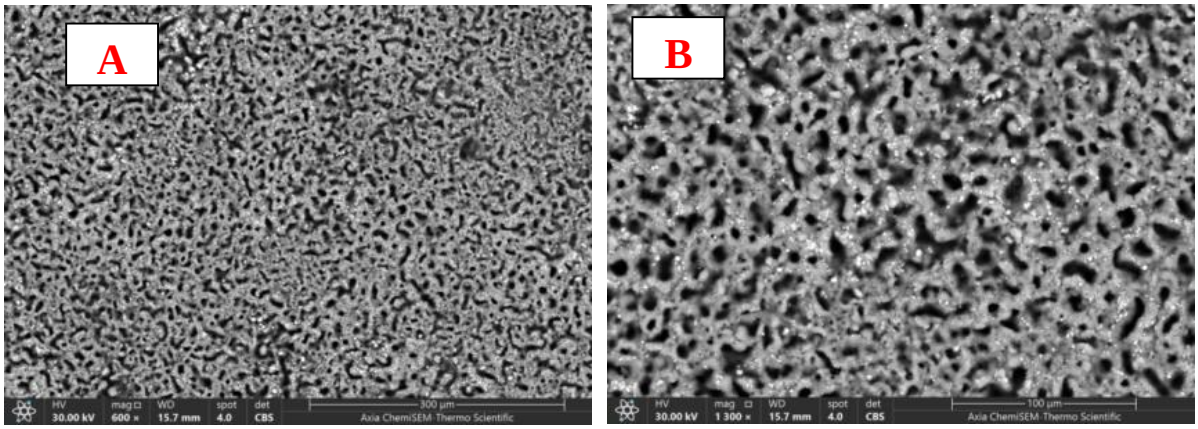

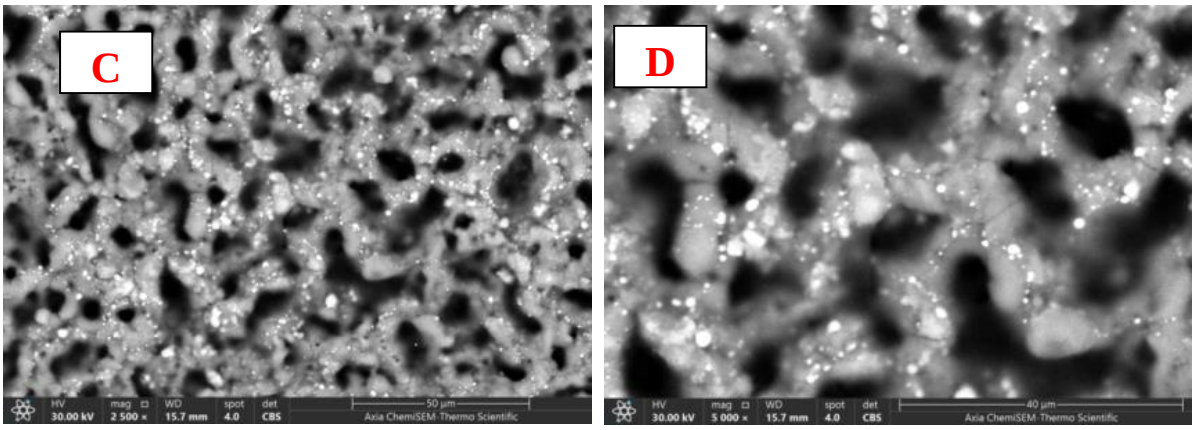

Figure (4-23): SEM results for coatings deposited using bauxite modified electrolyte ((G3)1 coating) at 15 min.

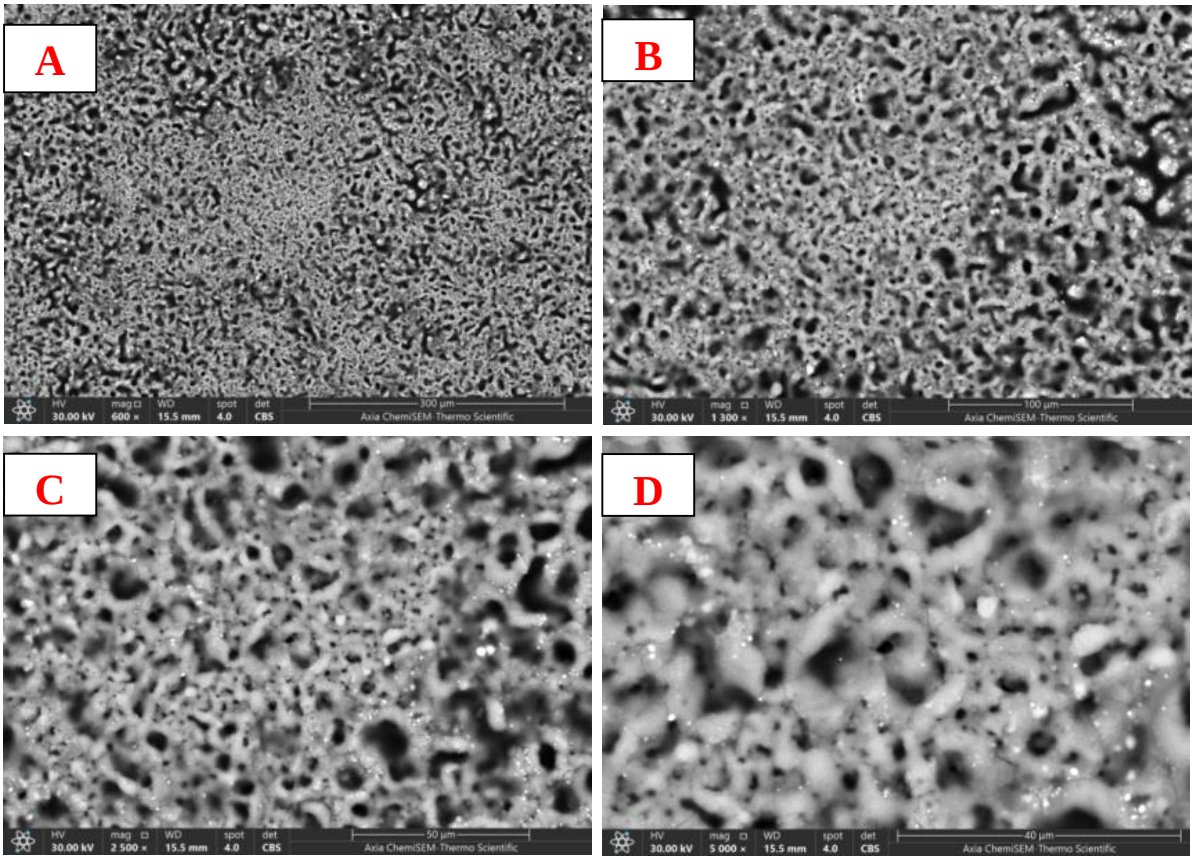

Figure (4-24): SEM results for coatings deposited using bauxite *modified electrolyte* (G5 *coating) at 15 min.*

As, Figure (4-25) to (4-26) the SEM image for coatings deposited using calcite, thassos and bauxite modified electrolytes. The coating CFG1 (at 20g/L calcite, 3g/L thassos and 3g/L bauxite) at 15 min, exhibited surface morphology of coating characterized by exhibiting higher micro pores content a typical crater-like porous structure with uniform distribution and it can be recorded the highest contact angle, due to post-treatment after the coating process.

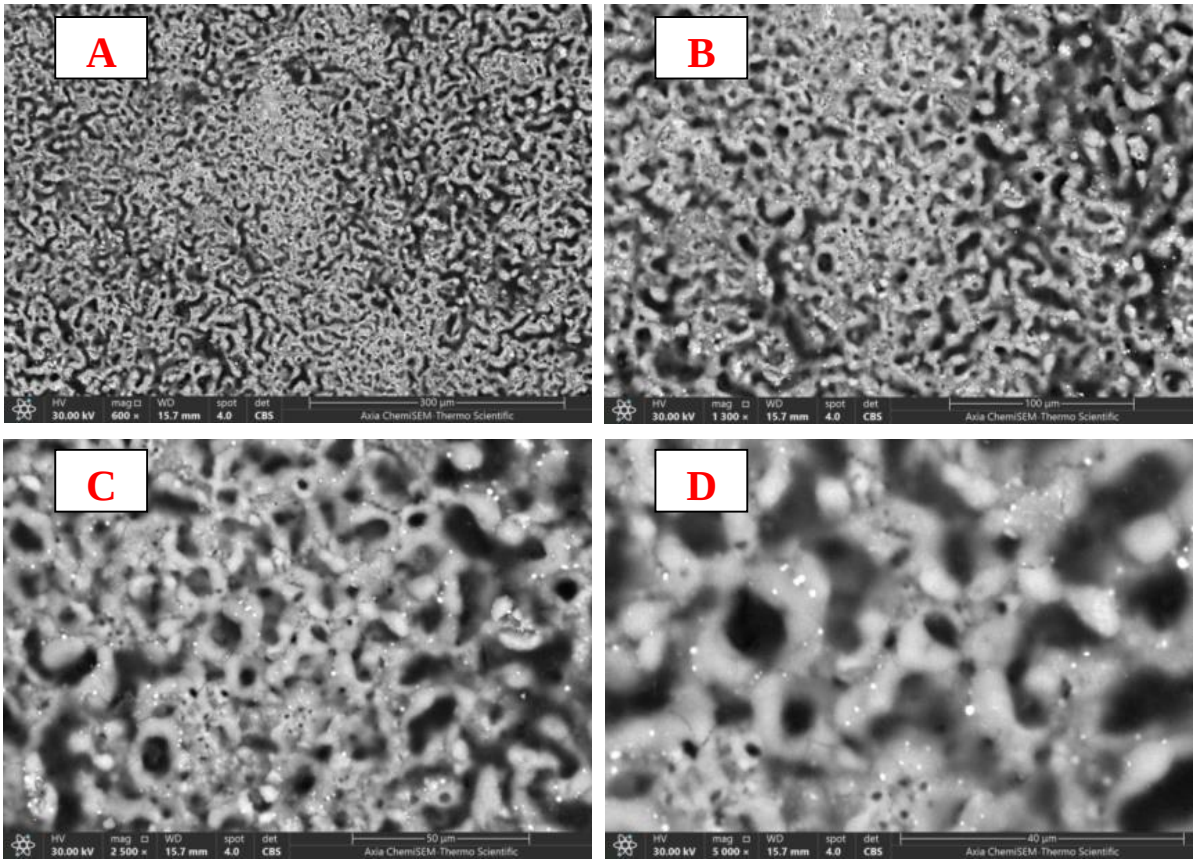

Figure (4-25): SEM results for coatings deposited using calcite, *thassos and bauxite modified electrolyte* (CFG1 *coating) at 15 min*.

As, figure (4-26) shows SEM image for the coating EFG3 (at 10g/L calcite, 7g/L thassos and 5g/L bauxite) at 45 min, it clearly that the highest hardness among all coatings, surface morphology refers to low pores content. In addition, the pores presented, although limited in number uniformly distributed across the surface of thecoating.

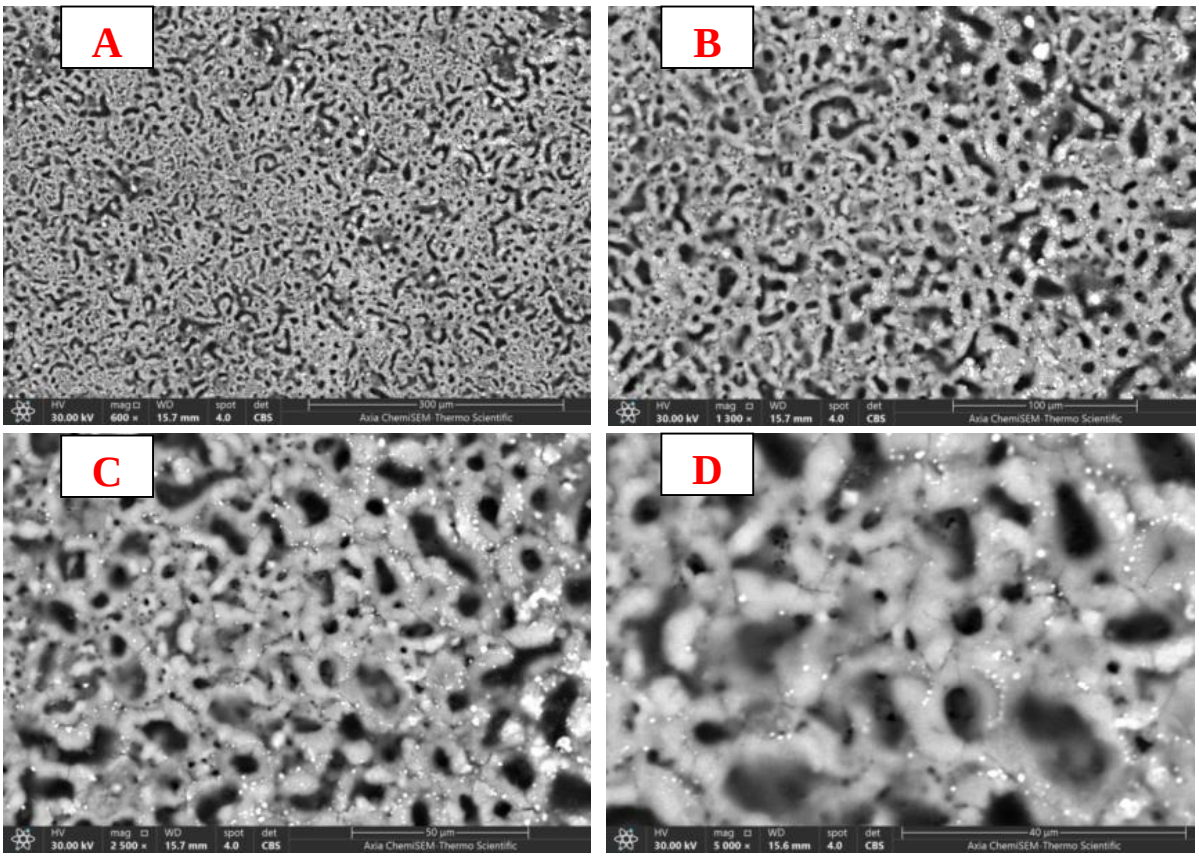

Figure (4-26): SEM results for coatings deposited using calcite, *thassos and bauxite modified electrolyte* (EFG3 *coating) at 45 min*.

4-6: EDS Results of Coatings

Results of coatings EDS are shown in figures (4.27) to (4.34) and table (4-2) to (4-9). It can be observed that the coating presented of aluminum (Al) and oxygen (O) elements in the coatings indicates the deposition of aluminum oxide (alumina).

Additionally, the use of different electrolytes has led to the incorporation of modification elements P (Phosphorus), Ca (Calcium) and Si (Silicon) in the coatings. These modification elements are present in different amounts, as indicated by their respective weights. This suggests that the coatings are not purely composed of aluminum oxide, but rather, they have been modified with these other elements through the electrolyte used during the coating process and post treatment after coating process for contact angle improvement. these proving the success of the study in deposition of ceramic coatings by MAO process using natural rock additive modified electrolyte containing calcite, thassos and bauxite additives.

4-6-1: EDS Results of Sample C4

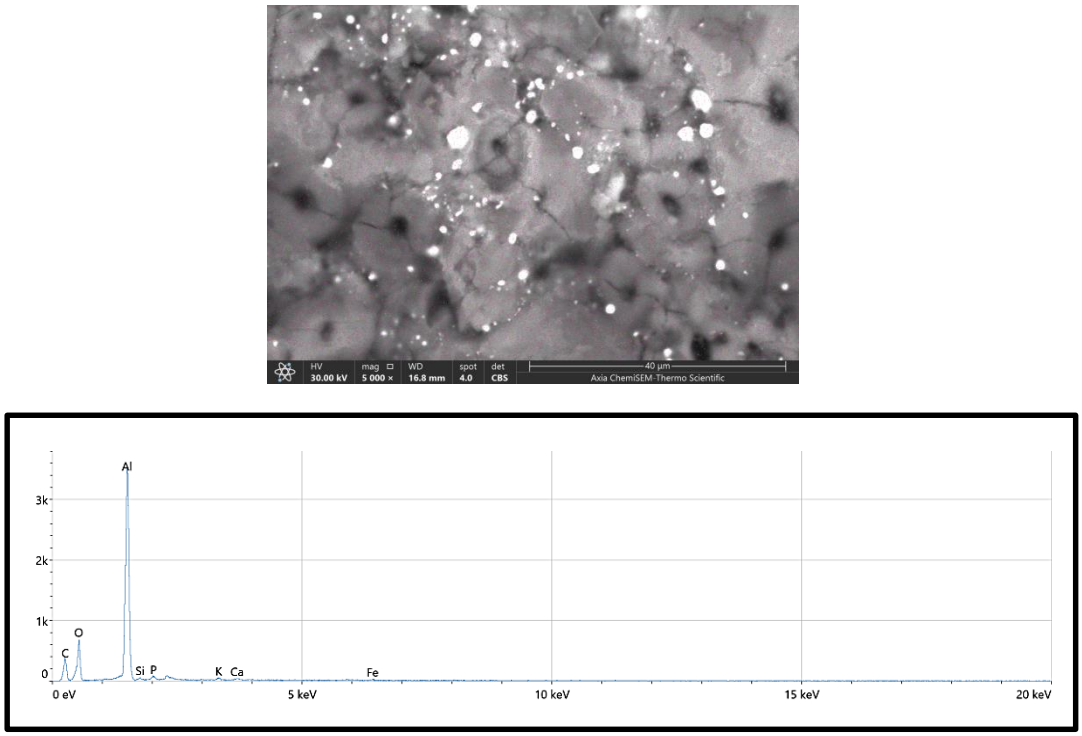

Figure (4-27): EDS results of sample C4 at 45 min.

Table (4-2): EDS Results of Sample C4.

Element	Atomic %	Atomic % Error	Weight %	Weight % Error
C	42.3	1.0	30.4	0.7
O	36.8	0.7	35.2	0.7
Al	19.7	0.1	31.7	0.2
Si	0.3	0.0	0.5	0.1
P	0.6	0.0	1.1	0.1
K	0.2	0.0	0.4	0.0
Ca	0.2	0.0	0.4	0.0
Fe	0.1	0.0	0.4	0.1

4-6-2: EDS Results of Sample D1

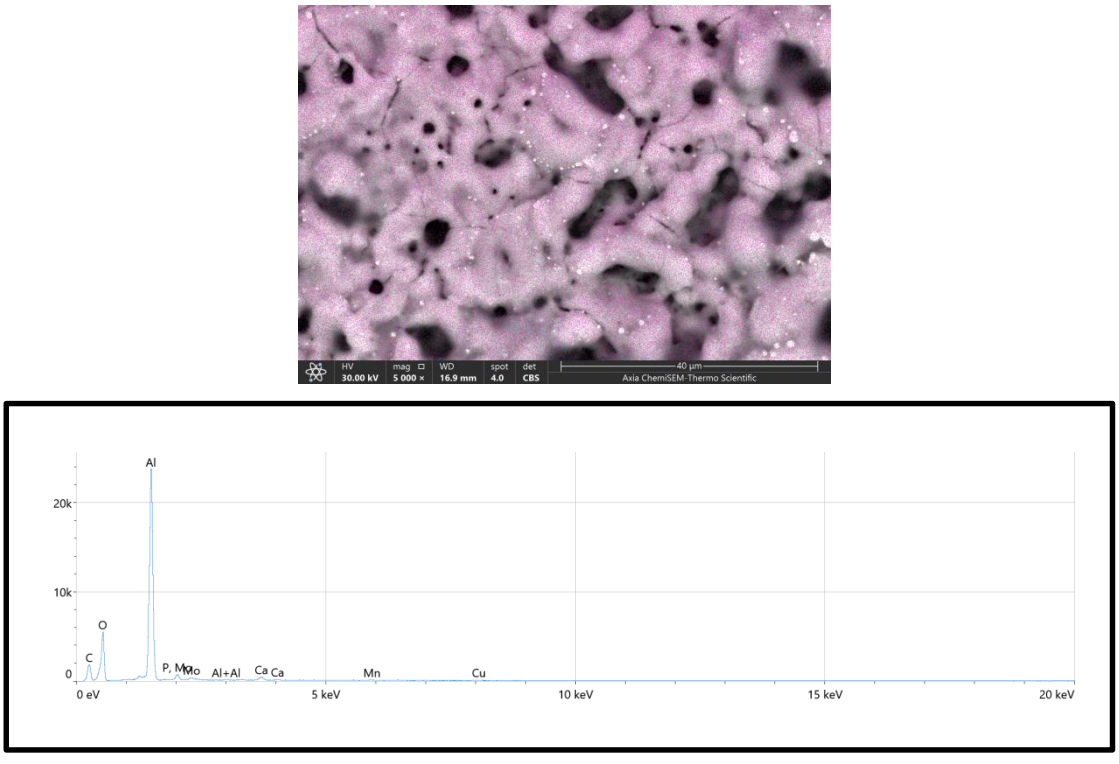

Figure (4-28): EDS results of sample D1 at 15 min.

Table (4-3): EDS Results of Sample D1.

Element	Atomic %	Atomic % Error	Weight %	Weight % Error
C	32.2	0.7	22.1	0.5
O	44.4	0.3	40.7	0.3
Al	22.1	0.1	34.1	0.1
P	0.7	0.0	1.3	0.0
Ca	0.4	0.0	0.8	0.0
Mn	0.1	0.0	0.2	0.0
Cu	0.1	0.0	0.4	0.1
Mo	0.1	0.1	0.3	0.3

4-6-3: EDS Results of Sample MC2

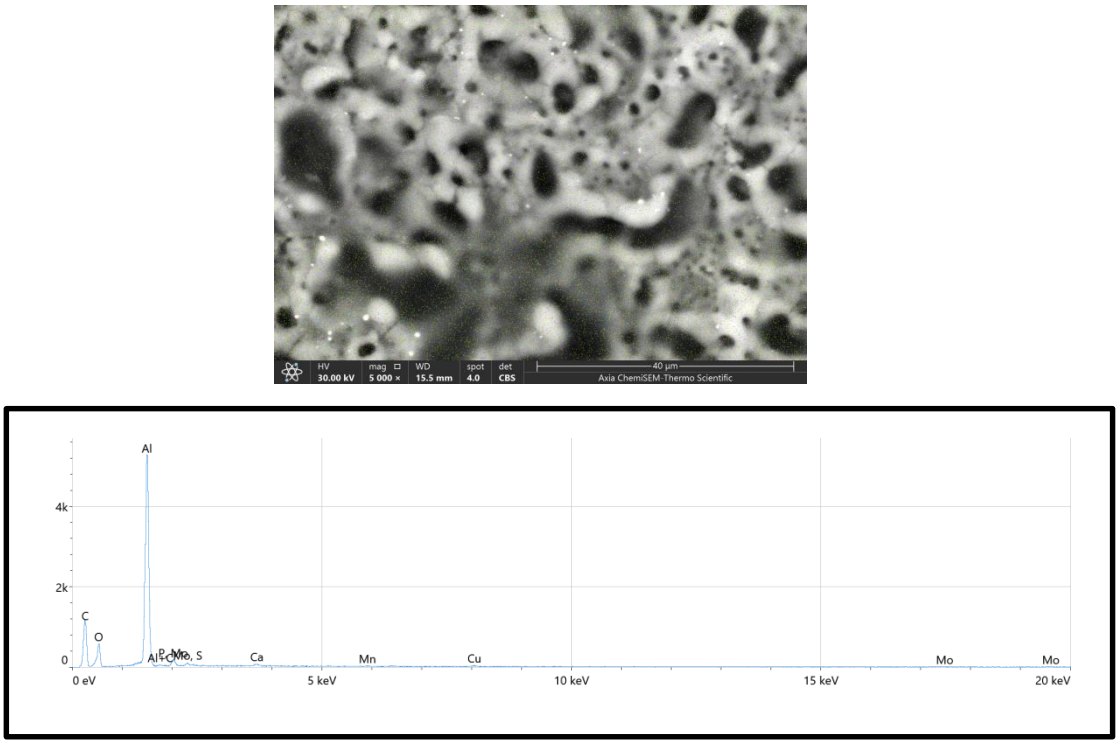

Figure (4-29): EDS results of sample MC2 at 45 min.

Table (4-4): EDS Results of Sample MC2.

Element	Atomic %	Atomic % Error	Weight %	Weight % Error
C	61.0	0.7	47.1	0.5
O	23.1	0.4	23.8	0.5
Al	14.8	0.1	25.7	0.1
P	0.6	0.0	1.2	0.0
S	0.0	---	0.0	---
Ca	0.1	0.0	0.3	0.0
Mn	0.0	0.0	0.2	0.0
Cu	0.1	0.0	0.6	0.1
Mo	0.2	0.1	1.1	0.5

4-6-4: EDS Results of Sample F2

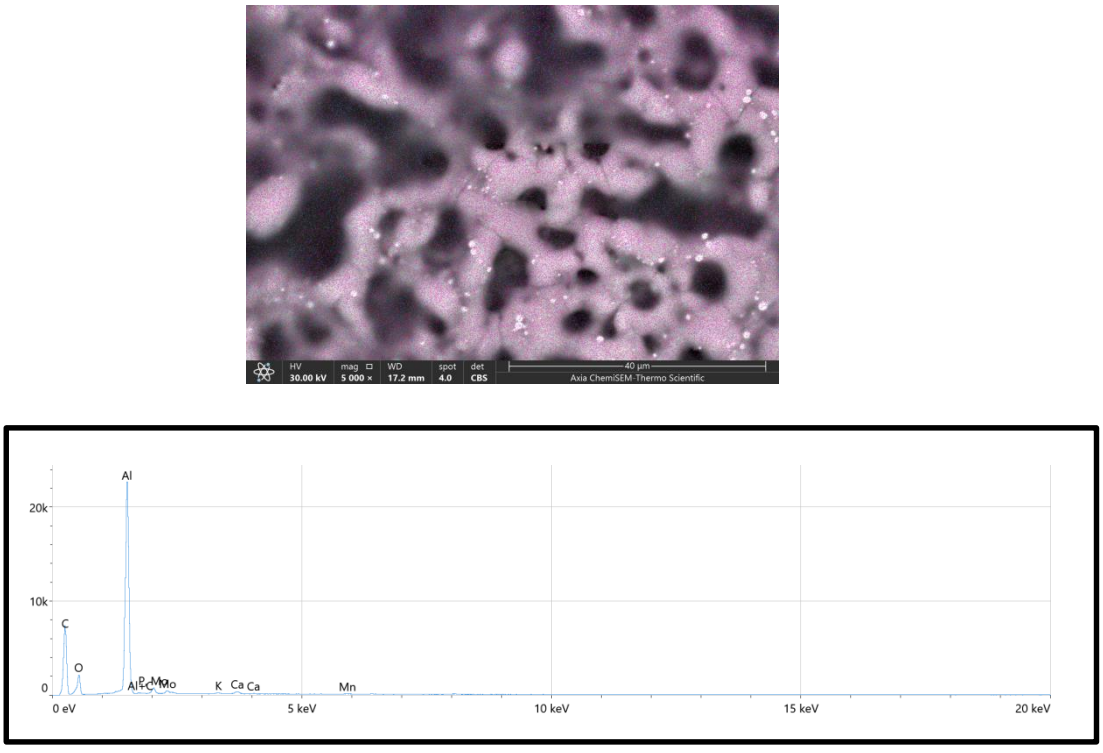

Figure (4-30): EDS results of sample F2 at 45 min.

Table (4-5): EDS Results of Sample F2.

Element	Atomic %	Atomic % Error	Weight %	Weight % Error
C	66.9	0.6	53.6	0.5
O	19.2	0.2	20.5	0.2
Al	13.2	0.1	23.7	0.1
P	0.4	0.0	0.9	0.0
K	0.1	0.0	0.2	0.0
Ca	0.1	0.0	0.4	0.0
Mn	0.1	0.0	0.2	0.0
Mo	0.1	0.0	0.6	0.3

4-6-5: EDS Results of Sample EF3

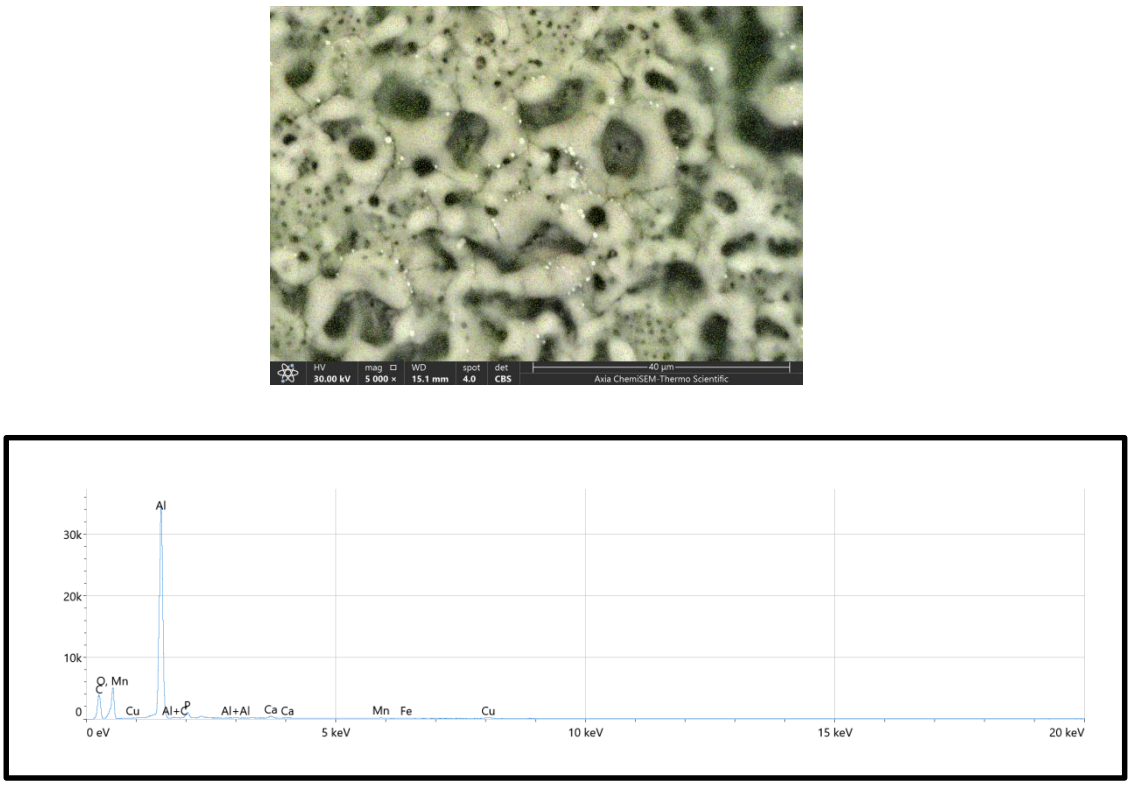

Figure (4-31): EDS results of sample EF3 at 45 min.

Table (4-6): EDS Results of Sample EF3.

Element	Atomic %	Atomic % Error	Weight %	Weight % Error
C	46.6	0.4	33.8	0.3
O	32.7	0.3	31.6	0.2
Al	19.5	0.1	31.8	0.1
P	0.8	0.0	1.5	0.0
Ca	0.2	0.0	0.4	0.0
Mn	0.1	0.0	0.2	0.0
Fe	0.0	0.0	0.2	0.0
Cu	0.2	0.0	0.7	0.1

4-6-6: EDS Results of Sample G5

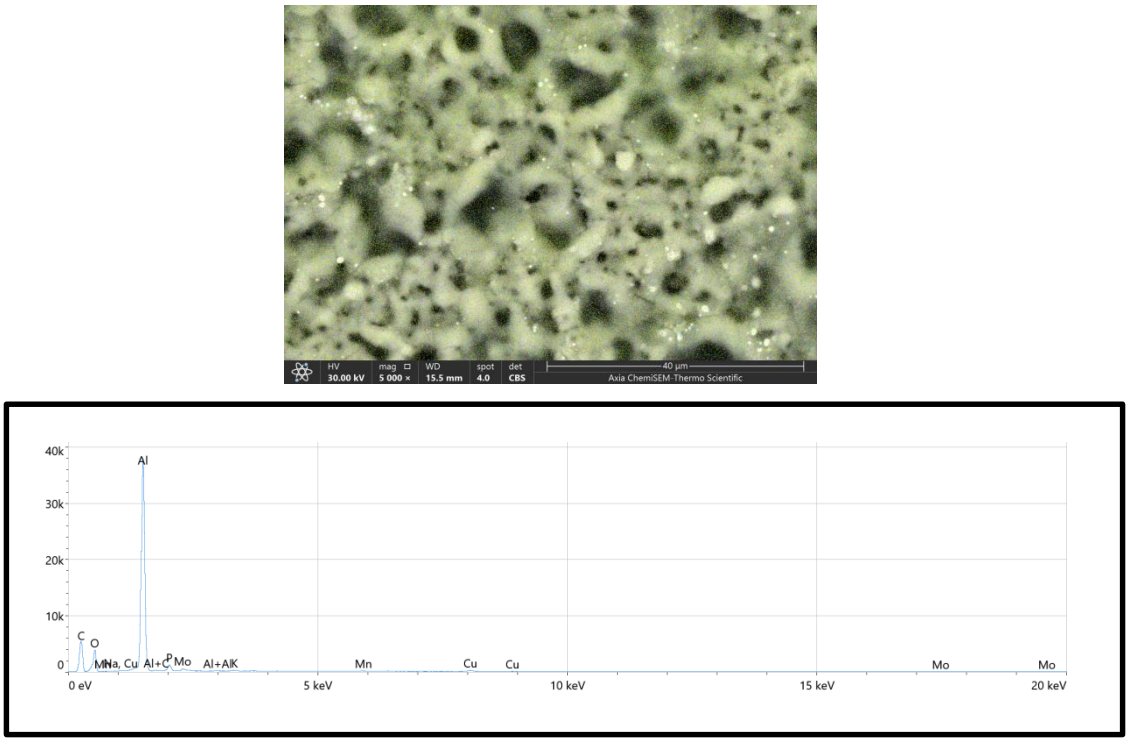

Figure (4-32): EDS results of sample G5 at 15 min.

Table (4-7): EDS Results of Sample G5.

Element	Atomic %	Atomic % Error	Weight %	Weight % Error
C	54.4	0.6	40.3	0.4
O	25.7	0.2	25.3	0.2
F	0.2	0.1	0.2	0.1
Na	0.1	0.0	0.1	0.0
Al	18.6	0.1	30.9	0.1
P	0.7	0.0	1.4	0.0
K	0.1	0.0	0.1	0.0
Mn	0.1	0.0	0.2	0.0
Cu	0.2	0.0	0.7	0.1
Mo	0.1	0.0	0.7	0.2

4-6-7: EDS Results of Sample CFG1

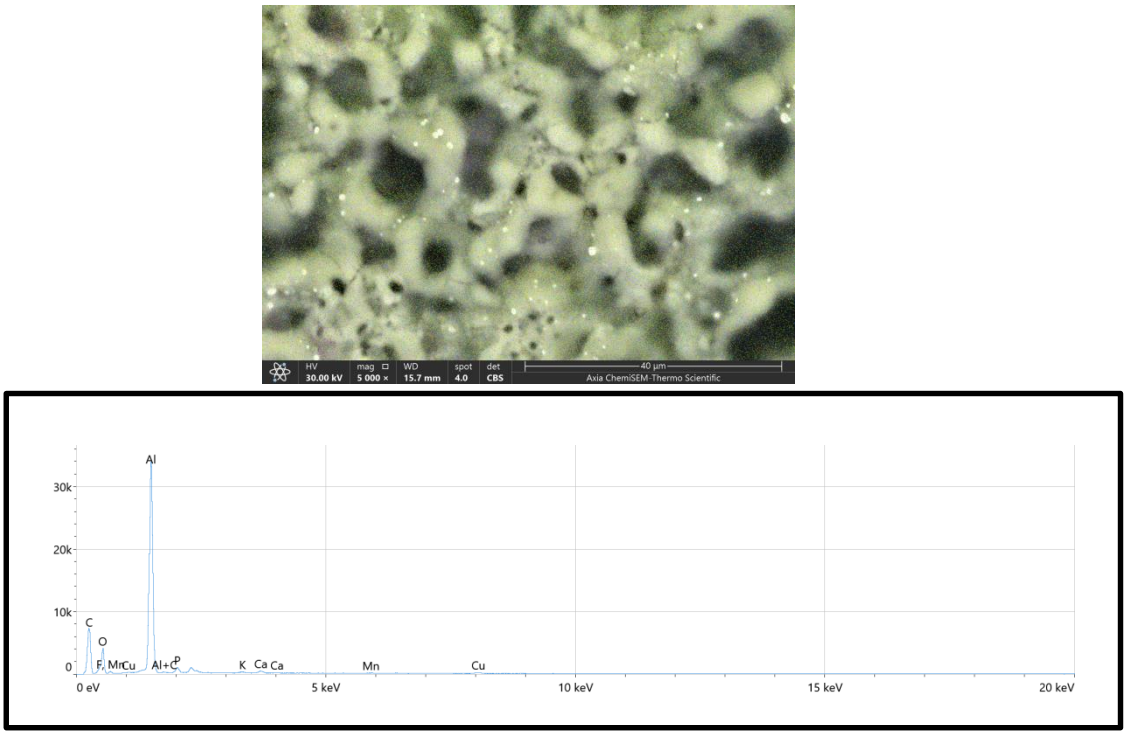

Figure (4-33): EDS results of sample CFG1 at 15 min.

Table (4-8): EDS Results of Sample CFG1.

Element	Atomic %	Atomic % Error	Weight %	Weight % Error
C	59.8	0.4	46.5	0.3
O	24.1	0.2	25.0	0.2
F	0.6	0.2	0.8	0.2
Al	14.5	0.1	25.4	0.1
P	0.5	0.0	1.1	0.0
K	0.1	0.0	0.2	0.0
Ca	0.2	0.0	0.4	0.0
Mn	0.0	0.0	0.2	0.0
Cu	0.1	0.0	0.5	0.1

4-6-8: EDS Results of Sample EFG3

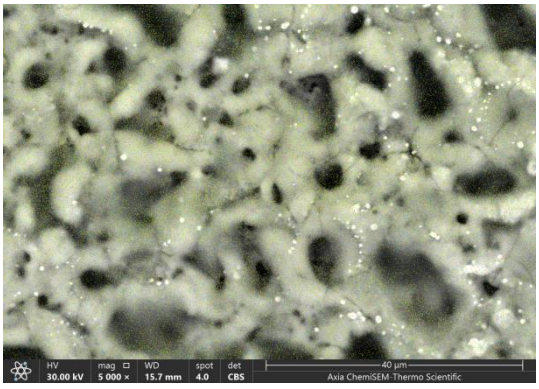

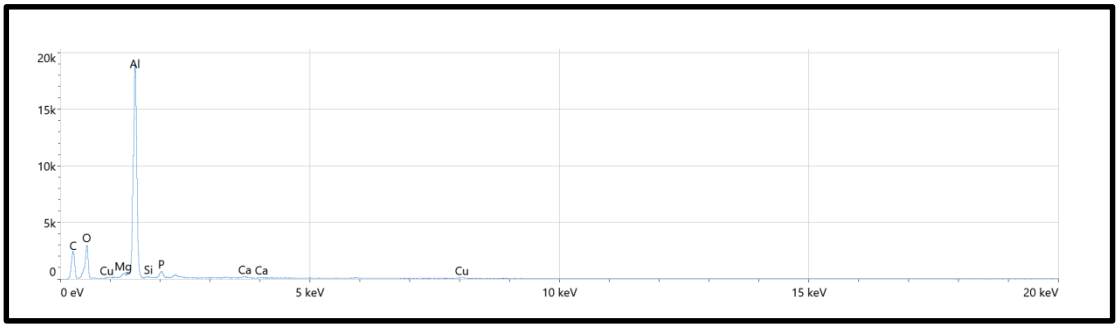

Figure (4-34): EDS results of sample EFG3 at 45 min.

Table (4-9): EDS Results of Sample EFG3.

Element	Atomic %	Atomic % Error	Weight %	Weight % Error
C	48.1	0.4	35.4	0.3
O	32.5	0.3	31.9	0.3
Mg	0.2	0.0	0.4	0.0
Al	18.0	0.1	29.8	0.1
Si	0.1	0.0	0.2	0.0
P	0.8	0.0	1.5	0.0
Ca	0.1	0.0	0.3	0.0
Cu	0.2	0.0	0.6	0.0

4-7: Hardness Results

Results of coatings hardness are shown in figure (4-35) to (4-36). It can be observed that the coatings hardness were in the range (154.7- 1700.7 HV) proving the success of the study in the deposition of ceramic coatings by MAO process using natural rock additive modified electrolyte containing calcite, thassos and bauxite additives. Measuring the hardness of a coating produced through the Micro-Arc Oxidation (MAO) process after post-treatment with a fatty acid can be challenging since the presence of the fatty acid may affect the coatings properties.

Generally, the higher hardness was obtained for the coatings deposition using calcite, thassos and bauxite modified electrolytes (1700.7 HV for EFG3 coating at 10g/L calcite, 7g/L, thassos and 5g/L bauxite) at 45 min. Due to the nature of these hard ceramic particles in providing the substrate material with improved mechanical properties.

The presence of MgO micro particles had a significant impact on the hardness of the MAO coatings [94]. Hardness of the coatings displayed an upward trend. In summary, the micro-arc discharge during the MAO process caused an increase in the Si content, particularly in the SiO_2 form, within the coatings [95]. This suggests a correlation between the composition of the coatings and their mechanical properties, specifically hardness. The exact mechanism behind this correlation could involve the interaction between Si content, MgO particles and the coatings structural properties [89] as shown in EDS and SEM images.

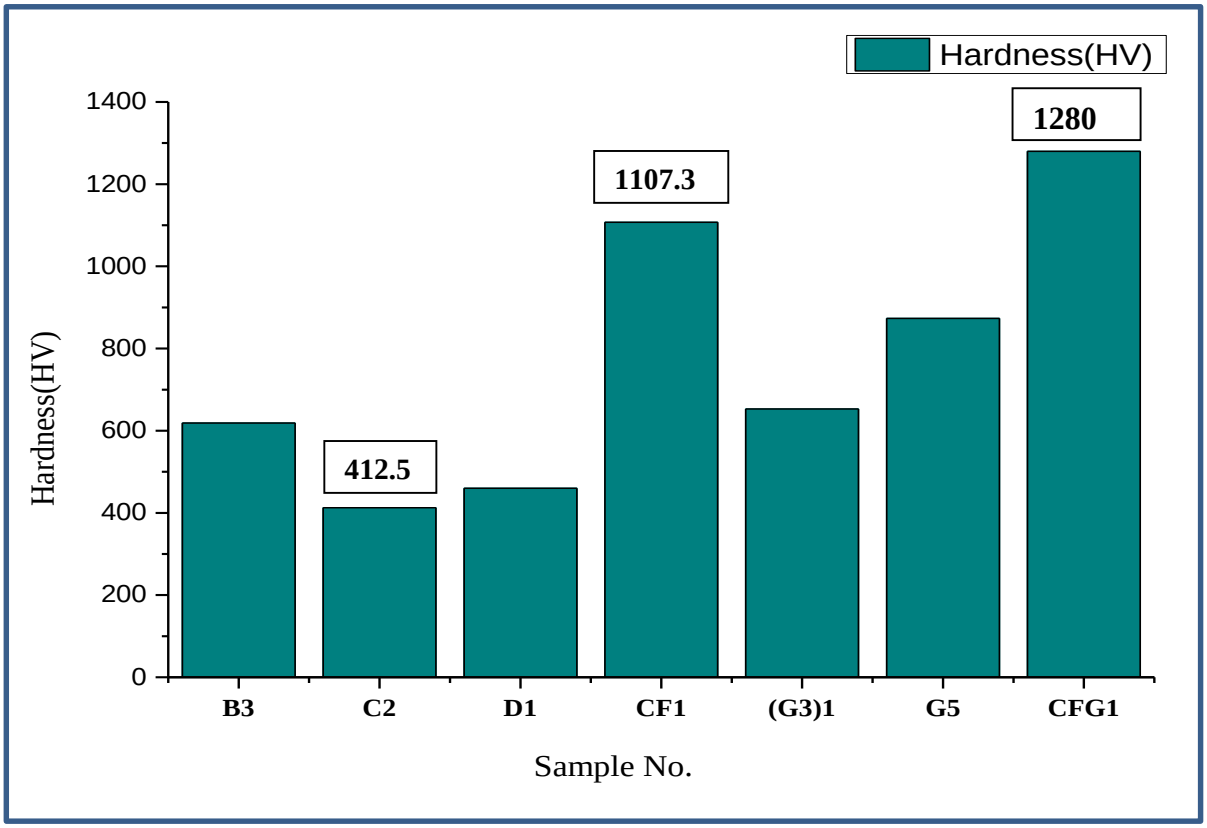

Figure (4-35): Hardness results for coatings using calcite, thassos and bauxite modified electrolyte at 15 min.

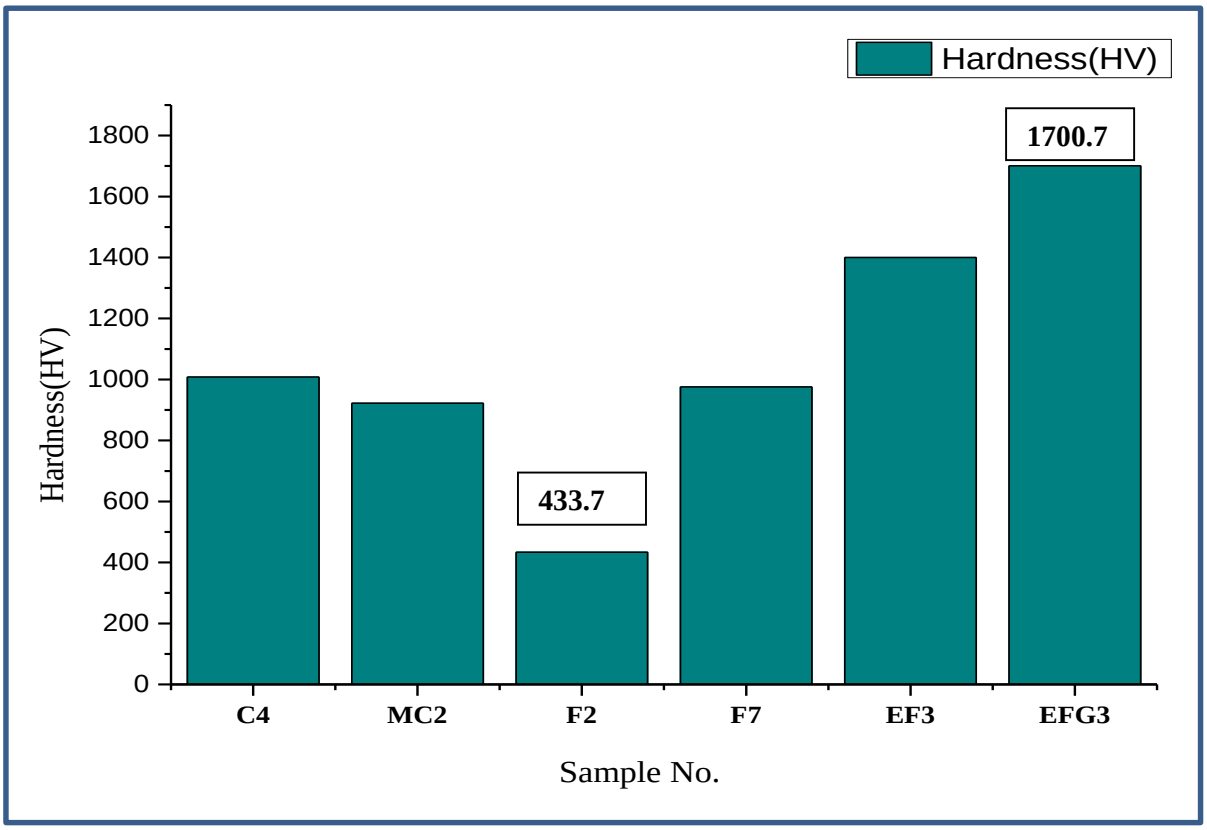

Figure (4-36): Hardness results for coatings using calcite, thassos and bauxite modified electrolyte at 45 min.

For the coatings deposited using basic electrolyte, the coating hardness were in the range (154.7-1008.3 HV) and the C4 (at 10g/L calcite) coating recorded the highest hardness among the others. Also, for coating D1 (at 15g/L calcite), it can be observed that the coating hardness decreased from 1008.3 HV to 460.1 HV with deposition time decreased from 45 min to 15 min. The decrease in hardness with reduced deposition time for coating implies that longer deposition times may contribute to a denser and harder coating. While shorter times result in thinner coatings with more pronounced porosity [96] as shown in the SEM images increased micro pores. For the coatings deposited using thassos modified electrolytes, the coatings hardness were in the range (246.9 HV- 975.9HV) and the F7 (at 7g/L thassos) coatings showed the highest hardness among the others.

For coatings F2 (at 2g/L thassos), it can be observed the coating hardness increased from 433.7 HV to 975.9 HV with increasing deposition time and addition ratio, due to the microstructure of the coating being altered by the incorporation of thassos particles into the coating. The compatibility between the particles and the coating matrix is crucial to ensure that the particles were effectively distributed throughout the coating. These particles could act as nucleation sites for crystal growth, leading to a more refined and organized microstructure that contributes to hardness improvement [97].

Furthermore, for the coatings deposited using calcite and thassos modified electrolytes, the coatings hardness were in the range (1107.36 HV -1400 HV) and the EF3 coating (at 10g/L calcite and 7g/L thassos) with deposition time to 45 min showed the highest hardness among the others. Also, for coatings CF1 (at 20g/L calcite and 3g/L thassos), it can be noted that the coating hardness increased from 1107.36 HV to 1400 HV with deposition time increasing from 15 min to 45 min. Because of the nature of those hard ceramic particles in providing the matrix material with improved mechanical properties including hardness and the coating thickness as explained previously [98].

In addition, for the coatings deposited using bauxite modified electrolytes, the coatings hardness were in the range (431.45 HV - 873.16 HV) and the G5 coating (at 5g/L bauxite) recorded the highest hardness for comparison among the others. As, for coating (G3)1 (at 3g/L bauxite), it can be observed that the coating hardness increased with depositing time to 15 min, due to the compatibility and distribution of bauxite particle size create a denser and less porous coating structure as shown in SEM image. For the coatings deposited using calcite, thassos and bauxite modified electrolytes, the coatings hardness were in the range (1280 HV- 1700.7 HV) and the EFG3 coatings (at 10 g/L calcite, 7g/L thassos and 5g/L bauxite) showed the highest hardness among the others.

Also, for coatings CFG1 (at 20g/L calcite, 3g/L thassos and 3g/L bauxite), it is clearly that the coating hardness increased from 1280 HV to 1700.7 HV with increasing deposition time from 15 min to 45 min.

4-8: AFM and Roughness Results

The Atomic Force Microscope (AFM) is a powerful tool for characterizing the surface topography and morphology of various materials, including coatings. The AFM images revealed the form and particle size distribution of the coated layer, which represented the asperities cups of the surface.

Figures (4-37) to (4-41) and table (4-10) show the results of AFM test. It can be observed from the figures, that the coating was dense with cups had different mean diameters and distribution in the surface topography. Such cups and their characterization by means of diameter (nm) and density (particles/mm^2) were given in table (4-10). In general, results of densities from table are in aggreament with those can be observed at the figures, Furthermore, the F7 coatings modified by thassos additives recorded the highest density among the others, while the G5 coatings modified by bauxite addition exhibited the lowest value, and there by the lowest contact angle (46.706°). CFG1 coatings topography showed mean diameter and density of 120.2 nm and 7066174 particles/ mm^2 respectively, which resulted in the highest contact angle (113.90°) among the other coatings. In addition, coatings modified by calcite addition showed less roughness and mean diameters with good densities in comparison to other coatings, because of the coating grown on the surface have a rough surface depending on the phenomenon of micro discharge resulting from the nature of MAO process [99]. Most likely, the calcite incorporation in coating layers were expected to have its significant effects on mechanical properties hardness and corrosion behavior in comparison to other properties such as (Ra) [100].

Seemingly, contact angle results and self-cleaning property were strongly affected by roughnesses, mean diameters and densities of the asperities at the surface topography. As in the lotus effect that in a natural phenomenon could observed on the surface of the lotus flower leaves and refers to the high water repellence they exhibit. Such repellency was originated due to formation of many nanostructured asperities with certain roughness, diameters and densities.

Table (4-10): AFM results.

Coating NO	**Ra (nm)**	**Mean diameter of particles (nm)**	**Density Particles/ mm^2**	**Contact angle (°)**
B3	69.46	175.3	4898730	78.113
C2	37.97	88.75	6408399	90.789
C4	53.75	99.9	9953720	80.787
D1	62.41	116.6	7177066	96.344
F2	113.4	278.2	1376657	94.733
F7	79.42	108	10886559	88.901
CF1	240.3	116.1	6472990	108.501
EF3	109.2	228.3	1953271	81.069
(G3)1	136.1	167.3	3897301	103.526
G5	186.1	354.4	1226169	46.706

CFG1	172.7	120.2	7066174	113.907
EFG3	110.9	231.6	3211679	96.437

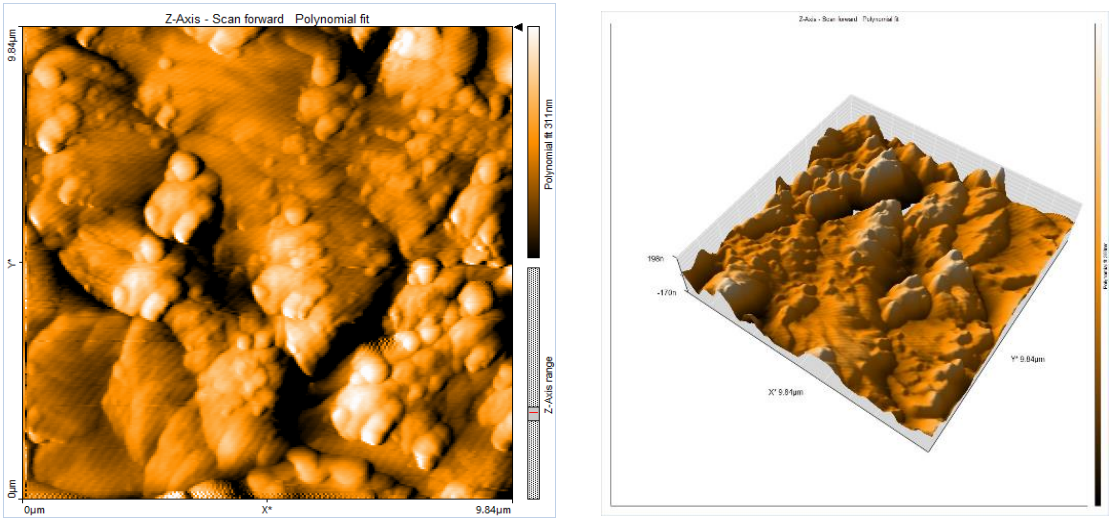

AFM image of B3 at 15 min

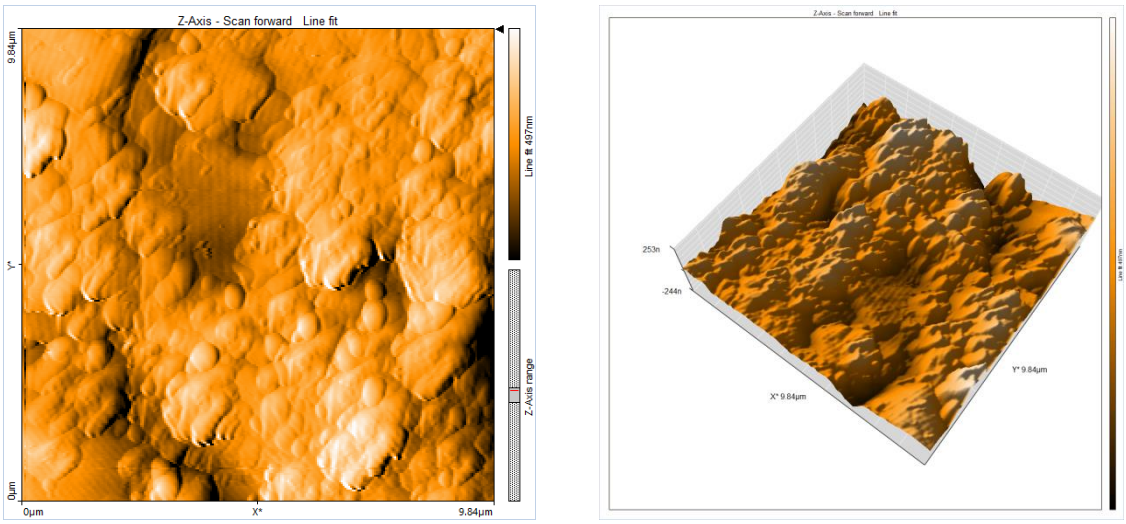

AFM image of C2 at 15 min.

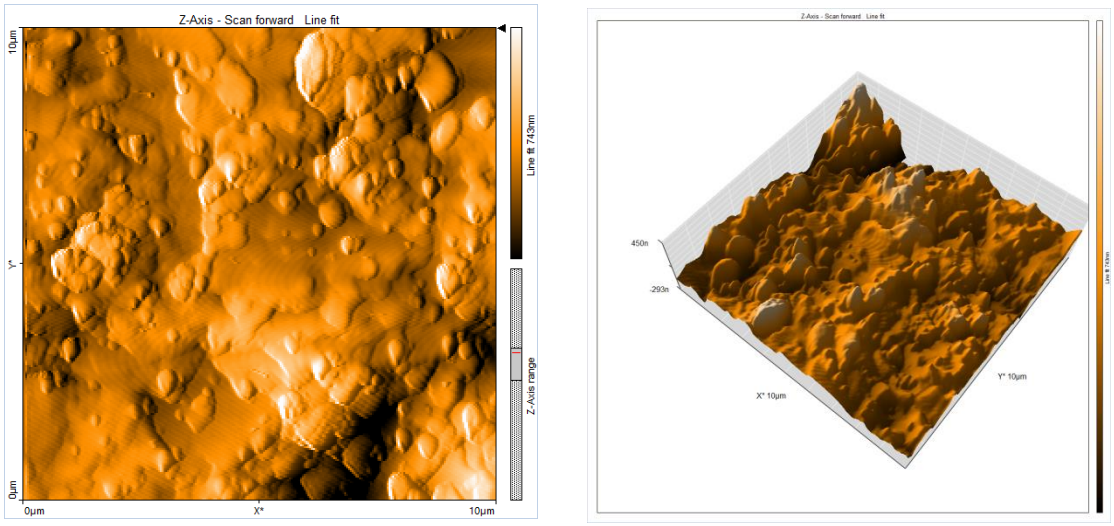

AFM image of C4 at 45 min.

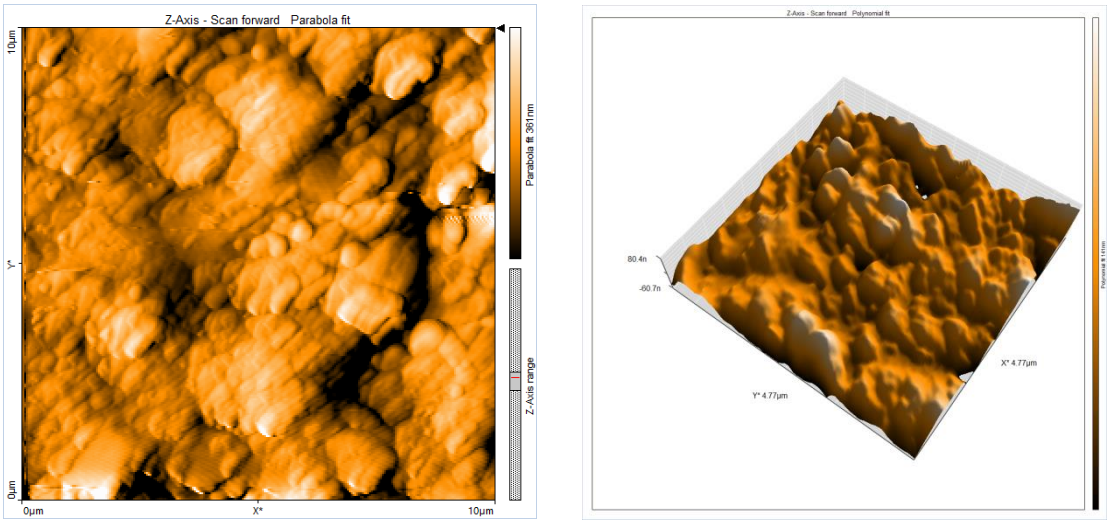

AFM image of D1 at 15 min.

Figure (4-37): AFM results for coatings using calcite basic electrolyte.

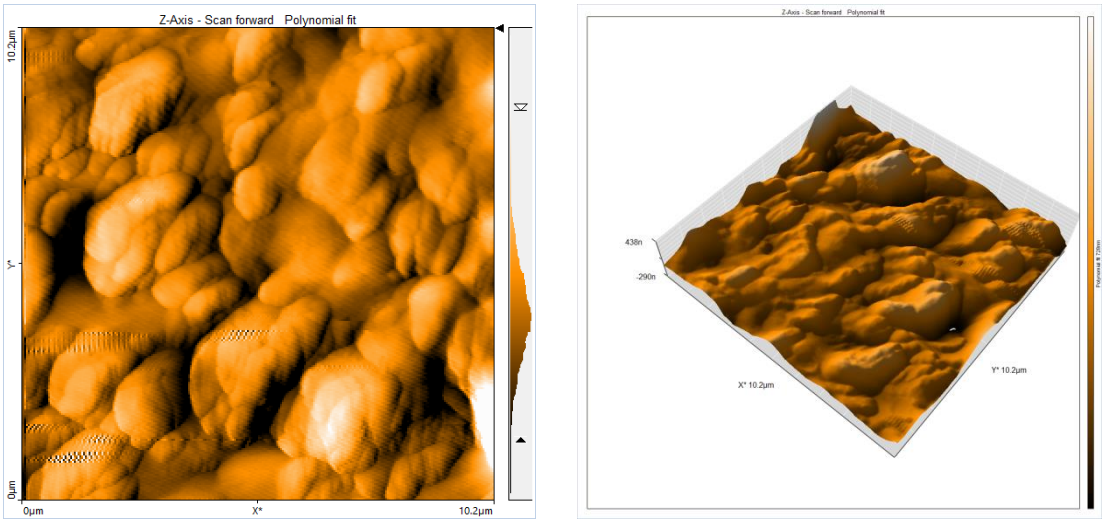

AFM image of F2 at 45 min.

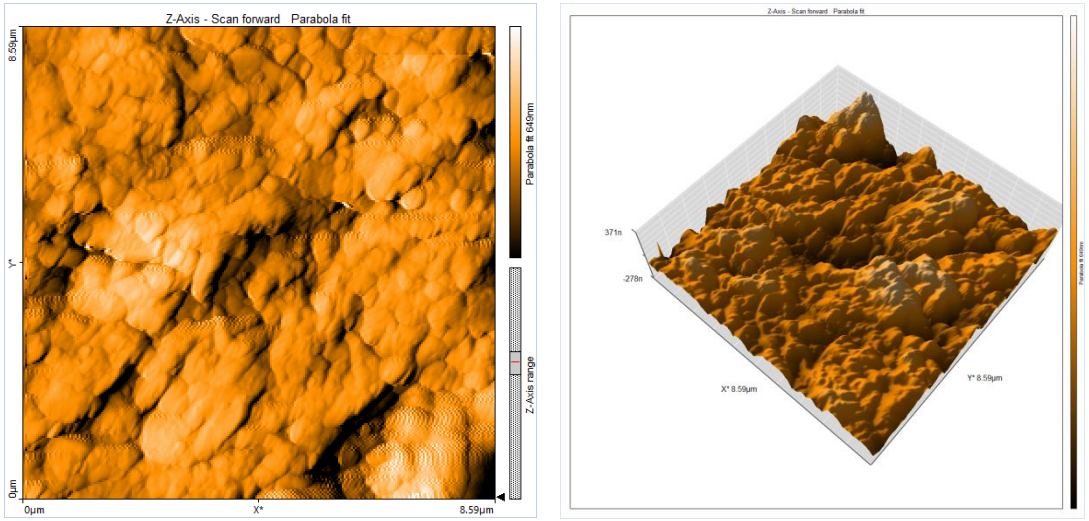

AFM image of F7 at 45 min.

Figure (4-38): AFM results for coatings using thassos modified electrolyte.

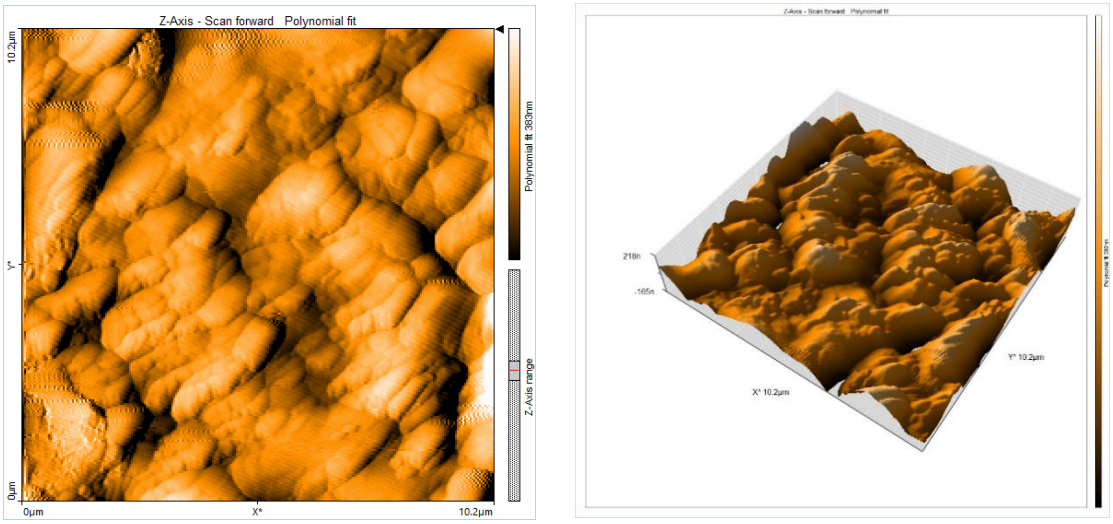

AFM image of CF1 at 15 min.

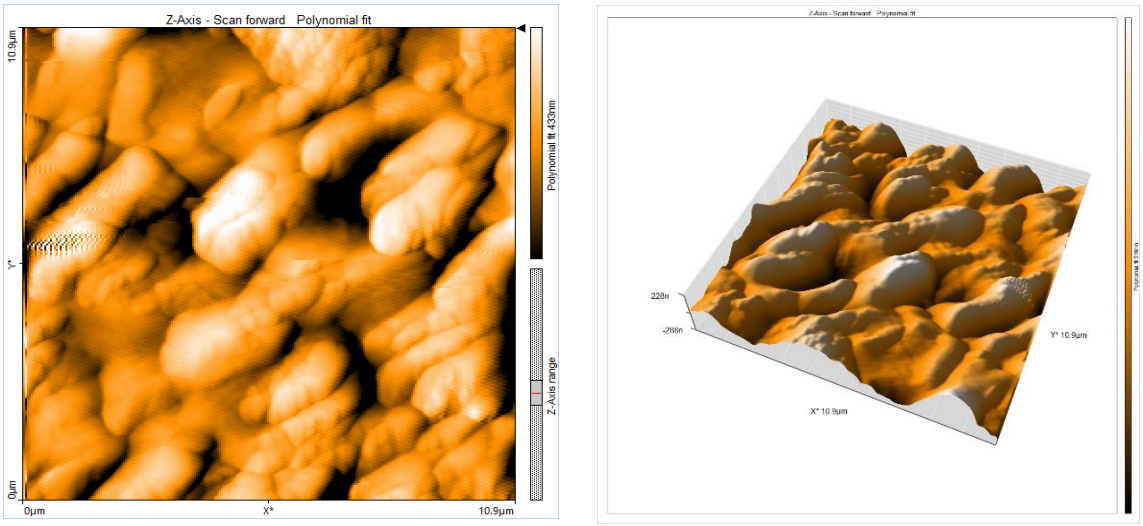

AFM image of EF3 at 45 min.

Figure (4-39): AFM results for coatings using calcite and thassos modified electrolyte.

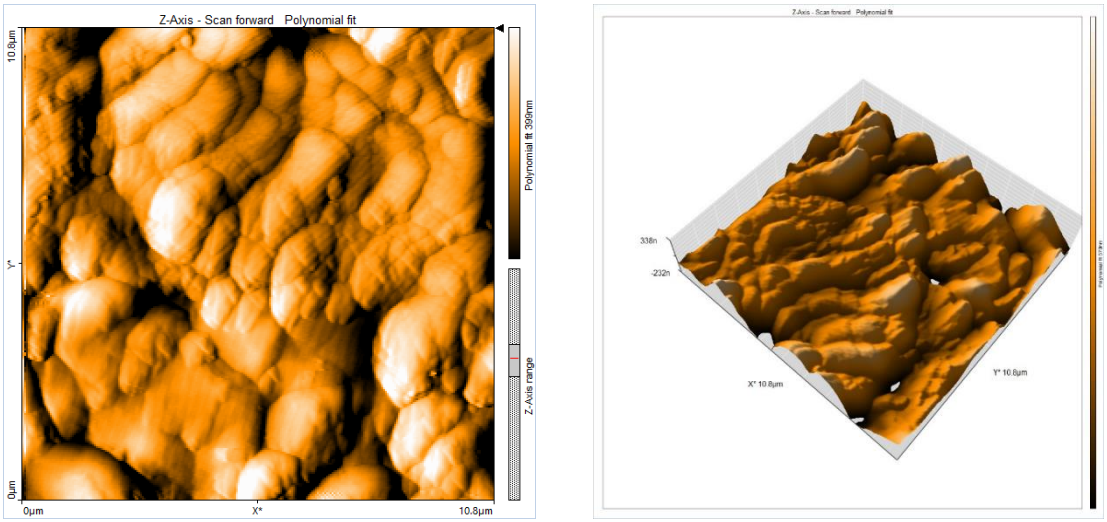

AFM image of (G3)1 at 15 min.

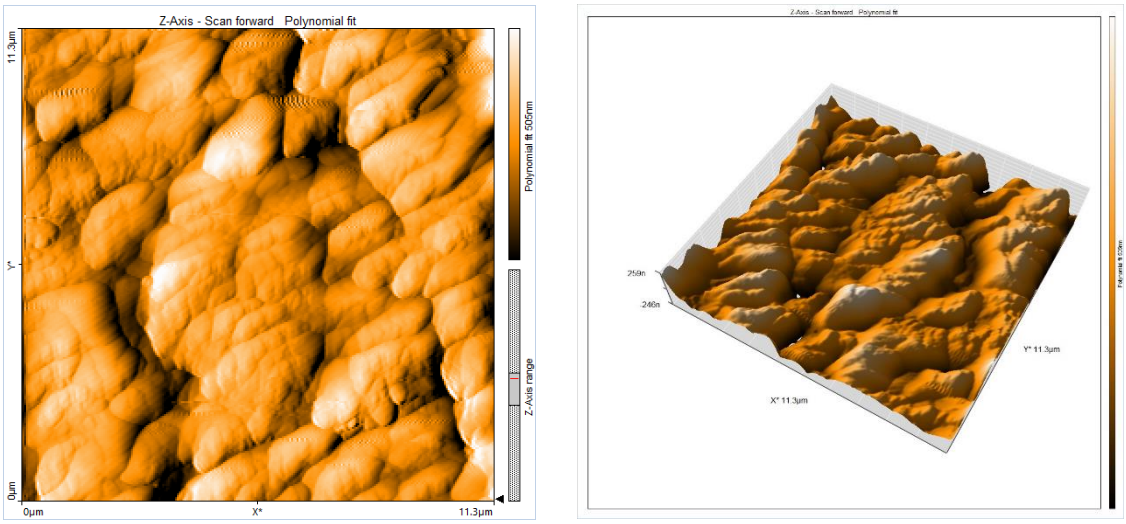

AFM image of G5 at 15 min.

Figure (4-40): AFM results for coatings using calcite and thassos modified electrolyte.

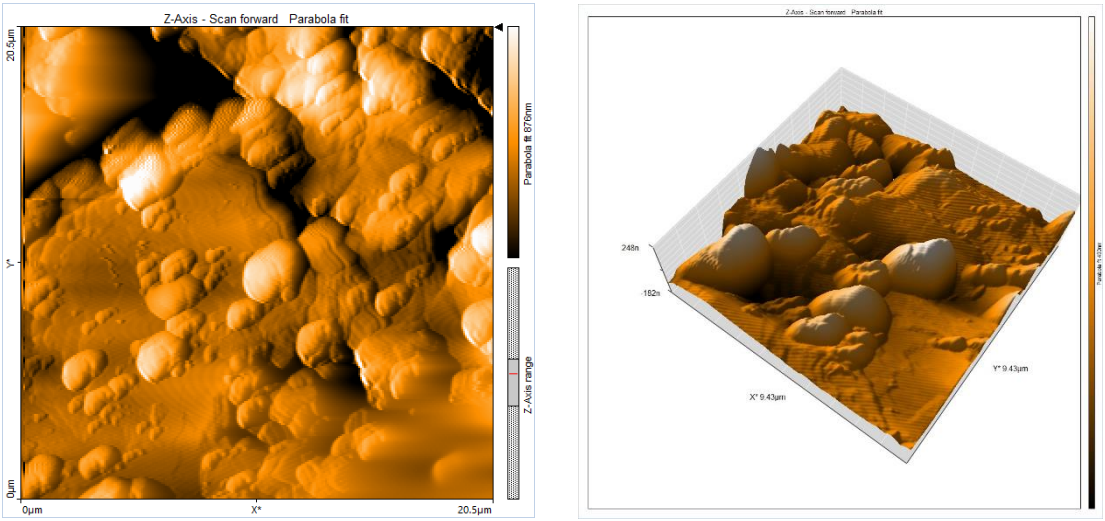

AFM image of CFG1 at 15 min.

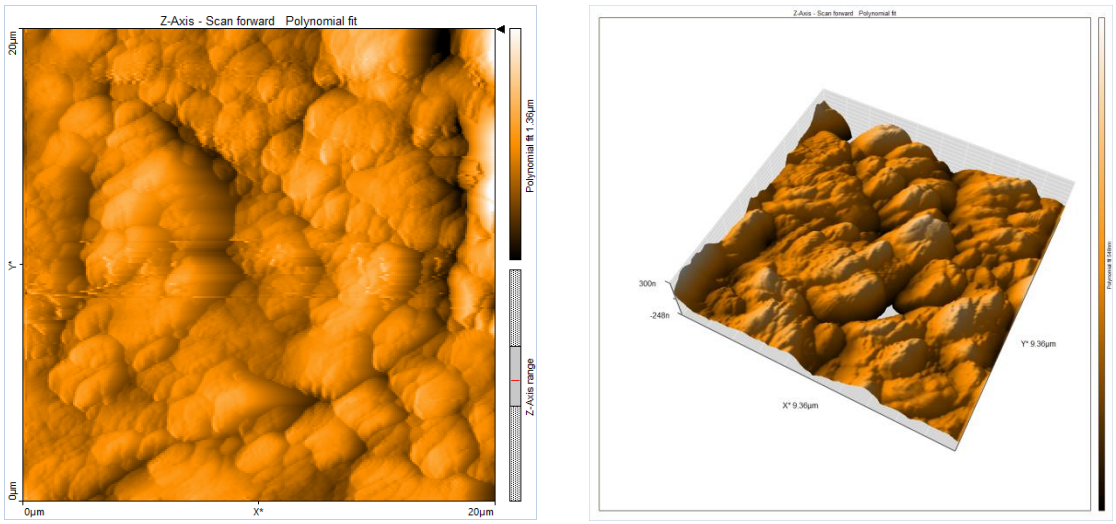

AFM image of EFG3 at 45 min.

Figure (4-41): AFM results for coatings using calcite, thassos and bauxite modified electrolyte.

4-9: Contact Angles (CA) Results

The wettability of surfaces was determined by the contact angle test after MAO coating and post-treatment, as explained in chapter 3. All coated specimens were examined to evaluate the properties of a surface. Whether it is hydrophilic or hydrophobic, results of coatings CA are shown in table (4-11) to (4-15) and figures (4-42) to (4-46). It can be observed that the coatings contact angle was in the range (46.706°-113.90°) proving the success of the study in the deposition of ceramic coatings by MAO process using natural rock additive modified electrolyte containing calcite, thassos and bauxite additives and post-treatment by fatty acid for hydrophobic Al_2O_3 ceramic coatings. Generally, the higher contact angle was obtained for the coatings deposited using calcite, thassos and bauxite additives modified electrolytes. (113.907° for CFG1 coating at 20g/L calcite, 3g/L thassos and 3g/L bauxite) at 15min, due to each material contributed to changes in surface roughness and topography, impacting increasing contact angle as shown in the AFM image.

The compatibility and dispersion of these materials lead to even distribution within the coating matrix as shown in the SEM image. Al alloy substrates after coating owns CA of (0.000), due to the coating formed by MAO is usually porous and rough, which the water drop was absorbed by the sample surface and does not allow the formation of a drop on the surface before coating. After several experiments, we achieved post treatment of MAO coatings using fatty acids because treatment layer work on closing all the pores at the substrates surfaces.

For the coatings deposited using calcite electrolytes, the contact angles were in the range (78.113°-96.977°) and the E (at 20 g/L calcite) coating showed the highest contact angle among the others.

Also, for coatings B3 (at 3g/L calcite) the least contact angle among the coatings, it can be noticed that D1(at 15g/L calcite) the coatings contact angle increased from 78.113° to 96.344° with increasing addition ratio from 3g/L to 15g/L and deposition time to 15min. When adding $CaCO_3$ due to the topography of the surface of the particles that make up the surface of the coatings and less roughness values, it gives the best result for the contact angle among the others additives as shown in particle analysis of AFM test.

Table (4-11): ***Contact angle results for coatings using calcite basic electrolyte.***

Sample No.	Time (min)	Calcite ratio (g/L)	Contact angle (°) before post treatment	Contact angle (°) after post treatment
B7	15	7	0	90.067^{O}
C2	15	10	0	90.789^{O}
D1	15	15	0	96.344^{O}
E	45	20	0	96.977^{O}

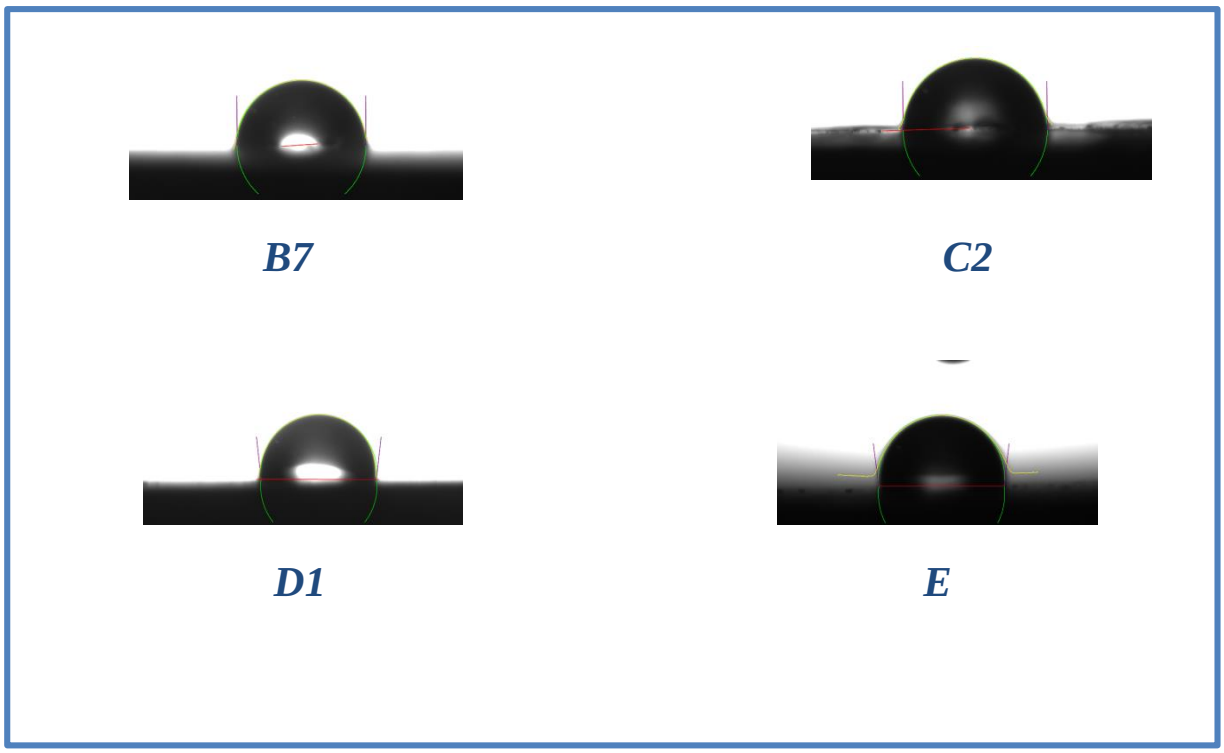

Figure (4-42): Contact angle results for coatings using calcite basic electrolyte at 15min, and 45 min.

As, for the coatings deposited using thassos modified electrolytes, the coatings contact angle were in the range (80.764°-95.120°) and the (F3)4 coating (at 3g/L thassos) showed the highest among other. As, for coatings F2 and (F3)4 (at 2g/L and 3g/L thassos) it can be exhibited the contact angle increased from 94.773° to 95.120° with deposition time to 45 min. While the F5 (at 7g/L thassos) coating recorded contact angle decreased from 95.120° to 90.326°.

Table (4-12): ***Contact angle results for coatings using thassos modified electrolyte.***

Sample No.	Time (min)	Thasoss ratio (g/L)	Contact angle (°) before post treatment	Contact angle (°) after post treatment
F2	45	2	0	94.773^{O}
(F3)4	45	3	0	95.120^{O}
F5	45	5	0	90.326^{O}

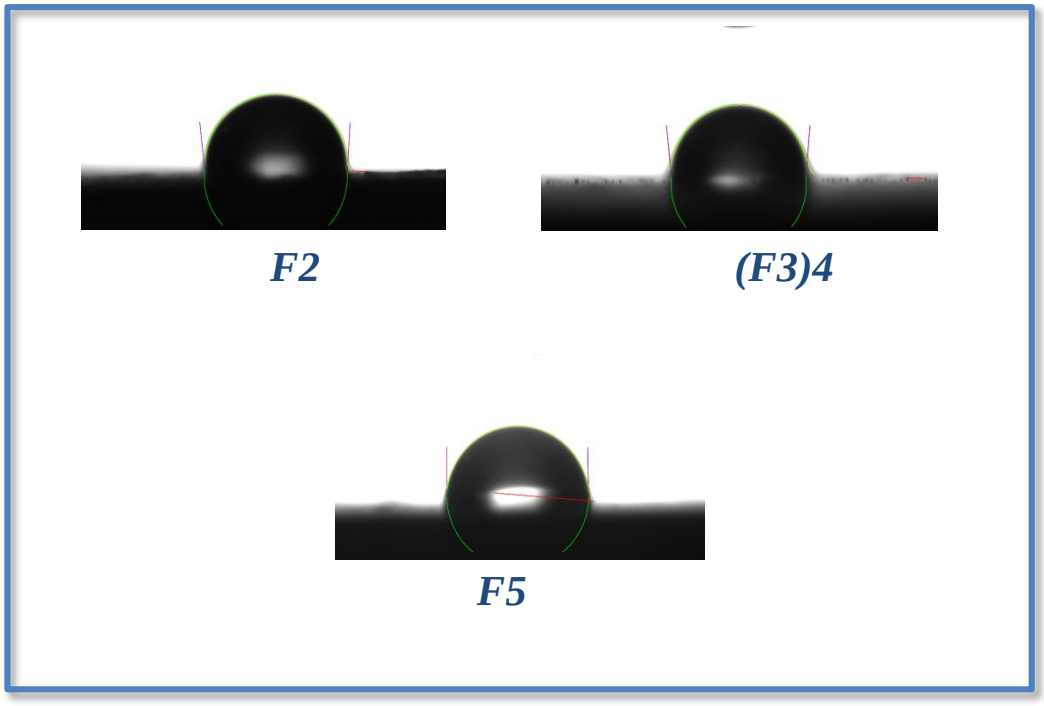

Figure (4-43): Contact angle results for coatings using thassos modified electrolyte at 45 min.

As, for the coatings deposited using calcite and thassos modified electrolytes, the coatings contact angle were in the range (81.069°-108.501°) and the CF1 coating (at 20g/L calcite and 3g/L thassos) showed the highest roughness value and thickness among the coatings. As, for coatings EF1 (10g/L calcite and 7g/L thassos) it can be exhibited the contact angle decreased from 108.501° to 90.535° with deposition time 15 min.

Table (4-13): ***Contact angle results for coatings using calcite and thassos modified electrolyte.***

Sample No.	Time(min)	Thasoss ratio (g/L)	CaCO3 ratio (g/L)	Contact angle (°) before post treatment	Contact angle (°) after post treatment
CF1	15	3	20	0	108.501^{O}
EF1	15	7	10	0	90.535^{O}

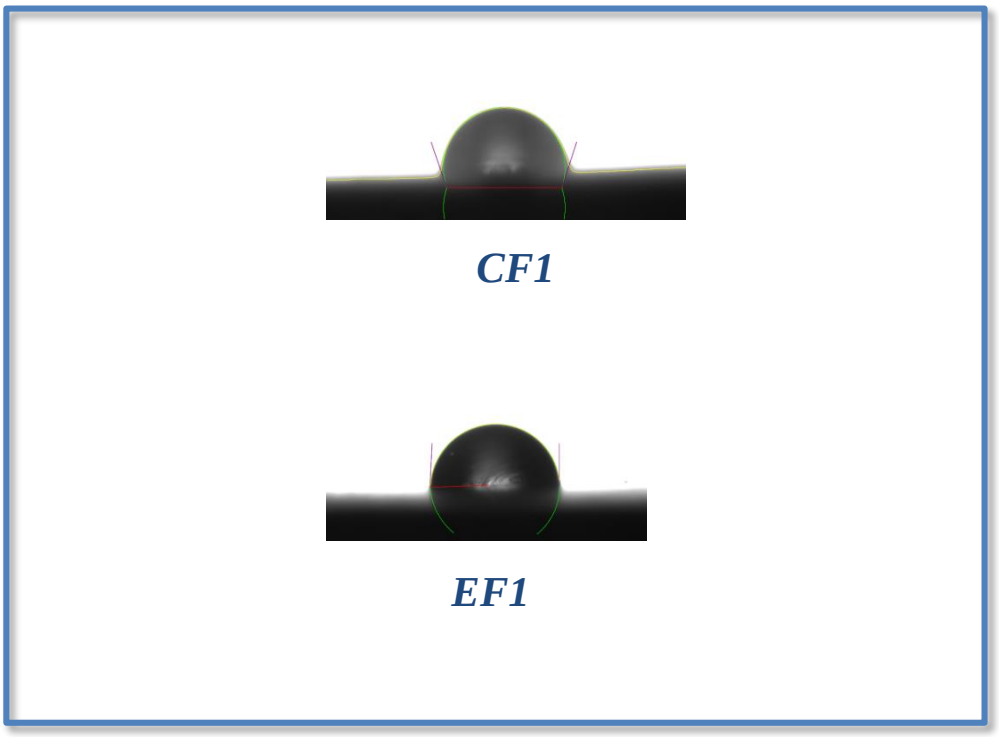

Figure (4-44): Contact angle results for coatings using calcite and thassos modified electrolyte at 15 min.

Where in, for the coatings deposited using bauxite modified electrolytes, the coatings contact angle were in the range (46.706°-103.526°) and the (G3)1 coating (at 3g/L bauxite) showed the highest contact angle among the coatings. As, for coatings G5 (at 5g/L bauxite) it can be showed the contact angle decreased from 103.526° to 46.706° with increasing addition ratio from 3g/L to 5g/L and deposition time to 15min, due to the coatings containing bauxite, the contact angle decreased because the minerals that make up bauxite are hydrophilic .

Table (4-14): ***Contact angle results for coatings using bauxite-modified electrolyte.***

Sample No.	Time(min)	Bauxite ratio (g/L)	Contact angle (°) before post treatment	Contact angle (°) after post treatment
(G3)1	15	3	0	103.526^{O}

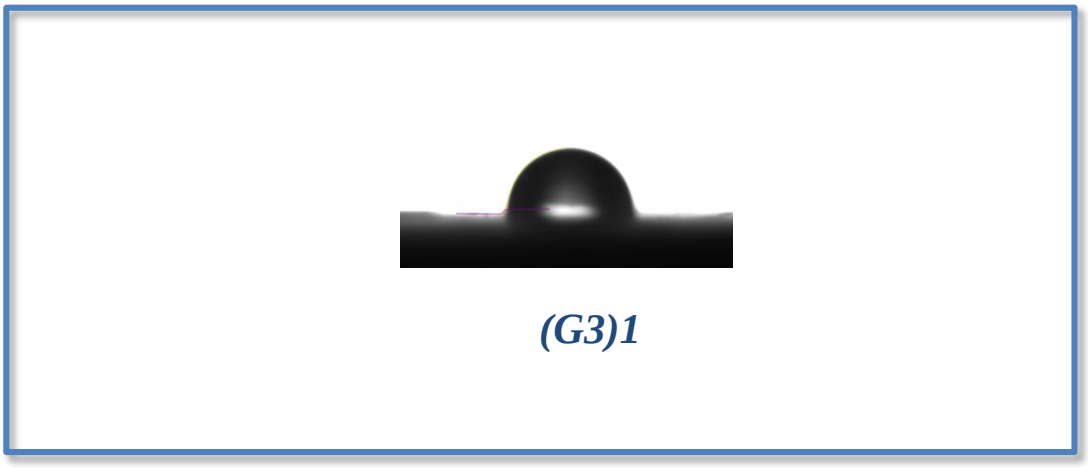

Figure (4-45): Contact angle results for coatings using bauxite-modified electrolyte at 15 min.

However, for the coatings deposited using calcite, thassos and bauxite modified electrolytes, the coatings contact angle were in the range (82.750°-113.907°) and the CFG1 coating (at 20g/L calcite, 3g/L thassos and 3g/L bauxite) showed the highest contact angle among all the coatings. As, it can be showed the contact angle decreased from 113.907° to 98.571° with increasing deposition time from 15min to 45min. Furthermore, for the EFG3 coatings (10g/L calcite, 7g/L thassos and 5g/L bauxite). It can be recorded the contact angle decreased from 103.587° to 82.750° with increasing deposition time from 15min to 45min.

Table (4-15): ***Contact angle results for coatings using calcite, thassos and bauxite modified electrolyte.***

Sample No.	Time(min)	Thasoss ratio (g/L)	$CaCO_3$ ratio (g/L)	Bauxite ratio(g/L)	Contact angle (°) before post treatment	Contact angle (°) after post treatment
CFG1	15	3	20	3	0	113.907^{O}
CFG3	45	3	20	3	0	98.571^{O}
EFG1	15	7	10	5	0	103.587^{O}
EFG3	45	7	10	5	0	96.437^{O}

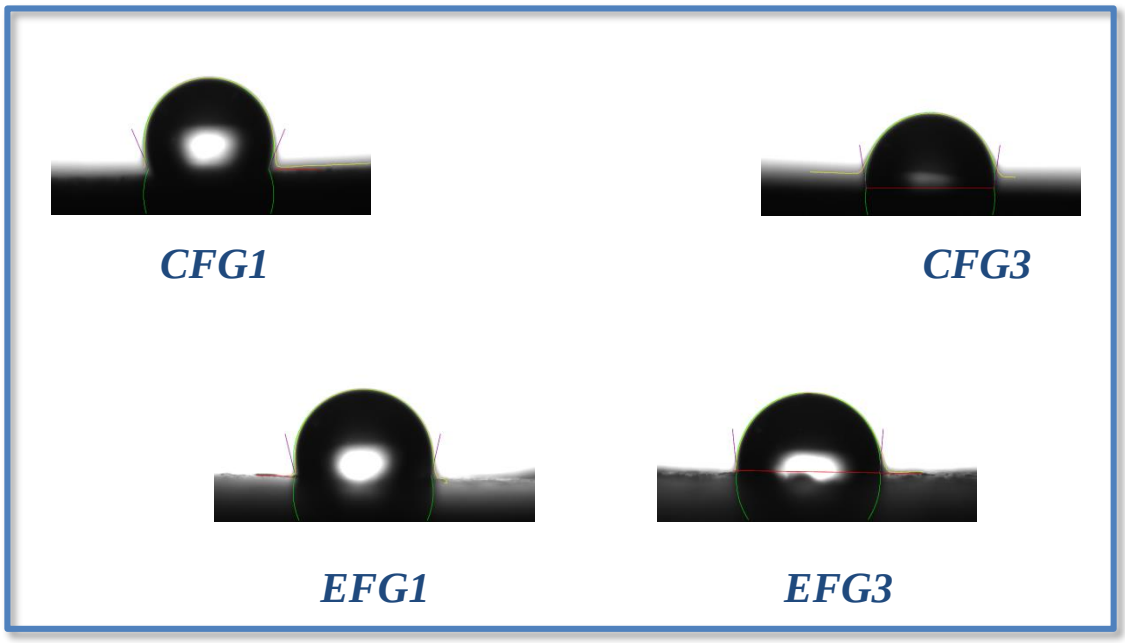

Figure (4-46): Contact angle results for coatings using calcite, thassos and bauxite-modified electrolyte at 15 min and 45min.

4-10: Corrosion Result

Tafel plots from electrochemical tests are used to determine anodic and cathodic processes. Corrosion current (I-corr) was obtained from these plots for both uncoated and MAO-coated substrates. Linear polarization results as shown in table (4-16) and figure (4-47). The natural rock additives (calcite, thassos, and bauxite) lead to a significant shift toward lower current densities. The Al alloy has the highest i_corr value, indicating greater susceptibility to pitting corrosion compared to MAO-treated specimens. Corrosion potential values for coated specimens range from 8.48 nA for CFG1 coating (3g/L thassos, 20g/L calcite and 3g/L bauxite) showed lower corrosion resistance compared to 8.49 nA for EFG3 coating (at 7g/L thassos, 10g/L calcite, and 5g/L bauxite). Results in table (4-16) indicate that CFG1 coating is more efficient; due to CFG1 coating exhibits the highest contact angle 113.907°, which valuable for corrosion resistance. A higher contact angle helps prevent water absorption into the sample, contributing to increased corrosion resistance. The MAO coating processes significantly improve the corrosion resistance of the Al alloy in the tested solutions. Natural rocks additives further enhance the protective properties of the coatings.

Table (4-16): ***Corrosion results for Al alloy and coatings using calcite, thassos and bauxite modified electrolyte.***

Sample No.	I-corr (nA)	E-corr (mV)
Al alloy	568.61	-765.0
CFG1	8.48	-626.1
EFG3	8.49	-752.3

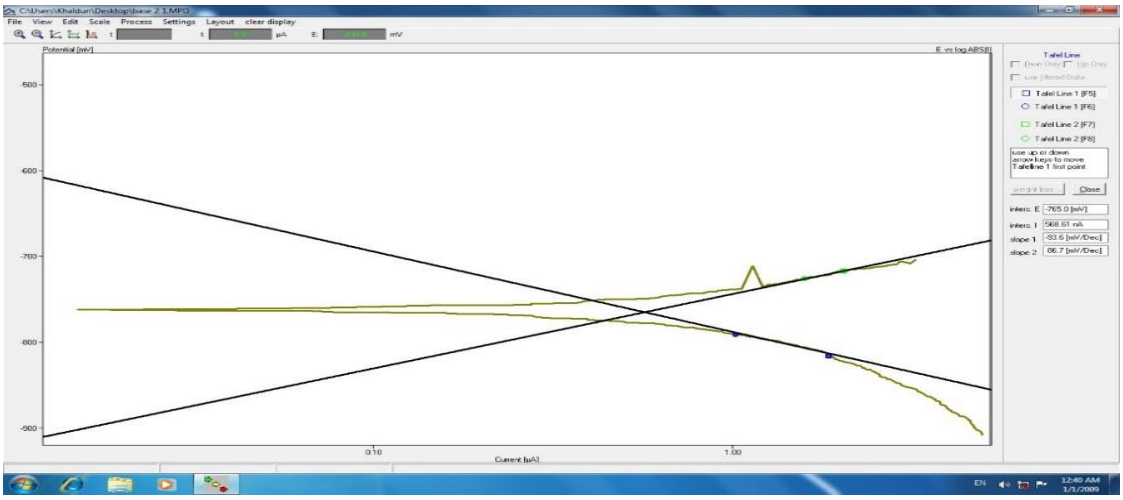

Corrosion results for Al alloy

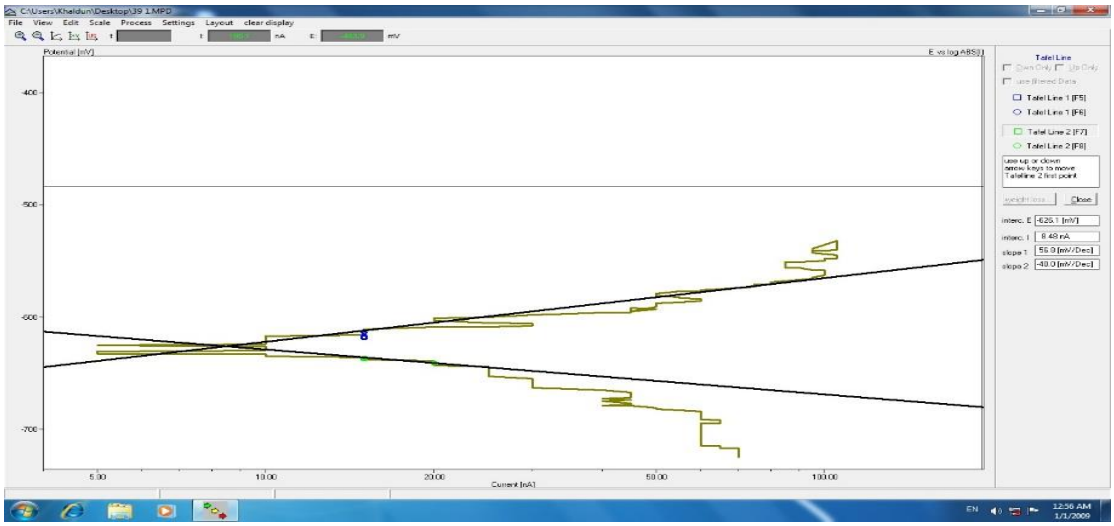

Corrosion results for CFG1

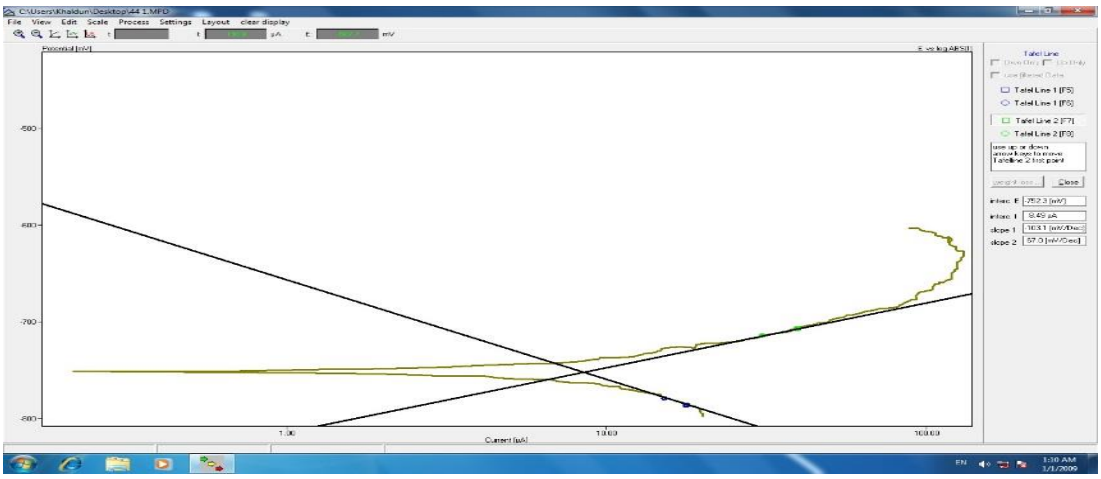

Corrosion results for EFG3

Figure (4-47) Corrosion results for Al alloy and coatings using calcite, thassos and bauxite modified electrolyte

Chapter Five

Conclusions & Recommendations

5-1: Conclusions

1- The success of the present work in using MAO technique with modified electrolytes containing Iraqi natural ceramic additives of (calcite, thassos, bauxite) and post treatments using fatty acids, specifically (mayrstic and stearic), as well as chloroform and methanol in depositing of composite ceramic Al_2O_3 coatings with notable properties of hardness and hydrophobicity together.

2- The results showed that porous and self-cleaning ceramic composite coatings with several noteworthy properties have thickness (445.2-2329 nm), hydrophobic and self-cleaning in terms of contact angle (90.004°-113.907°), hardness (154.7-1700.7 HV), roughness (37.97-240.3 Ra) values could be obtained and corrosion resistance (568.61- 8.48nA).

3- The addition (20g/L) of calcite (3g/L) of thassos and (3g/L) of bauxite led to an enhancement in the contact angle of the coating to (113.907°), which indicated the greater hydrophobicity.

4- Generally , the hardness values improved after adding bauxite (5g/L), calcite (10g/L) and thassos(7g/L) to electrolytes provided the highest hardness of coatings (1700.7 HV).

5- The higher finding for contact angle was found at a deposition time of 15 min, whereas the greatest results for hardness were found at a coating deposition time of 45 min.

6- Due to The morphology of the coated surfaces, which was characterized by irregularity and the formation of lumps of additives on the surface, the addition of 1g of MOS_2 did not produce the desired effects of the contact angle with addition of calcite and thassos of (10, 3) g/L respectively, while on improve in hardness to (750.8 HV) and (922.26 HV), could be obtained.

7- The morphology of the coated surfaces showed a typical crater-like porous structure. Characterized by a clear and uniform distribution of (calcite, thassos and bauxite) particles evenly dispersed throughout the coating material. Overall, the porous morphology and distribution of particles in the coated surfaces suggest that the coatings have unique microstructures that can influence their performance characteristics in self-cleaning.

8- XRD and EDS results proved the deposition of γ- Al2O3 with different contents and other modification elements.

9- Using of rock additives calcite, bauxite and thassos improve the corrosion resistance of Al alloy, they increased corrosion resistance from (568.61nA) to (8.48nA) which prove the successes of using these additives to deposit ceramic coatings with good corrosion resistance.

10- The results showed that the research was successful in protecting the surfaces of Al alloy with self-cleaning composite coatings of high hardness , which will help to maintain environmental cleanliness and aesthetics while also protecting them from scratching and external weather conditions.

5-2: *Suggestions for Future Work*

1- Fabrication of a ceramic material of super hydrophobic properties with high hardness for a range of applications. From calcite, thassos and bauxite combines by MAO and anodizing process.

2- By integrating laser-based secondary treatments with Al alloy coatings, it can tailor the surface properties to meet specific requirements, such as superhydrophobicity (self-cleaning) and high hardness.

References

1. Wu, Y. (2022, March). Application of aluminum alloy in aircraft. In *Journal of Physics: Conference Series* (Vol. 2228, No. 1, p. 012024). IOP Publishing.

2. Polmear, I., StJohn, D., Nie, J. F., & Qian, M. (2017). *Light alloys: metallurgy of the light metals*. Butterworth-Heinemann.

3. Ali, H. M., Qasim, M. A., Malik, S., & Murtaza, G. (2018). Techniques for the fabrication of super-hydrophobic surfaces and their heat transfer applications. Heat Transf. Models Methods Appl, 1, 283-315.

4. Zheng, S., Li, C., Fu, Q., Hu, W., Xiang, T., Wang, Q& Chen, Z. (2016). Development of stable superhydrophobic coatings on aluminum surface for corrosion-resistant, self-cleaning, and anti-icing applications. *Materials & Design*, *93*, 261-270.

5. Dehnavi, V., Luan, B., Liu, X. Y., Shoesmith, D. W., & Rohani, S. (2013). Production of ceramic coatings on AA6061 aluminum alloy using plasma electrolytic oxidation. *Coatings for Corrosion and Wear-resistance Applications*.

6. Liu, S., Chen, J., Zhang, D., Wang, Y., He, Z., & Guo, P. (2022). Properties of micro-arc oxidation coatings on 5052 Al alloy sealed by SiO2 nanoparticles. *Coatings*, *12*(3), 373.

7. Wu, Y. L., Hong, J., Peterson, D., Zhou, J., Cho, T. S., & Ruzic, D. N. (2013). Deposition of aluminum oxide by evaporative coating at atmospheric pressure (ECAP). *Surface and Coatings Technology*, *237*, 369-378.

8. Lu, X., Mohedano, M., Blawert, C., Matykina, E., Arrabal, R., Kainer, K. U., & Zheludkevich, M. L. (2016). Plasma electrolytic oxidation coatings with particle additions–A review. *Surface and Coatings Technology*, *307*, 1165-1182.

9. Cao, G. P., & Song, R. G. (2018). Microstructure and properties of ceramic coatings prepared by micro-arc oxidation on 7075 aluminum alloy. *Materials Research Express*, *5*(2), 026407.

10. 10. Yilmaz, M. S., Sahin, O. (2018). Applying high voltage cathodic pulse with various pulse durations on aluminum via micro-arc oxidation (MAO). Surface and Coatings Technology, 347, 278-285.

11. Z. Kolozsváry (2013) IFHTSE Global 21: heat treatment and surface engineering in the twenty-first century, International Heat Treatment and Surface Engineering, 7:4, 152-158

12. الاكساء بالغمر" رسالة ماجستير تقدم بها المهندس زهير طالب خليف الطائي الى قسم هندسة المواد/كلية الهندسة/جامعة بابل2005

13. Awad, S. H., & Qian, H. C. Deposition of duplex Al_2O_3/TiN coatings on aluminum alloys for tribological applications using a combined microplasma oxidation (MPO) and arc ion plating (AIP). (2006). *Wear*, *260*(1), 215-222

14. Sikdar, S., Menezes, P. V., Maccione, R., Jacob, T., & Menezes, P. L. (2021).Plasma electrolytic oxidation (PEO) process—processing, properties, and applications. *Nanomaterials*, *11*(6), 1375.

15. Pfeiffer, O. P., Liu, H., Montanelli, L., Latypov, M. I., Sen, F. G., Hegadekatte, V., ... & Homer, E. R. (2022). Aluminum alloy

compositions and properties extracted from a corpus of scientific manuscripts and US patents. *Scientific Data*, *9*(1), 128.

16. Davis, J. R. (1993). *Aluminum and aluminum alloys*. ASM international.

17. "Aluminum Electrical Conductor Handbook **",** Third Edition 1989, The Aluminum Association 900 19th street, N.W., Washington, D.C. 20006.

18. Liu, R. (2009). An Overview of Aluminum Protective Coating Properties and Treatments. *OPTI, the University of Arizona*.

19. Mackenzie, D. S., & Totten, G. E. (Eds.). (2003). *Handbook of aluminum*. New York: Dekker.

20. Auerkari, P. (1996). Mechanical and physical properties of engineering alumina ceramics (Vol. 23). Espoo: Technical Research Centre of Finland.

21. Andersson, J. M. (2005). *Controlling the formation and stability of alumina phases* (Doctoral dissertation, Institutionen för fysik, kemi och biologi).

22. Riedel, R., & Chen, I. W. (Eds.). (2011). *Ceramics science and technology, volume 2: materials and properties* (Vol. 2). John Wiley & Sons.

23. Sierka, M., Döbler, J., Sauer, J., Santambrogio, G., Brümmer, M., Wöste, L& Asmis, K. R. (2007). Unexpected structures of aluminum oxide clusters in the gas phase. *Angewandte Chemie International Edition*, *46*(18), 3372-3375.

24. Ghulam, N. A., Abbas, M. N., & Sachit, D. E. (2019). Preparing of Alumina From Aluminium Waste. *Int. J. Innov. Sci. Res. Technol*, *4*, 32019.

25. Zahra, A. L. T., & Tammemi, Z. (2021). Nanoparticles of Alumina (Al 2 O 3): An Overview and Their Applications in Medical Surgery. *Nanomedicine*, *4*(1).

26. Fürstner, R., Barthlott, W., Neinhuis, C., & Walzel, P. (2005). Wetting and self-cleaning properties of artificial superhydrophobic surfaces. *Langmuir*, *21*(3), 956-961.

27. Lafuma, A., & Quéré, D. (2003). Superhydrophobic states. *Nature materials*, *2*(7), 457-460.

28. Ganesh, V. A., Raut, H. K., Nair, A. S., & Ramakrishna, S. (2011). A review on self-cleaning coatings. *Journal of Materials Chemistry*, *21*(41), 16304-16322.

29. Latthe, S. S., Sutar, R. S., Kodag, V. S., Bhosale, A. K., Kumar, A. M., Sadasivuni, K. K., ... & Liu, S. (2019). Self–cleaning superhydrophobic coatings: Potential industrial applications. *Progress in Organic Coatings*, *128*, 52-58.

30. Zheng, S., Li, C., Zhang, Y., Xiang, T., Cao, Y., Li, Q., & Chen, Z. (2021). A general strategy towards superhydrophobic self-cleaning and anti-corrosion metallic surfaces: An example with aluminum alloy. *Coatings*, *11*(7), 788.

31. Baudrand, D. (2005). Conversion coatings for aluminum and magnesium. *Plating and surface finishing*, *92*(1), 30-34.

32. Hussein, R. O., & Northwood, D. O. (2014). Production of anti-corrosion coatings on light alloys (Al, Mg, Ti) by plasma-electrolytic oxidation (PEO). *Developments in corrosion protection*, 201-239.

33. Sankara Narayanan, T. S. N. (2005). Surface pretretament by phosphate conversion coatings-A review. *Reviews in Advanced Materials Science*, *9*, 130-177.

34. Miramontes, J. C., Gaona Tiburcio, C., García Mata, E., Esneider Alcála, M. Á., Maldonado-Bandala, E., Lara-Banda, M., ... & Almeraya Calderón, F. (2022). Corrosion Resistance of Aluminum Alloy AA2024 with Hard Anodizing in Sulfuric Acid-Free Solution. *Materials*, *15*(18), 6401.

35. Bhat, K. U., Panemangalore, D. B., Kuruveri, S. B., John, M., & Menezes, P. L. (2022). Surface modification of 6xxx Series aluminum alloys. *Coatings*, *12*(2), 180.

36. Li, L., Yang, E., Yan, Z., Xie, X., Wei, W, Li, W. (2022). Effect of Pre-Anodized Film on Micro-Arc Oxidation Process of 6063 Aluminum Alloy. *Materials*, *15*(15), 5221.

37. Tian, J., Luo, Z., Qi, S., & Sun, X. (2002). Structure and antiwear behavior of micro-arc oxidized coatings on aluminum alloy. *Surface and Coatings Technology*, *154*(1), 1-7.

38. Akbar, A., Qaiser, M. A., Hussain, A., Mustafa, R. A., & Xiong, D. (2017). Surface modification of aluminum alloy 6060 through plasma electrolytic oxidation. *International Journal of Engineering Works*, *4*(6), 114-123.

39. XUE W, WANG C, LI Y. Effect of micro-arc discharge surface treatment on the tensile properties of Al-Cu-Mg alloy [J]. Materials Letters, 2002,56: 737-743.

40. Yuting, D., Zhiyang, L., & Guofeng, M. (2020). The research progress on micro-arc oxidation of aluminum alloy. In *IOP Conference Series: Materials Science and Engineering* (Vol. 729, No. 1, p. 012055). IOP Publishing.

41. Yao, M., Chen, J., Yang, P., Shan, W., Hu, B., & Yao, X. (2013). Preparation and breakdown property of aluminum oxide thin films deposited onto anodized aluminum substrate. *Ferroelectrics*, *455*(1), 21-28.

42. Fotovvati, B., Namdari, N., & Dehghanghadikolaei, A. (2019). On coating techniques for surface protection: A review. *Journal of Manufacturing and Materials processing*, *3*(1), 28.

43. Zhang, J., Dai, W., Wang, X., Wang, Y., Yue, H., Li, Q., ... & Li, C. (2023). Micro-arc oxidation of Al alloys: Mechanism, microstructure, surface properties, and fatigue damage behavior. *Journal of Materials Research and Technology*.

44. Arslan, E., Totik, Y., Demirci, E. E., & Efeoglu, I. (2013). Wear and adhesion resistance of duplex coatings deposited on Ti6Al4V alloy using MAO and CFUBMS. *Surface and Coatings Technology*, *214*, 1-7.

45. Cenk MISIRLI Trakya University Faculty of Eng. and Arch. Dept. Mech. Eng. 22180, Edirne-Turkey, A GENERAL OVERWIEV OF THE MAO PROCESS ON ALUMINUM ALLOYS, INTERNATIONAL SCIENTIFIC CONFERENCE 19 – 20 November 2010, GABROVO.

46. Rodriguez, L., Paris, J. Y., Denape, J., & Delbé, K. (2023). Micro-Arcs Oxidation Layer Formation on Aluminium and Coatings Tribological Properties—A Review. Coatings, 13(2), 373.

47. Golubkov, P. E., Pecherskaya, E. A., Shepeleva, Y. V., Martynov, A. V., Zinchenko, T. O., & Artamonov, D. V. (2018, December). Methods of applying the reliability theory for the analysis of micro-arc oxidation process. In *Journal of Physics: Conference Series* (Vol. 1124, No. 8, p. 081014). IOP Publishing.

48. Yang, G., Lü, X., Bai, Y., Cui, H., & Jin, Z. (2002). The effects of current density on the phase composition and microstructure properties of micro-arc oxidation coating. *Journal of Alloys and Compounds*, *345*(1-2), 196-200.

49. Li, Z. Y., Cai, Z. B., Cui, Y., Liu, J. H., & Zhu, M. H. (2019). Effect of oxidation time on the impact wear of micro-arc oxidation coating on aluminum alloy. *Wear*, *426*, 285-295.

50. Yang, H., Wang, X., Zhu, Z., & Liu, R. (2022). Discharge Characteristic of Micro-Arc Oxidation on Aluminum Alloy under the Changing Electrolyte Temperature. *Journal of Materials Science and Chemical Engineering*, *10*(11), 24-35.

51. Jin, S., Ma, X., Wu, R., Wang, G., Zhang, J., Krit, B., ... & Liu, B. (2022). Advances in micro-arc oxidation coatings on Mg-Li alloys. *Applied Surface Science Advances*, *8*, 100219.

52. W. Gebarowski, and S. Pietrzyk, "Growth characteristic of formation the oxide layer on aluminum the process of plasma electrolytic oxide" 2014, Archives of metallurgy and materials Vol. 59, Issue 1

53. A.L. Yerokhin, X. Nie, A. Leyland, A. Matthews, and S.J. Dowey, "Plasma electrolysis for surface engineering", 1999, Surface and Coatings Technology, 122,73-93.

54. Voevodin, A. A., Yerokhin, A. L., Lyubimov, V. V., Donley, M. S., & Zabinski, J. S. (1996). Characterization of wear protective Al□ Si□ O coatings formed on Al-based alloys by micro-arc discharge treatment. *Surface and Coatings Technology*, *86*, 516-521.

55. Al Bosta, M. M., & Ma, K. J. (2014). Suggested mechanism for the MAO ceramic coating on aluminium substrates using bipolar current mode in the alkaline silicate electrolytes. *Applied surface science*, *308*, 121-138.

56. Joseph, K. R., & Neto, C. (2010). On the superhydrophobic properties of crystallized stearic acid. *Australian journal of chemistry*, *63*(3), 525-528.

57. Acid, L. (1987). Final report on the safety assessment of oleic acid, laurie acid, palmitic acid, myristic acid, and stearic acid. *J. Am. Coll. Toxicol*, *6*, 321-401.

58. Ott, J., Gronemann, V., Pontzen, F., Fiedler, E., Grossmann, G., Kersebohm, D. B., ... & Witte, C. (2000). Methanol. *Ullmann's encyclopedia of industrial chemistry*.

59. Watts, P., Long, G., & Meek, M. E. (2004). *Chloroform* (No. 58). World Health Organization.

60. Al Omari, M. M. H., Rashid, I. S., Qinna, N. A., Jaber, A. M., & Badwan, A. A. (2016). Calcium carbonate. *Profiles of drug substances, excipients and related methodology*, *41*, 31-132.

61. Febrida, R., Setianto, S., Herda, E., Cahyanto, A., & Joni, I. M. (2021). Structure and phase analysis of calcium carbonate powder prepared by a simple solution method. *Heliyon*, *7*(11), e08344.

62. Declet, A., Reyes, E., & Suárez, O. M. (2016). Calcium carbonate precipitation: a review of the carbonate crystallization process and applications in bioinspired composites. *Reviews on Advanced Materials Science*, *44*(1).

63. Brečević, L., Kralj, D. (2007). On calcium carbonates: from fundamental research to application. *Croatica Chemica Acta*, *80*(3-4), 467-484.

64. Al-Amer, E. M. H., & Al-Kadhemy, M. F. H. (2015). Improving the Physical Properties of Iraqi Bauxite Refractory Bricks. *Al-Nahrain Journal of Science*, *18*(3), 67-73.

65. Esham, M. I. M., Othman, M. H. D., Ismail, A. F., Rahman, M. A., Jaafar, J., & Ismail, N. J. (2019). Effect of sintering temperature on physical properties of bauxite-based hollow fiber membrane.

66. Merzah, A. S. (2017). Iraqi Bauxite and Porcalinite Rocks Based Refractory, Preparation and Studying Properties. *Al-Khwarizmi Engineering Journal*, *13*(1), 70-78.

67. Evans, K., Nordheim, E., & Tsesmelis, K. (2016). Bauxite residue management. *Light metals 2012*, 63-66.

68. Reddy, P. S., Reddy, N. G., Serjun, V. Z., Mohanty, B., Das, S. K., Reddy, K. R., & Rao, B. H. (2021). Properties and assessment of applications of red mud (bauxite residue): current status and research needs. *Waste and Biomass Valorization*, *12*, 1185-1217.

69. A Buker, R., & M Ramadhan, O. (2013). Application of Iraqi Natural Rich-Bauxite Mineral Clays doped with Chromium Oxides in Upgrading of Iraqi Kerosene. *Journal of Education and Science*, *26*(4), 21-28.

70. Connecticut Stone, ‘‘Thassos Marble.’’ https://www.connecticutstone.com/thassos-marble.

71. Khwayyir, H. H., Hachim, D. M., Aboodi, A. M., & Alwan, K. J. (2022). Investigating the Unique Thermal properties of Thassos marble. *Journal of The Institution of Engineers (India): Series D*, *103*(1), 217-224. ISO 690

72. Alghamdy, S., Alleman, J. E., & Alowaibdi, T. (2021). Cool white marble pavement thermophysical assessment at Al Masjid Al-Haram, Makkah City, Saudi Arabia. *Construction and Building Materials*, *285*, 122831.

73. De Luca, R., Barca, D., Bloise, A., Dominici, R., Lezzerini, M., Sica, M. M., & Miriello, D. (2020). Provenance of White Marbles from the Roman City of Tauriana (Palmi, Reggio Calabria, Italy). *Minerals*, *10*(4), 297.

74. Herrmann, J., & Newman, R. (2002). New sculptures in Thasian dolomite: Turkey, Greece, Egypt, Italy. *ASMOSIA V*, 215-224.

75. Maniatis, Y., Tambakopoulos, D., Dotsika, E., STEFANIDOU-TIVERIOU, T. H. (2010). Marble provenance investigation of Roman sarcophagi from Thessaloniki. Archaeometry, 52(1), 45-58.

76. Aal, A, Shoukry, H, Sayed, M, Ghramh, H. A. (2018). Physical characteristics of heat-dissipating smart marble at Al Masjid Al-Haram, Makkah City, Saudi Arabia. *Arabian Journal of Geosciences*, *11*, 1-10.

77. Vishnoi, M., Muthupandi, Murugan, S. (2017). Characterization of hydrophobic coating developed by micro arc oxidation on AA2014 alloy.

78. Al-Dulamy, N. F. S., & Rubay, S. H. A. (2017). Effects of rice husks ash addition on alumina layers deposited on 2024 aluminum alloys by micro-arc oxidation (MAO). Advances in Natural and Applied Sciences, 11(1), 19-31.

79. Farqad Saleem Murad. S. Rubay, S. H. A. (2018). Deposition of Aluminium Oxide on Al alloy by Micro Arc Oxidation using different additives.

80. Yılmaz, M. S., Şahin, O. (2019). Investigation of High Energy Single Pulse Effect on Micro Arc Oxidation (MAO) Process on Aluminum.

81. Li, X. J., Zhang, M., Wen, S., Mao, X., Huo, W. G., Guo, Y. Y., & Wang, Y. X. (2020). Microstructure and wear resistance of micro-arc oxidation ceramic coatings prepared on 2A50 aluminum alloys. Surface and Coatings Technology, 394, 125853.

82. Dong, X., Meng, J., Hu, Y., Wei, X., Luan, X., Zhou, H. (2020). Fabrication of self-cleaning superhydrophobic surfaces with improved

corrosion resistance on 6061 aluminum alloys. Micro machines, 11(2), 159.

83. Mo‹ Q.‹ Qin‹ G.‹ Wei‹ W.‹ Zhang‹ Z.‹ Li‹ W. (2022). Hydrophobic composite layers for enhancing long-term corrosion resistance of Al alloy micro-arc oxidation coating. Surface and Coatings Technology, 450, 128979.

84. Liu, C., Wen, X., Bai, P., Meng, Y., & Tian, Y. (2022). Tribological behavior of cathode plasma electrolytic deposited Al2Y4O9 coating on aluminum alloy. Journal of Bio-and Tribo-Corrosion, 9(1), 14.

85. Lv, P., Zhang, X., Yin, T., Wang, Z., Dong, Q., He, L., Zheng, S. (2023). Processing and Analysis of Micro-Arc Oxidation Coating on 319S Aluminum Alloy. Coatings, 13(6), 1024.

86. Feng, L., Che, Y., Liu, Y., Qiang, X., Wang, Y. (2013). Fabrication of superhydrophobic aluminum alloy surface with excellent corrosion resistance by a facile and environment-friendly method. Applied Surface Science, 283, 367-374.

87. Tillmann, W., Khalil, O., & Abdulgader, M. (2019). Porosity characterization and its effect on thermal properties of APS-sprayed alumina coatings. *Coatings*, *9*(10), 601.

88. Marcinauskas, L., Valatkevičius, P. (2010). The effect of plasma torch power on the microstructure and phase composition of alumina coatings. *Materials Science-Poland*, *28*(2), 451-458.

89. Lv, P., Zhang, X., Yin, T., Wang, Z., Dong, Q, He, L, Zheng, S. (2023). Processing and Analysis of Micro-Arc Oxidation Coating on 319S Aluminum Alloy. *Coatings*, *13*(6), 1024.

90. Laveissière, M., Cerda, H., Roche, J., Cassayre, L., & Arurault, L. (2019). In-depth study of the influence of electrolyte composition on coatings prepared by plasma electrolytic oxidation of TA6V alloy. *Surface and Coatings Technology*, *361*, 50-62.

91. N. Yu. Dudareva, R.V. Kalschikov, I.A. Butusov, R.R. Grin, I.V. Alexandrov, and F.F. Musin,"The Investigation of the Effect of Micro-Arc Oxidation Modes on the Adhesion Strength of Coatings", 2014, Journal of Engineering Science and Technology Review 7 (5), 5-8.

92. Grigoriev, S., Peretyagin, N., Apelfeld, A., Smirnov, A., Yanushevich, O., Krikheli, N, Peretyagin, P. (2022). Investigation of MAO coatings characteristics on titanium products obtained by EBM method using additive manufacturing. *Materials*, *15*(13), 4535.

93. Luo, S., Wang, Q., Ye, R., & Ramachandran, C. S. (2019). Effects of electrolyte concentration on the microstructure and properties of plasma electrolytic oxidation coatings on Ti-6Al-4V alloy. *Surface and Coatings Technology*, *375*, 864-876.

94. Cosan, K. A., Gunduz, K. O., Tarakcı, M., & Gencer, Y. (2022). Plasma electrolytic oxidation of as-cast and heat-treated binary Al-Ni alloys. *Surface and Coatings Technology*, *450*, 128998.

95. Li, W., Chen, Q., Shen, D., Yang, R., & Zhang, X. (2023). Composited MAO coating with SiO2 particles on TA2 alloy by laser treatment. *Surface and Coatings Technology*, *472*, 129966.

96. Peng, Z., Xu, H., Liu, S., Qi, Y., & Liang, J. (2021). Wear and corrosion resistance of plasma electrolytic oxidation coatings on 6061 Al alloy in electrolytes with aluminate and phosphate. *Materials*, *14*(14), 4037.

97. Lelevic, A. (2018). Ni-P coatings electroplating-A review, Part I: Pure Ni-P alloy. *arXiv preprint arXiv:1807.04693*.

98. Dervishi, E., McBride, M., Edwards, R., Gutierrez, M., Li, N., Buntyn, R., & Hooks, D. E. (2022). Mechanical and tribological properties of anodic Al coatings as a function of anodizing conditions. *Surface and coatings technology*, *444*, 128652.

99. Ogden, H.R. and Holden, F.C. (1958) „Metallography of titanium alloys“ (No. TML-103), Battelle Memorial Inst, Titanium Metallurgical Lab., Columbus, Ohio.

100. S. Liua, B. Lib, C. Langb, H. Wangb, Z. Qiao "Formation mechanism and adhesive strength of a hydroxyapatite/ TiO2 composite coating on a titanium surface prepared by micro-arc oxidation "Applied Surface Science 362 (2016) 109–114.

1- Mixing of basic electrolyte based on the calcite addition as shown in table Group I.

Substrate / *Materials*	*A1*	*A2*	*A3*	*A4*	*B3*	*B5*	*B7*	*C1*	C2	C3	C4	*D1*	*D2*	*E*	*MC1*	*MC2*
KH_2PO_4	*20g/L*	20g/L	20g/L	20g/L	20g/L	20g/L	20g/L	20g/L	20g/L	20g/L	20g/L	*20g/L*	*20g/L*	*20g/L*	*20g/L*	*20g/L*
KOH	*2 g/L*	2 g/L	2 g/L	2 g/L	2 g/L	2 g/L	2 g/L	2 g/L	2 g/L	2 g/L	2 g/L	2 g/L	2 g/L	2 g/L	2 g/L	2 g/L
Na_2SiO_3	—	—	—	—	—	—	—	—	—	—	—	*10g/L*	—	*10g/L*	—	—
$(NH_3)_2MO_7O_{24}$	*12g/L*	12g/L	12g/L	12g/L	12g/L	12g/L	12g/L	12g/L	12g/L	12g/L	12g/L	12g/L	12g/L	12g/L	12g/L	12g/L
H_3PO_4	*8 ml*	8 ml	8 ml	8 ml	8 ml	8 ml	8 ml	8 ml	8 ml	8 ml	8 ml	*8ml*	*8 ml*	*8ml*	*8ml*	*8 ml*
$CaCO_3$	*1g/L*	1g/L	1g/L	1g/L	3g/L	5g/L	7g/L	10g/L	10g/L	10g/L	10g/L	15g/L	15g/L	20g/L	10g/L	10g/L
MOS2	___				—	—	___	—				—	___	—	*1g/L*	*1g/L*
PH	*4-5*															
Temp.(˚C)	*20-30*	*15-20*	*15-20*	*15-20*	*15-20*	*15-20*	*15-20*	*15-20*	*15-20*	*15-20*	*15-20*	*15-20*	*15-20*	*15-20*	*15-20*	*15-20*
Time(min)	*10*	*15*	*30*	*45*	*15*	*15*	*15*	*10*	*15*	*30*	*45*	*15*	*45*	*45*	*15*	*45*
voltage	*320-330*															
current	*0.1-0.3*															

2- Mixing of Modified electrolyte by thassos addition as shown in table Group II.

Substrate / *Materials*	*F1*	*F2*	*(F3)1*	(F3)2	*(F3)3*	*(F3)4*	*F5*	*F7*	*MF1*	*MF2*
KH_2PO_4	*20g/L*	*20g/L*	*20g/L*	*20g/L*	*20g/L*	*20g/L*	*20g/L*	*20g/L*	*20g/L*	*20g/L*
KOH	*2 g/L*	*2 g/L*	*2 g/L*	*2 g/L*	*2 g/L*	*2 g/L*	*2 g/L*	*2 g/L*	*2 g/L*	*2 g/L*
Na_2SiO_3	—	—	—				*10g/L*	*10g/L*	—	—
$(NH_3)_2MO_7O_{24}$	*12g/L*	*12g/L*	*12g/L*	*12g/L*	*12g/L*	*12g/L*	*12g/L*	*12g/L*	*12g/L*	*12g/L*
H_3PO_4	*8 ml*	*8ml*	*8ml*	*8 ml*	*8 ml*	*8 ml*	*8 ml*	*8ml*	*8ml*	*8 ml*
Thassos	*1g/L*	*2g/L*	*3g/L*	*3g/L*	*3g/L*	*3g/L*	*5g/L*	*7g/L*	*3g/L*	*3g/L*
MOS_2	—	—	—				—	—	*1g/L*	*1g/L*
PH	*4-5*									
Temp.(˚C)	*15-25*	*15-25*	*15-25*	*15-25*	*15-25*	*15-25*	*15-25*	*15-20*	*15-20*	*15-20*
Time(min)	*45*	*45*	*10*	*15*	*30*	*45*	*45*	*45*	*15*	*45*
voltage	*320-330*									
current	*0.1-0.3*									

3- Mixing of Modified electrolyte by calcite and thassos addition as shown in table Group III.

Substrate / *Materials*	*CF1*	*CF2*	*CF3*	EF1	*EF2*	*EF3*
KH_2PO_4	*20g/L*	*20g/L*	*20g/L*	*20g/L*	*20g/L*	*20g/L*
KOH	*2 g/L*	*2 g/L*	*2 g/L*	*2 g/L*	*2 g/L*	*2 g/L*
Na_2SiO_3	—	—	—	---	---	---
$(NH_3)_2MO_7O_{24}$	*12g/L*	*12g/L*	*12g/L*	*12g/L*	*12g/L*	*12g/L*
H_3PO_4	*8 ml*	*8ml*	*8ml*	*8 ml*	*8 ml*	*8 ml*
$CaCO_3$	*20g/L*	*20g/L*	*20g/L*	*10g/L*	*10g/L*	*10/L*
Thassos	*3g/L*	*3g/L*	*3g/L*	*7g/L*	*7g/L*	*7g/L*
MOS_2	—	—	—	—	—	—
PH	*4-5*					
Temp.(˚C)	*15-20*	*15-20*	*15-20*	*15-20*	*15-20*	*15-20*
Time(min)	*15*	*30*	*45*	*15*	*30*	*45*
voltage	*320-330*					
current	*0.1-0.3*					

4-Mixing of Modified electrolyte by bauxite addition as shown in table Group IV.

Substrate / *Materials*	*G1*	*(G3)1*	*(G3)2*	(G3)3	*G5*	*G7*
KH_2PO_4	*20g/L*	*20g/L*	*20g/L*	*20g/L*	*20g/L*	*20g/L*
KOH	*2 g/L*	*2 g/L*	*2 g/L*	*2 g/L*	*2 g/L*	*2 g/L*
Na_2SiO_3	—	—	—	---	---	---
$(NH_3)_2MO_7O_{24}$	*12g/L*	*12g/L*	*12g/L*	*12g/L*	*12g/L*	*12g/L*
H_3PO_4	*8 ml*	*8ml*	*8ml*	*8 ml*	*8 ml*	*8 ml*
Bauxite	*1g/L*	*3g/L*	*3g/L*	*3g/L*	*5g/L*	*7g/L*
MOS_2	—	—	—	—	—	—
PH	*4-5*					
Temp.(˚C)	*15-20*	*15-20*	*15-20*	*15-20*	*15-20*	*15-20*
Time(min)	*15*	*15*	*30*	*45*	*15*	*15*
voltage	*320-330*					
current	*0.1-0.3*					

4- Mixing of Modified electrolyte by calcite, bauxite and thassos addition as shown in table Group V.

Substrate / *Materials*	*CFG1*	*CFG2*	*CFG3*	EFG1	*EFG2*	*EFG3*
KH_2PO_4	*20g/L*	*20g/L*	*20g/L*	*20g/L*	*20g/L*	*20g/L*
KOH	*2 g/L*	*2 g/L*	*2 g/L*	*2 g/L*	*2 g/L*	*2 g/L*
Na_2SiO_3	—	—	—	---	---	---
$(NH_3)_2MO_7O_{24}$	*12g/L*	*12g/L*	*12g/L*	*12g/L*	*12g/L*	*12g/L*
H_3PO_4	*8 ml*	*8ml*	*8ml*	*8 ml*	*8 ml*	*8 ml*
$CaCO_3$	*20g/L*	*20g/L*	*20g/L*	*10g/L*	*10g/L*	*10/L*
Thassos	*3g/L*	*3g/L*	*3g/L*	*7g/L*	*7g/L*	*7g/L*
Bauxite	*3g/L*	*3g/L*	*3g/L*	*5g/L*	*5g/L*	*5g/L*
MOS_2	—	—	—	—	—	—
PH	*4-5*					
Temp.(˚C)	*15-20*	*15-20*	*15-20*	*15-20*	*15-20*	*15-20*
Time(min)	*15*	*15*	*30*	*45*	*15*	*15*
voltage	*320-330*					
current	*0.1-0.3*					

Table (1): Results of coatings thickness and hardness for samples.

N	Substrates	Time (min)	Before contact Angle (°)	After contact angle (°)	Hardness
1	A1	10	0	88.005	154.7
2	A2	15	0	90.672	285.4
3	A3	30	0	94.739	309.5
4	A4	45	0	88.205	352.8
5	B3	15	0	78.113	618.8
6	B5	15	0	89.152	439.7
7	B7	15	0	90.067	391.8

8	C1	10	0	87.295	225.2
9	C2	15	0	90.789	412.5
10	C3	30	0	87.256	408.6
11	C4	45	0	80.787	1008.3
12	D1	15	0	96.344	460.1
13	D2	45	0	90.004	500.5
14	E	45	0	96.977	591
15	MC1	15	0	68.506	600.9
16	MC2	45	0	75.382	922.26
17	F1	45	0	88.596	547.4
18	F2	45	0	94.773	433.7
19	$(F3)_1$	10	0	80.764	246.9
20	$(F3)_2$	15	0	90.278	347.6
21	$(F3)_3$	30	0	87.69	382.4
22	$(F3)_4$	45	0	95.120	669.2
23	F5	45	0	90.326	724.56
24	F7	45	0	88.901	975.9
25	MF1	15	0	88.417	750.8
26	MF2	45	0	88.698	577.9
27	CF1	15	0	108.501	1107.366
28	CF2	30	0	90.923	1397.6
29	CF3	45	0	87.246	1155.9
30	EF1	15	0	90.535	1117
31	EF2	30	0	82.483	1384.8
32	EF3	45	0	81.069	1400
33	G1	15	0	85.944	431.45
34	$(G3)_1$	15	0	103.526	653.05
35	$(G3)_2$	30	0	96.203	595.65
36	$(G3)_3$	45	0	88.018	775.35
37	G5	15	0	46.706	873.16
38	G7	15	0	83.755	765.6
39	CFG1	15	0	113.907	1280

40	CFG2	30	0	106.381	1385
41	CFG3	45	0	98.571	1371
42	EFG1	15	0	103.587	1376.2
43	EFG2	30	0	82.750	1641.75
44	EFG3	45	0	96.437	1700.7

Table (2): Thickness results of coatings.

N	*Substrates*	*Time (min)*	*Thickness* (nm)	*Roughness (nm)*
1	B3	10	683.1	69.46
2	C2	15	445.2	37.97
3	C4	45	520.4	53.75
4	D1	15	687.0	62.41
5	F2	45	933.9	113.4
6	F7	45	830.8	79.42
7	CF1	15	2329	240.3
8	EF3	45	976.5	109.2
9	(G3)1	15	1452	136.1
10	X5	15	2022	186.1
11	CFG1	15	2191	172.7
12	EFG3	45	920.5	110.9

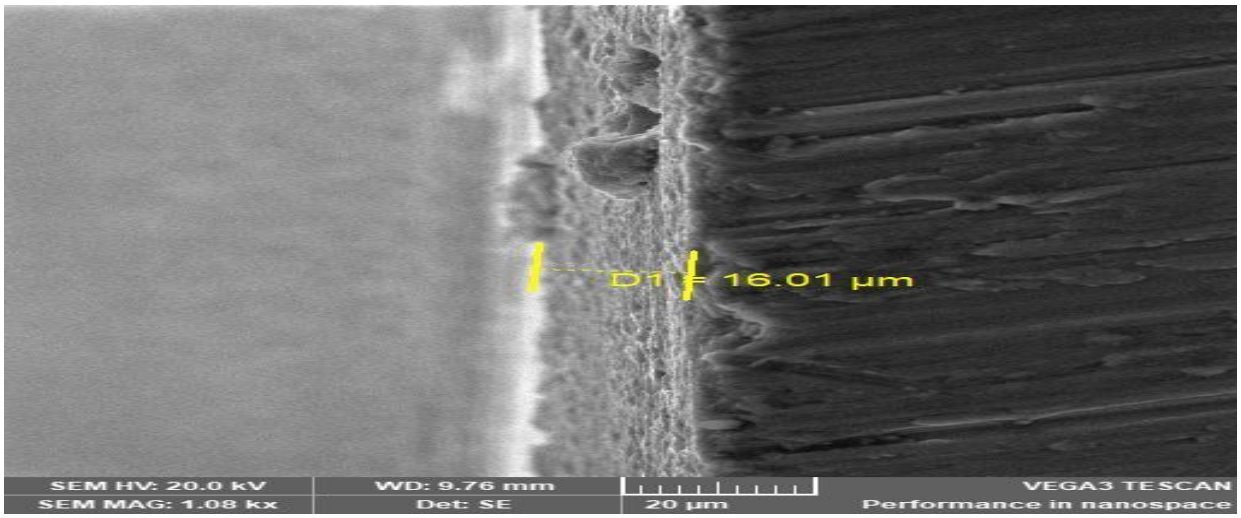

Figure (1): Thickness results of coatings by SEM.

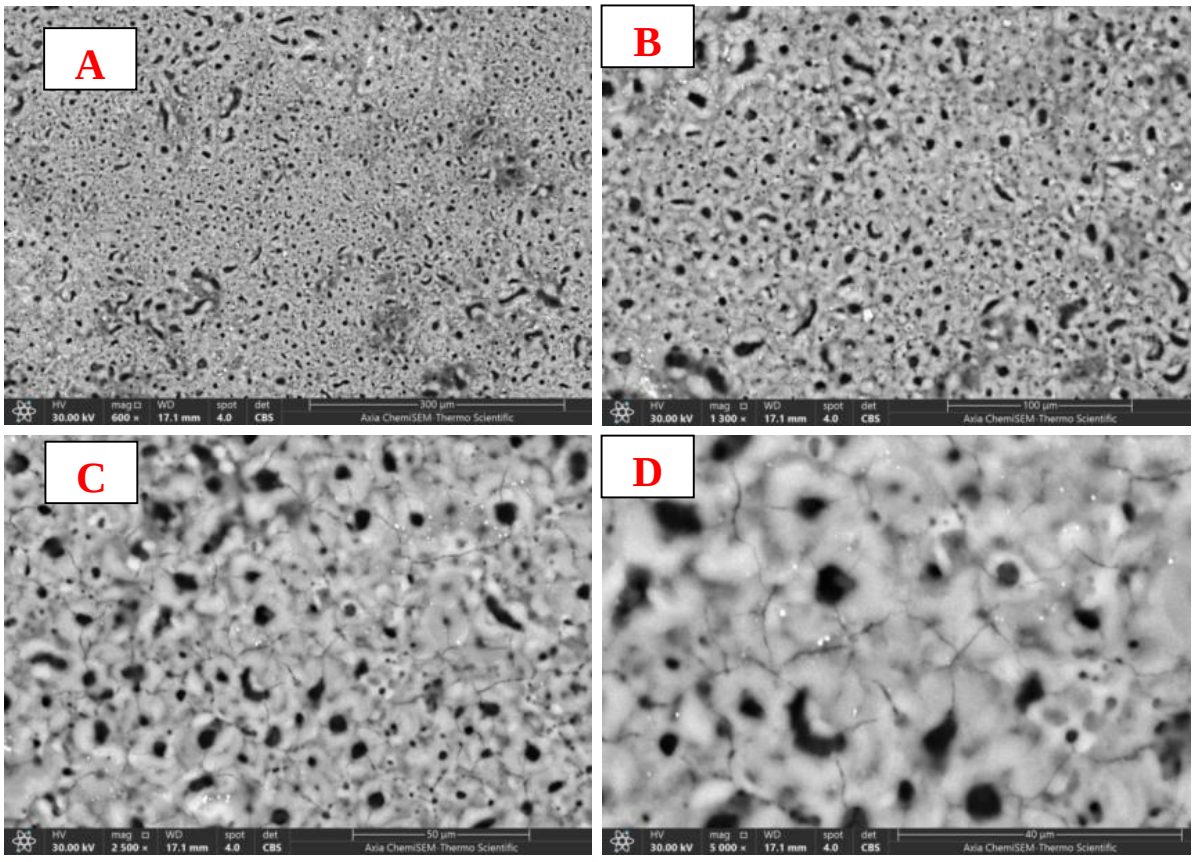

Figure (2): SEM results for coatings deposited using *basic electrolyte* (B3 *Coating).*

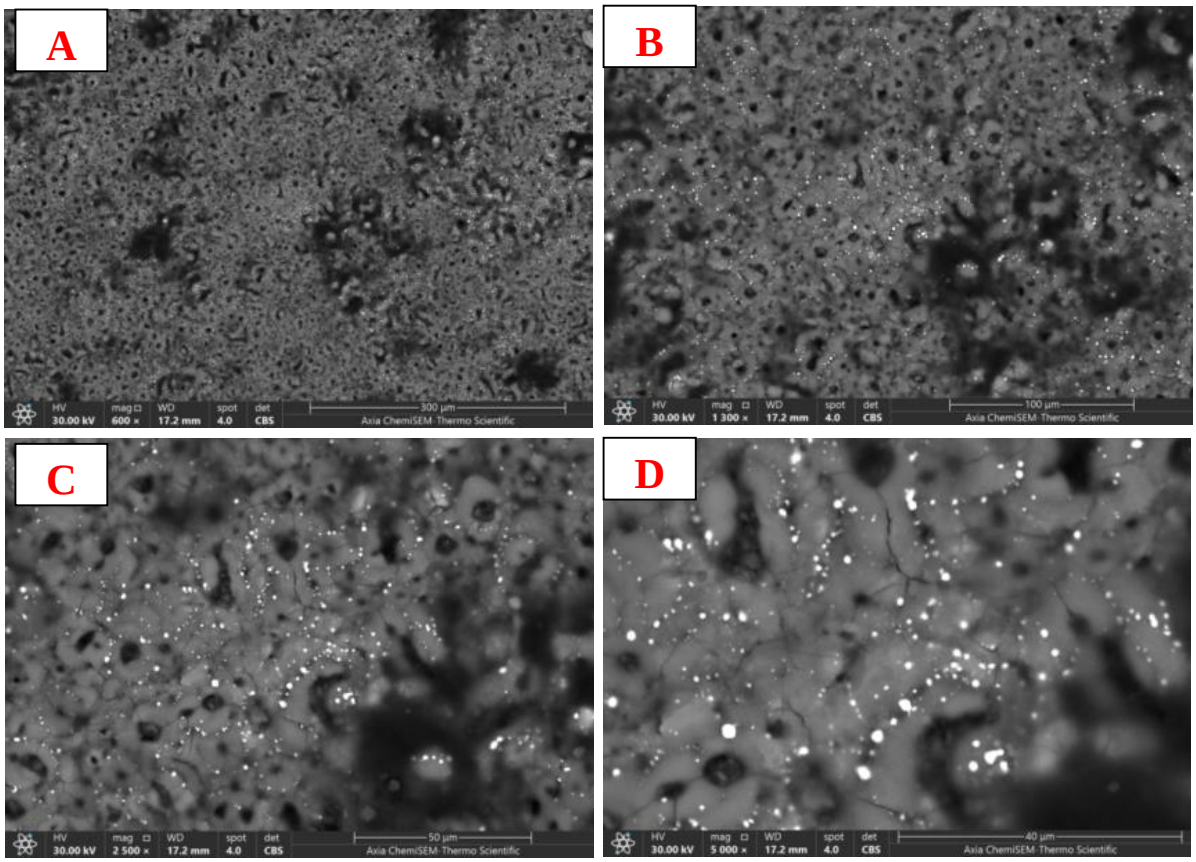

Figure (3): SEM results for coatings deposited using *basic electrolyte* (C2 *Coating)*.

جمهورية العراق

وزارة التعليم العالي والبحث العلمي

جامعة بابل

قسم السيراميك ومواد البناء

تحضير وتوصيف طبقة أوكسيدية سيراميكية صلدة ذاتية التنظيف بأستخدام طريقة الأكسدة المايكروية من إضافات صخرية مختلفة

رسالة

مقدمة الى كلية هندسة المواد / جامعة بابل وهي جزء من متطلبات نيل درجة الماجستير في هندسة المواد / السيراميك

من قبل

رشا نايف راشد جاسم

إشراف

أ . د .

سمير حامد عواد

2023 م **1445هـ**

الخلاصة

لقد شهدت السنوات الاخيرة أهتمام كبير ومتزايد في هندسة سطوح سبائك الالمنيوم بأستخدام تقنيات مختلفة لترسيب طلاءات سيراميكية كارهة للماء لتحسين خصائص مقاومة البلى والتأكل والسطوح ذاتية التنظيف.

الدراسة الحالية هي محاولة في استخدام الاضافات السيراميكية العراقية الصخرية الطبيعية في تطوير المحاليل الالكتروليتية المستخدمة في تقنية الاكسدة المايكروية MAO لترسيب طلاءات الألومينا Al_2O_3 السيراميكية الصلدة الكارهة للماء في نفس الوقت على سبائك الالمنيوم للتطبيقات الترايبولوجية شديدة ظروف التحميل ولتطبيقات السطوح ذاتية التنظيف. طلاء مكونات الالمنيوم للجسور والسور بمواد التنظيف الذاتي الى تقليل تكاليف الصيانة وتعزيز طول عمر هذه الهياكل في البيئات الخارجية وتطبيق التنظيف الذاتي ومقاومة التأكل لطلاءات سبائك الالمنيوم على الاسطح المعمارية، مثل واجهات المباني الخارجية، للحد من تراكم الاوساخ والملوثات والنمو البيولوجي وهذا لا يحافظ على المظهر الجمالي فحسب بل يقلل أيضا من متطلبات الصيانة.

تم في هذه الدراسة استخدام مساحيق صخور الكالسايت $CaCO_3$ كمضافات ومكونات اساسية في المحاليل , واستخدام كل من مساحيق صخور البوكسايت (7,5,3,1) غم/لتر والثاسوس (7,5,3,1) غم/لتر كمضافات مطورة للمحاليل . تم ترسيب طلاءات على سطوح سبائك الالمنيوم باستخدام منظومة ترسيب صممت وصنعت محلياً لمتطلبات البحث بفولتية (320-350 فولت), تيار (0.1 - 0.3 امبير) وبدرجة حرارة ترسيب مسيطر عليها ضمن المدى (15-25°C) باستخدام التبريد والخلط الميكانيكي لمكونات المحلول وأوقات الترسيب (10-45 دقيقة) . تم معالجة الطلاءات بعد الترسيب باستخدام حوامض الميريستيك والستيريك لتحسين مواصفات السطوح ذاتية التنظيف.

تم استخدام عدة تقنيات وطرق فحص لتوصيف المساحيق والطلاءات (البنية , الاطوار المترسبة, والخصائص الميكانيكية والفيزيائية) مثل SEM , XRD , الخشونة , AFM , فحص البلى, الصلادة, السمك وقياس زاوية التماس .

أثبتت النتائج نجاح أستخدام تقنية MAO بمحاليل مطورة بالإضافات الطبيعية الصخرية العراقية السيراميكية من الكالسايت، البوكسايت والثاسوس ومعالجة الطلاءات بعد الترسيب بالحوامض في ترسيب طلاءات Al_2O_3 ذات طبيعة مسامية منتظمة (Ra240.3-53.75) وسمك (445.2-2329

نـانو) بمواصـفات متميـزة مثـل الصـلادة العاليـة (HV 1700.7-154.7) وكراهيـة المـاء (90.004-113.907°)، وبمقاومة تأكل جيدة (8.48-568.61 نانو أمبير).

أعلـى زاويـة تمـاس (113,907°) تـم الحصـول عليهـا عنـد اسـتخدام نسـب اضـافات (20غم/لتـر مـن الكالسايت, 3غم/ لتر من كل من البوكسايت والثاسوس) بفولتية ترسيب (325 فولت) وزمن ترسيب (15 دقيقة) هكذا زاوية تماس عالية تثبت كراهية السطوح للماء , أعلـى قيمـة صـلادة (HV 1700,7) تـم تسـجيلها عنـد نسـب اضـافات (10غم/لتـر مـن الكالسـايت ,7غـم /لترثاسـوس ,5غم/لتـر بوكسـايت) بفولتية ترسيب (330 فولت) وزمن ترسيب (45 دقيقة) .صفات الطلاءات المحسنة في هذا البحث سوف تساهم في حفظ تلك الطلاءات ذاتية التنظيف ومقاومة للبلى والخدش والظروف الجوية الشديدة.